CAPITAL UNIVERSITY OF SCIENCE AND
TECHNOLOGY, ISLAMABAD

Numerical Study of Heat and Mass Transfer of MHD flow over a stretching sheet

by

Muhammad Bilal

A thesis submitted in partial fulfillment for the
degree of Doctor of Philosophy

in the

Faculty of Computing
Department of Mathematics

2018

Numerical Study of Heat and Mass Transfer of MHD flow over a stretching sheet

By

Muhammad Bilal

(PA 131003)

Dr. Masoud Nickaeen

Center for Cell Analysis & Modeling, UConn Health, Farmington, USA

(Foreign Evaluator No. 1)

Dr. Abderrahim Ouazzi

Technische Universitt Dortmund Fakultt fr Mathematik, Dortmund, Germany

(Foreign Evaluator No. 2)

Dr. Muhammad Sagheer

(Thesis Supervisor)

Dr. Muhammad Sagheer

(Head, Department of Mathematics)

Dr. Muhammad Abdul Qadir

(Dean, Faculty of Computing)

DEPARTMENT OF MATHEMATICS

CAPITAL UNIVERSITY OF SCIENCE AND TECHNOLOGY

ISLAMABAD

2018

CAPITAL UNIVERSITY OF SCIENCE & TECHNOLOGY
ISLAMABAD

Expressway, Kahuta Road, Zone-V, Islamabad
Phone:+92-51-111-555-666 Fax: +92-51-4486705
Email: info@cust.edu.pk Website: https://www.cust.edu.pk

CERTIFICATE OF APPROVAL

This is to certify that the research work presented in the thesis, entitled "**Numerical Study of Heat and Mass Transfer of MHD Flow Over a Stretching Sheet**" was conducted under the supervision of **Dr. Muhammad Sagheer**. No part of this thesis has been submitted anywhere else for any other degree. This thesis is submitted to the **Department of Mathematics, Capital University of Science and Technology** in partial fulfillment of the requirements for the degree of Doctor in Philosophy in the field of **Mathematics**. The open defence of the thesis was conducted on **19 March, 2018**.

Student Name : Mr. Muhammad Bilal (PA131003)

The Examining Committee unanimously agrees to award PhD degree in the mentioned field.

Examination Committee :

(a)	External Examiner 1:	Dr. Muhammad Ashraf Professor BZU, Multan
(b)	External Examiner 2:	Dr. Sirajul Haq Professor, GIK Institute, Topi
(c)	Internal Examiner :	Dr. Abdul Rehman Kashif Associate Professor Capital University of Science & Technology, Islamabad
Supervisor Name :		Dr. Muhammad Sagheer Professor Capital University of Science & Technology, Islamabad
Name of HoD :		Dr. Muhammad Sagheer Professor Capital University of Science & Technology, Islamabad
Name of Dean :		Dr. Muhammad Abdul Qadir Professor Capital University of Science & Technology, Islamabad

AUTHOR'S DECLARATION

I, **Mr. Muhammad Bilal (Registration No. PA131003)**, hereby state that my PhD thesis titled, '**Numerical Study of Heat and Mass Transfer for Newtonian and Non-Newtonian Fluids**' is my own work and has not been submitted previously by me for taking any degree from Capital University of Science and Technology, Islamabad or anywhere else in the country/ world.

At any time, if my statement is found to be incorrect even after my graduation, the University has the right to withdraw my PhD Degree.

(**Mr. Muhammad Bilal**)

Dated: 19 March, 2018

Registration No : PA131003

PLAGIARISM UNDERTAKING

I solemnly declare that research work presented in the thesis titled "**Numerical Study of Heat and Mass Transfer for Newtonian and Non-Newtonian Fluids**" is solely my research work with no significant contribution from any other person. Small contribution/ help wherever taken has been duly acknowledged and that complete thesis has been written by me.

I understand the zero tolerance policy of the HEC and Capital University of Science and Technology towards plagiarism. Therefore, I as an author of the above titled thesis declare that no portion of my thesis has been plagiarized and any material used as reference is properly referred/ cited.

I undertake that if I am found guilty of any formal plagiarism in the above titled thesis even after award of PhD Degree, the University reserves the right to withdraw/ revoke my PhD degree and that HEC and the University have the right to publish my name on the HEC/ University Website on which names of students are placed who submitted plagiarized thesis.

(Mr. Muhammad Bilal)
Registration No. PA131003

Dated: 19 March, 2018

This work is dedicated to my Friends, Family and my Teachers

List of Publications

It is certified that following publication(s) have been made out of the research work that has been carried out for this thesis:-

1. **M. Bilal**, S. Hussain and M. Sagheer, "Boundary layer flow of magneto-micropolar nanofluid flow with Hall and ion-slip effects using variable thermal diffusivity", *Bulletin of the Polish Academy of Sciences*, 65(3), 383-390, 2017.

2. **M. Bilal**, M. Sagheer and S. Hussain, "Three dimensional MHD upper-convected Maxwell nanofluid flow with nonlinear radiative heat flux", *Alexandria Engineering Journal*, http://dx.doi.org/10.1016/j.aej.2017.03.039, 2017.

3. **M. Bilal**, M. Sagheer and S. Hussain, "On MHD 3D upper convected Maxwell fluid flow with thermophoretic effect using non-linear radiative heat flux", *Canadian Journal of Physics*, https://doi.org/10.1139/cjp-2017-0250, 2017.

Muhammad Bilal
(PA131003)

Acknowledgements

Veneration for **ALLAH** almighty, who created us among the humans, the supreme beings, the Muslims and bestowed with the discernment to distinguish the right from wrong. Obeisance to the Omniscient who adorned the Universe with the Holy Prophet, **HAZRAT MUHAMMAD (Sallallahu Alaihay Wa'alihi Wasalam)** the prime cause of the creation of macrocosm, the one who transformed the twilight of the deserts of ignorance into the illuminated oasis of knowledge and directed humanity towards the path of heaven.

I owe honour, reverence and indebtedness to my accomplished supervisor and mentor **Dr. Muhammad Sagheer** whose affectionate guidance, authentic supervision, keen interest and ingenuity was a source of inspiration for commencement, advancement and completion of the present study. I would like to acknowledge CUST to providing me such a favourable environment to conduct this research.

A lot of appreciation is extended to **Dr. Shafqat Hussain**, Associate professor for his devotion, commitment, dedication and help during this project. He provided me the opportunity to learn the method that finally lead to this thesis.

Sincere and heartiest salutations are due to my Parents and siblings whose life long toil and nature made me what I am today. I also feel grateful to life partner who never let me down and was a source of fortification during the trial period of research.

I gratefully acknowledge the funding source that made my Ph.D work possible. I was funded by the Higher Education Commission of Pakistan.

Last but not the least, my sincere thanks goes to my friends Dr. Khalid Mehmood, Mr. Yasir Mehmood, Mr. Mian Tanvir Sajid and Mr. Sajid Shah for very good company and entertainment activities in free hours at the university.

In the end, I pray to Almighty Allah to shower his countless blessings on all who assisted me in anyway during my thesis.

Abstract

In this thesis, the boundary layer flow of Newtonian and non-Newtonian fluid models over unidirectional and bidirectional linearly stretching sheets are considered for the heat and mass transfer purpose. Upper convected Maxwell fluid model is used as a non-Newtonian fluid model. Flow is triggered due to linearly stretched sheet. For the enhancement of thermophysical properties of such fluids, the concept of nanofluid is utilized. Magnetic field is applied across the fluid flow which allows further manipulation of heat transfer and hydrodynamics characteristics. When the strong magnetic field is applied athwart the fluid having the low density, the conductivity of the fluid decreases because of the spiral movement of electrons about the lines of the magnetic force and the Hall current and ion-slip effects are produced. In addition, during the study of the nanofluids for the heat transfer purpose, the effects of thermal radiation cannot be denied. Particularly when there is a big temperature difference, we are encouraged to consider the non-linear thermal radiation. Further, the effects of heat generation/absorption, variable thermal conductivity, Joule heating, viscous dissipation and mixed convection are also contemplated for different problems. Using the boundary layer approximations, the physical flow model in the form of differential equations are governed. The partial differential equations which are non-linear in nature are reduced into a set of ordinary differential equations. Shooting technique with fourth order of Runga-Kutta integration scheme is used to calculate the numerical results of obtained differential equations. The quantities of physical significance such as velocities, concentration, temperature, Nusselt number, Sherwood number and skin-friction coefficients for various values of the emerging parameters, are computed numerically and are analyzed in detail. For the validation of the results obtained by the shooting method, a MATLAB built-in function bvp4c is also employed. Both the methods show an excellent agreement. To further strengthen the reliability of our MATLAB code, the results presented in the already published articles are reproduced successfully.

Contents

List of Figures

List of Tables

Symbols

a	a real constant
A^*	space dependent heat generation/absorption
B^*	temperature dependent heat generation/absorption
b	constants of dimension $(time)^{-1}$
B	magnetic induction vector
B_0	magnetic field strength
C	concentration of fluid
c	stretching ratio parameter
Cf_x	skin friction coefficient along x-axis
Cf_z	skin friction coefficient along z-axis
C_w	concentration at wall
C_∞	ambient concentration
c_p	specific heat
D	diffusion coefficient
D_B	Brownian diffusion coefficient
D_T	thermophoretic diffusion coefficient
E	electric field intensity
e	charge of an electron
Ec	Eckert number
f, g	dimensionless stream functions
f_w	mass transfer parameter
g	dimensionless transvers velocity
g_c	gravitational acceleration

Gr_c	mass Grashof number
Gr_x	thermal Grashof number
G	microrotation parameter
G_1	spin gradient viscosity
h	microrotation function
h_w	heat flux coefficient
J	electric current density
j_w	surface mass flux
K_0	vortex viscosity
K_1	thermophoretic coefficient
k	thermal conductivity
κ_p	permeability parameter
k^*	permeability of porous medium
Le	Lewis number
M	magnetic parameter
N	microrotation component
Nb	Brownian motion parameter
Nt	thermophoresis parameter
Nu_x	local Nusselt number
N_1	coupling constant parameter
n_e	density number of electrons
Pr	Prandtl number
q^m	non-linear coefficient of heat generation/absorption
q_r	radiative heat flux
q_w	surface heat flux
Rd	thermal radiation parameter
Re_x	local Reynolds number
Sc	Schmidt number
Sh_x	local Sherwood number
T	temperature of fluid
T_w	temperature at wall

T_∞	ambient temperature
u_x	stretching velocity
V	velocity vector
V_T	thermophoretic velocity
V_w	suction injection velocity
(u, v, w)	velocity components
(x, y, z)	coordinate axises
α	thermal diffusivity
α_0	thermal diffusivity at wall temperature
β_c	concentration coefficient
β_T	thermal expansion coefficient
β_2	fluid nature dependent parameter
β_e	Hall current parameter
β_i	ion-slip parameter
ν	kinematic viscosity
ν_e	electron atom collision frequency
θ	dimensionless temperature
θ_w	temperature ratio parameter
ϕ	dimensionless concentration
λ	fluid relaxation time
Λ	Deborah number
ψ	stream function
σ	electric conductivity
σ^*	Steffan-Boltzman constant
ω	collision frequency
ρ	density of fluid
τ	ratio of nanoparticle heat capacity and base fluid heat capacity
τ_1	thermophoretic parameter
τ_{wx}	wall shear stress in x-direction
η	dimensionless normal distance
$\aleph$	mean absorption coefficient

Chapter 1

Introduction

1.1 Introduction

This chapter contains some basic information regarding non-Newtonian and Newtonian fluids. A brief history and importance of the boundary layer flow of Newtonian and non-Newtonian fluids, micropolar fluids, nanofluids, magnetohydrodynamics flows, Hall and ion slip effects, thermophoretic effects, porous media, heat generation/absorption, linear and non-linear radiation for the mass and heat transfer induced by a stretching surface is presented. The main shortcoming in the literature, motivations and objectives of the thesis are also highlighted.

1.2 History

In resent few years, study of the non-Newtonian fluids is curiously expanded because of their extensive dimension, useful technological and industrial applications. Shampoos, blood at low shear rate, soaps, apple sauce, mud, chyme, sugar solution, emulsion, etc are some real life examples of non-Newtonian fluids. In polymer, chemical and biomedical industries, the importance of non-Newtonian fluids cannot be denied. In almost all the industrial and biological fluids, the relationship between the rate of deformation and the stress is not linear. The sole properties

of all non-Newtonian fluids cannot be completely described by any concrete single equation/relation. Due to this, researchers have suggested various mathematical models of non-Newtonian fluids. Amongst these models, Maxwell fluids and viscoelastic fluids have ample range of industrial applications such as glass blowing, extrusion of polymer sheets, manufacturing of plastic films, hot rolling, crystal growing etc. The viscoelastic fluid models such as second order and/or Walter-B fluid models are recommended for fluids having small level of elasticity [1]. These fluid models violate some established rules of thermodynamics [2]. For highly viscoelastic polymers, second grade fluid models with high Deborah number do not give the meaningful results [3, 4], which reduces their significance in the polymer industry. Consequently, some more realistic fluid models, such as Oldroyd-B or upper-convected Maxwell fluid models have been considered for the application purpose [5]. Indeed these two models for viscoelastic fluid flow have been studied on stretching and non-stretching sheets. Ali and Ashrafi [6] have investigated the upper convected Maxwell fluid with high Weissenberg number over a linearly stretching sheet. Velocity and heat transfer analysis of the fluid flow is carried out by using the shooting technique. Mushtaq et al. [7] analyzed the Sakiadis flow of upper-convected Maxwell fluid through a stretching sheet using Cattaneo-Christov model. Omowaye and Animasaum [8] studied the MHD UCM(upper convected Maxwell) fluid over a melting surface subject to thermal stratification with variable thermo-physical properties. They concluded that velocity profile is enhanced for the higher values of Deborah number. Krupalakshmi et al. [9] found the numerical solution of UCM fluid in the existence of dust particles over convectively heated stretching sheet. They incorporated the magnetic field and discussed the effects of viscous dissipation, non-linear thermal radiation, and heat source/sink. Waini et al. [10] considered the inclined magnetic field through a continuously stretched sheet for the study of heat and fluid flow of UCM fluid. They concluded that the magnetic field's strength is enhanced when the inclination of the aligned magnetic field is high, and resultantly it increases the temperature and reduces the velocity of the fluid. Magnetohydrodynamics 3-dimensional flow of UCM fluid

over bidirectional sheet with non-Fourier heat flux model and heat generation/absorption effects was discussed by Saleem et al. [11]. Some recent articles regarding the importance and significance of Maxwell fluid can be seen in literature [12–17].

The boundary layer flow over moving surfaces has a large number of applications in engineering and industrial sectors. Sakiadis [18, 19] proposed the concept of the boundary layer flow through a constantly stretching surface. Erickson [20] extended his work by adding the case of mass transfer. Due to very wide range of practical applications of stretching surface, many researchers have contributed in this direction. Rizwan et al. [21] discussed the MHD slip flow with convective boundary conditions over a stretching surface for carbon nanotubes. Ramesh [22] studied the influence of the heat source on the stretching surface for the stagnation point flow of Jeffery nanofluids. Gireesha et al. [23] analyzed the MHD Casson fluid with chemical reaction effects for the flow, mass and heat transfer in a porous medium.

The idea of nanofluid was first introduced by Choi [24] in 1995. The homogeneous mixture of very small particles of size $10^{-9}m$ and base fluid is called nanofluid. Usually $Al, Cu, Ag, TiO_2, Al_2O_3$ etc are used as nanoparticles with base fluids like oil, ethylene glycol, water, etc. While using the nanofluids, the maximum possible thermal properties are targeted to achieve with the least feasible concentration by systematic dispersion and substantial suspension of nanoparticles in the base fluids [25, 26]. These fluids are fit for enhancing the thermophysical properties, for example, thermal diffusivity, convective heat transfer coefficient, viscosity, and thermal conductivity when compared with those of the base liquids like ethylene, tri-ethylene glucose, water or other coolants, polymer solutions and biofluids as expatiated by Choi [27] and Wong and Leon [28]. These fluids possess the distinguished physical and chemical properties and can easily pass through the microchannels and capillaries and don't block the flow. Fuel cells, hybrid-powered instruments, automotive, food handling industry and refrigeration are few pertinent examples of nanofluids. Buongiorno [29] considered the Brownian diffusion and thermophoresis slip mechanism for the relative velocity of the base fluid and nanoparticles. He proposed a mathematical model involving

thermophoresis and the Brownian motion effects to examine the thermal effects of the host fluid. Later on, another model based on the solid volume fraction of nanoparticles was introduced by Tiwari and Das [30] for the heat transfer enhancement of the host fluid. Ashikin et al. [31] addressed the issue of heat transfer for the MHD Maxwell nanofluid flow past a vertical permeable sheet. Mansur et al. [32] studied the magnetohydrodynamic stagnation point flow of a nanofluid over a stretching/shrinking sheet with suction. Noreen et al. [33] analyzed the Hall effects on the flow of pressure driven pseudoplastic fluid having viscous dissipation effects. Three dimensional mixed convection viscoelastic nanofluid flow was analyzed by Hayat et al. [34] analytically. In another article, Hayat et al. [35] studied the unsteady magneto-nanofluid flow with double stratification over an inclined stretching sheet. Shehzad et al. [36] worked on the Maxwell mixed convection nanofluid flow with doubly stratified heat generation/absorption. Very recently, Hayat et al. [37] investigated analytically the MHD flow of Maxwell nanofluid with thermal radiation and heat generation/absorption effects over a stretched sheet. Alsaedi et al. [38] analyzed the gyrotactic micro-organisms stratified bio-convective flow of MHD nanofluid. Inclined magnetic field is applied along with the additional effects of viscous dissipation and Joule heating. Study about the water based nanofluid flow with carbon nanotubes through a porous space with homogeneous-heterogeneous reactions and convective boundary conditions over a stretching cylinder was studied by Hayat et al. [39]. They concluded that single wall carbon nanotubes have more heat transfer coefficient as compared to multiwall carbon nanotubes. Mustafa et al. [40] presented the solutions of rotating flow of nanofluid over a convectively heated exponentially deforming sheet numerically. They used the zero mass flux condition for the nanoparticles. Hussanan et al. [41] investigated the time dependent free convection flow of micropolar nanofluid over a vertical plate using the Laplace transformation method. They considered five different types of nanoparticles, which are aluminum oxide, titanium oxide, copper oxide, iron oxide and graphene oxide with three different types of base fluids, which are kerosene oil, water and engine oil.

Eringen [42, 43] forthput a theory of micropolar fluids based on the characteristic

of inertial properties of the structure particles which undergo rotation. The microscopic effects and micro motion of structure fluid elements describe the micropolar fluids. In mathematical modeling, the interaction of microrotation field and macro velocity field can be portrayed by a new material constant in classical Newtonian fluids. Eringen's fluid model based on the classical Navier-Stokes equations is a special case for the incompressible and viscous fluids. These models are also suitable for the study of colloidal fluids flow, polymers, lubricants, cerebro fluids, animal blood, liquid crystals, real fluids with suspensions and ferro fluids etc., for which the classical Navier-Stokes theory is inadequate. In the micropolar fluid equation, a gyration parameter and microrotation vectors appear along with the classical Navier-Stokes equations. Mabood et al. [44] examined the non-Darcian magneto-micropolar fluid over an extending sheet with thermal radiation and non-uniform heat source/sink impacts. Mirzaaghaian and Ganji [45] used differential transformation method to investigate the heat and fluid flow of micropolar fluid through permeable walls. Ali et al. [46] figured the analytical solutions of the oblique stagnation point flow of micropolar fluid over a flat plate. They utilized the modified Hiemenz flow which happens in the $hjkns - skms$ boundary layer close orthogonal stagnation point flow. Exact solutions of mixed convective MHD micropolar fluid over a porous deformable plate with heat generation/absorption were calculated by Turkyilmazoglu [47]. Shehzad et al. [48] analyzed the unsteady mircopolar fluid flow through a convectively heated stretching sheet for heat and fluid flow. Realizing the significance and applications of micropolar fluids, many other researchers have also worked in this area [49–54].

The analysis of the effect of magnetohydrodynamics on the heat and mass transfer of fluid flowing over a stretching sheet in the presence of viscous dissipation and Joule heating is of great importance due to its extensive use in industrial and engineering sector. Amin [55] considered the MHD mixed convection flow over a non-isothermal cylinder with the additional effects of Joule heating and viscous dissipation in a porous medium. Alam et al. [56] discussed the Joule heating and viscous dissipation on an inclined isothermal permeable surface with MHD and thermophoresis effects. MHD natural convection flow over a porous medium

with the effects of viscous dissipation and Joule heating on a moving vertical plate was studied for the chemical reaction and Soret effects by Ibrahim and Reddy [57]. Hayat et al. [58] analyzed the incompressible unsteady 3-dimensional MHD flow over an exponentially stretching sheet with Joule heating and viscous dissipation. Mushtaq et al. [59] used the non-linear radiative heat flux on three dimensional upper convected Maxwell fluid for the analysis of fluid and heat flow on bidirectional stretching sheet.

Magnetic nanofluids is another imperative subbranch of nanofluids as it has momentous contribution in number of industrial and engineering fields [60]. Hydrodynamic characteristics and heat transfer rate is further manipulated when the magnetic field is applied across the flow of nanofluids. Often aluminum oxide and magnetite are oppressed during the formulation of such fluids. Sheikholeslami et al. [61] investigated the force convection heat transfer of magnetic nanofluids flow in a lid driven semi-annulus enclosure. They used the two phase model for the simulation of nanofluids. They concluded that higher values of Lewis and Hartmann number decrease the rate of heat flux, but it is augmented for the larger values of Reynolds number. Abbasi et al. [62] considered the boundary layer flow of two dimensional Jeffrey nanofluid with hydromagnetic effects over a linearly stretched sheet.

Mostly, Hall current and ion-slip effects are neglected because of their ignorable contribution while applying Ohm's law for small magnetohydrodynamics [63]. However, these have strong effect when the magnetic field is high [64], due to the strong electromagnetic force. Hall effect plays an important role when the Hall parameter is high. Hall parameter is the ratio of electron cyclotron frequency to atom-electron collision frequency. So the Hall current effect is high when the electron-atom collision frequency is low [63]. Steady MHD boundary layer flow with free convection over a porous inclined plate was explored by Alam et al. [65] with variable suction and Soret effect in the existence of Hall current. Eldahab [66] studied the free convective MHD flow along with the Hall effects through a stretching sheet. Thamizsudar [67] discussed the impact of Hall current and rotation on the heat and mass transfer of MHD fluid flowing over an exponentially

accelerated vertical plate. Nabil et al. [68] investigated the Hall effects on peristaltic flow of third order fluid with porosity factor. One dimensional unsteady MHD micropolar fluid flow with the effect of Hall current was analyzed by Islam et al. [69]. It is known that the mass of ions is much greater than the mass of electrons, and ultimately their motion will be different from each other. As a result of different velocities of electrons and ions, their diffusion velocities will also be different. As the current density mainly depends upon the diffusion velocity, the current density of electrons is much higher than that of ions. However if the magnetic field is high, then the diffusion velocity of ions is not negligible. The combined effect of diffusion velocities of ions and electrons is called ion-slip effect. Hall and ion-slip effects are involved in many engineering technologies such as Hall sensors, Hall accelerators, construction of centrifugal and turbines, etc. Attia et al. [70] discussed the heat transfer of Couette flow of a dusty fluid with ion-slip effect and uniform suction and injection. MHD mass transfer problem by free convection flow of an ionized incompressible viscous micropolar fluid across the infinite vertical plate under the action of Hall current and ion-slip parameter has been discussed by Anika et al. [71]. Ziya Uddin et al. [72] considered the Hall and ion-slip effect on MHD boundary layer flow of a micropolar fluid past a wedge. Motsa et al. [73] studied the micropolar fluid with chemical reaction and Hall and ion-slip effects with thermal diffusivity.

Applied and theoretical research in porous media for the flow, heat and mass transfer has gained an immense attention during last few years. The usefulness of porous media can be seen in many research areas and has a wide range of engineering applications such as geothermal reservoirs, geophysics, exploration of petroleum, thermal insulation engineering, water movements in geothermal reservoirs, and gas fields etc [74]. Hayat et al. [75] have made a comparative study about the MHD flow of viscous nanofluids with convective boundary conditions over an exponentially stretching sheet embedded in a porous medium. Silver, copper, titanium oxide and alumina are considered as nanoparticles. Thermally radiative mixed convective flow of nanofluid with magnetic field and porous medium in a stretchable channel was investigated numerically by Rauf et al. [76]. They have

further incorporated the effects of viscous dissipation, Brownian motion and thermophoresis in the energy equations. Nadeem and Muhammad [77] focus on the flow of viscous fluid, saturated with porous medium over a stretching sheet with stratification and Cattaneo-Christov heat flux model. They concluded that higher values of porosity parameter will enhance the velocity field. Sheikholeslami [78] presented the MHD natural convection flow of viscous nanofluid flow in a porous curved cavity. He applied the innovative numerical approach namely CVFEM. It was found that temperature profile is enhanced for the higher values of Darcy number.

Heat is transferred due to difference in temperature. If there is a large temperature difference, then assumption of constant thermal conductivity will lead to a noticeable error. Thus to minimize this type of error, it is necessary to consider a temperature dependent variable thermal conductivity within the thermal boundary layer region. The exploration of heat absorption/generation becomes in demand due to capricious applications in scientific instrumentation and nuclear reactor engineering. Many engineering procedures such as fossil fuel combustion, solar power technology, space vehicle re-entry and astrophysical flows occur at extremely high temperature. Radiative heat transfer in these processes perform a very meaningful role. When there is a significant difference of temperature between the ambient and the surface temperature, the effects of thermal radiation gain a significant importance. But a linear radiation is not valid for high temperature difference. To overcome this obstacle, the effects of non-linearthermal radiation are considered. In non-linear thermal radiation, the problem is governed by three parameters which are the radiation parameter, Prandtl number, and the temperature ratio parameter, whereas in linearized Rosseland approximation, only the effective Prandtl number is involved.

Thermophoresis is a process in which the fluid particles move towards a cooler region from the warmer [79]. This movement occurs because molecules from the warmer region having high kinetic energy impinge with the molecules having low energy in the cooler region. The velocity gained by the particles is thermophoretic velocity and the force experienced by the particles is called the thermophoretic

force [80]. Particles deposition due to thermophoresis was measured accurately by Tsai et al. [81]. Applications of thermophoresis can be seen in aerosol technology, radioactive particle expulsion in the nuclear reactor safety simulation, heat exchanger corrosion and deposition of silicon thin film. Layers of glass (SiO_2 and GeO_2) are built up by the deposition of particles on the tube wall with the help of modified chemical vapour deposition process. For very small sized chips, the potential failures increase due to the micro contamination by the particle deposition. The process of thermophoresis can be used to inhibit the deposition of small particles on the electronic chips for the purpose of efficiency. The thermophoretic transport of particles in one-dimensional flow for the thermophoretic velocity was studied first time by Goldsmith and May [82]. A theoretical analysis of thermophoresis of aerosol particles in the laminar flow over a horizontal flat plate was presented by Goren [83]. Since then, many researchers have considered thermophoresis as an effective parameter in a variety of flow problems for different types of fluids [84–88].

The aforementioned literature survey specifies that up till now a enormous literature regarding Newtonian and non-Newtonian fluid flow over a stretching sheet is presented. The importance of heat and mass transfer over the sheet has a number of practical applications in industrial and engineering sectors. Nanotechnology has introduced a new type of fluid which has higher physical and thermal properties as compared to the ordinary fluid. Due to the insertion of nanoparticles in the base fluid, the rate of heat and mass transfer is enhanced. In spite of all the earlier works done by various researchers, there is still a lot to do on boundary layer flow of magneto-nanofluid flow and heat and mass transfer, specially in the presence of strong magnetic field, Hall and ion-slip effects and non-linear thermal radiation. The purpose of this thesis is to explore the combined effects of MHD and nanofluid flow over the stretching sheet for the flow, heat and mass transfer of Newtonian and non-Newtonian liquids. Upper convected Maxwell fluid is considered as a non-Newtonian fluid. Along with nanofluid and MHD effects, we have also considered Hall and ion slip effects, variable thermal diffusivity, heat generation/absorption effects, non-linear thermal radiation, thermophoretic effects and

different boundary conditions for the different geometries. Similarity factors are utilized to change the partial differential equations into ordinary differential equations and these are solved numerically by implementing the shooting technique with Runge-Kutta integration scheme. It is a very efficient method with very low computational cost. Results are further compared with MATLAB built-in function bvp4c. Numerical results are plotted graphically and are discussed in detail for the fluid flow, heat and mass transfer. The effects of prominent parameters on skin friction, local Nusselt number and Sherwood number are discussed with the help of numerical results arranged in the form of tables. Results are further compared with previously published results in the limiting case.

The remaining thesis layout is as follows:
In **Chapter 2**, some fundamental laws governing the mathematical equations of fluid flow are derived. Continuity equation, momentum equations, energy equation and concentration equations are discussed which are based on the law of conservation of mass, Newton's second law of motion, first law of thermodynamics and Fick's law respectively. Tensor analysis is carried out for the upper convected Maxwell fluid. After this, the numerical scheme i.e., the shooting method is explained briefly with an example.

Chapter 3 examines the boundary layer flow of micropolar nanofluid over a linearly stretching porous sheet. Effects of magnetohydrodynamics, Hall and ion-slip are also discussed. During the formulation of energy equation, the concept of variable thermal conductivity is also considered. This Chapter is published in "Bulletin of the Polish Academy of Sciences, Technical Science", Vol. 65, No. 3, 2017, DOI: 10.1515/bpasts-2017-0043.

In **Chapter 4**, the effect of Hall current on boundary layer flow of magneto-nanofluid flow with mixed convection and non-linear heat generation/absorption is analyzed numerically. Non-linear differential equations are solved by the shooting method.

In **Chapter 5**, three dimensional flow of upper convected Maxwell fluid over a bidirectional linearly stretching sheet with the effects of magnetohydrodynamics

and non-linear thermal radiation is investigated. Again shooting method is used to solve the problem. This chapter is published in "Alexandria Engineering Journal", (2017) doi.org/10.1016/j.aej.2017.03.039.

Chapter 6 is comprised of the discussion on the MHD three dimensional flow of upper convected Maxwell fluid over linearly stretching sheet. Non-linear thermal radiation along with viscous dissipation, thermophoretic effect and Joule heating are also considered. This chapter is accepted in "Canadian Journal of Physics" (2017), https://doi.org/10.1139/cjp-2017-0250.

Chapter 7 consists of the conclusion of the thesis and the future outlook.

Chapter 2

Basic Governing Laws and Solution Methodology

In this chapter the basic concept of Boundary layer thickness, basic conservation laws of linear momentum, mass, energy and concentration diffusion are discussed. The constitutive relationship of upper-convected Maxwell fluid is given. Basic idea of shooting method is elaborated with an example. MATLAB built-in function bvp4c is highlighted briefly.

2.1 Boundary Layer [89]

"Skin friction drag is due to the viscous shearing that takes place between the surface and the layer of fluid immediately above it. This occurs on surfaces of objects that are long in the direction of flow compared to their height. Such bodies are called streamlined. When a fluid flows over a solid surface, the layer next to the surface may becomes attached to it (it wets the surface). This is called the no slip condition. The layers of the fluid above the surface are moving so there must be shearing taking place between the layers of the fluid. The shear stress acting between the wall and the first moving layer next to it is called the wall shear stress and denoted τ_w.

The result is that the velocity of the fluid u increases with height y. The boundary layer thickness δ is taken as the distance required for the velocity to reach 99% of u_0. This layer is called the Boundary layer and δ is the boundary layer thickness. Figure 2.1 shows how the velocity u varies with height y for a typical boundary layer. In a pipe, this is the only form of drag and it results in a pressure and

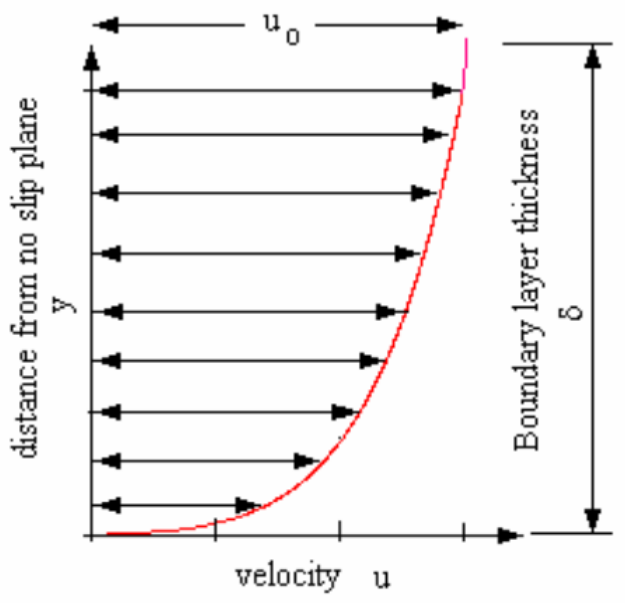

FIGURE 2.1: Boundary layer thickness over a flat surface

energy lost along the length. A thin flat plate is an example of a streamlined object. Consider a stream of fluid flowing with a uniform velocity u_0. When the stream is interrupted by the plate (Figure. 2.2) the boundary layer forms on both sides. The diagram shows what happens on one side only. The boundary layer thickness δ grows with distance from the leading edge. At some distance from the leading edge, it reaches a constant thickness. It is then called a fully developed boundary layer. The Reynolds number for these cases is defined as

$$(Re)_x = \frac{\rho u_0 x}{\nu} \tag{2.1}$$

x is the distance from the leading edge. At low Reynolds numbers, the boundary layer may be laminar throughout the entire thickness. At higher Reynolds numbers, it is turbulent. This means that at some distance from the leading edge the flow within the boundary layer becomes turbulent. A turbulent boundary

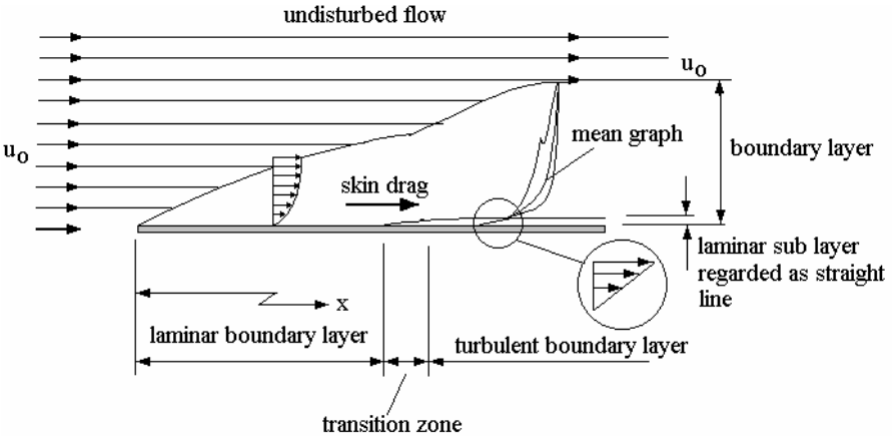

FIGURE 2.2: Boundary layer thickness in a pipe

layer is very unsteady and the streamlines do not remain parallel. The boundary layer shape represents an average of the velocity at any height. There is a region between the laminar and turbulent section where transition takes place."

2.2 Fundamental Laws

2.2.1 Mass Conservation (Continuity Equation)[90]

The expression for the law of conservation of mass is as follows:
"For any fluid, conservation of mass is expressed by the scalar equation

$$\frac{\partial \rho}{\partial t} + \nabla.(\rho \mathbf{V}) = 0, \tag{2.2}$$

where ρ is density of the fluid and $\mathbf{V}$ is the velocity field. Hence, a velocity profile represents an admissible (real) flow, if and only if it satisfies the continuity equation. For incompressible fluids, Eq. (2.2) reduces to

$$\nabla.\mathbf{V} = 0 \tag{2.3}$$

In Cartesian coordinates

$$\frac{\partial u}{\partial x} + \frac{\partial v}{\partial y} + \frac{\partial w}{\partial z} = 0 \tag{2.4}$$

Here, u, v and w are the velocity components along x, y and z direction respectively."

2.2.2 Momentum Equation (Conservation Law of Linear Momentum) [90]

The law of conservation of momentum is stated as follows: "This law states that the total linear momentum of the system is conserved. It is derived from Newton's second law. The mathematical form of momentum equation for any fluid is

$$\frac{\partial}{\partial t}(\rho \mathbf{V}) + \nabla.[(\rho \mathbf{V})\,\mathbf{V}] - \nabla.\tau_1 - \rho \mathbf{g} = 0. \tag{2.5}$$

The Cauchy stress tensor is defined as:

$$\tau_1 = -p\mathbf{I} + \mathbf{S}, \tag{2.6}$$

the momentum equation takes the form

$$\rho\left(\frac{\partial \mathbf{V}}{\partial t} + \mathbf{V}.(\nabla \mathbf{V})\right) = \nabla.(-p\mathbf{I} + \mathbf{S}) + \rho \mathbf{g}, \tag{2.7}$$

where, $\mathbf{g}$ is the body force, p the pressure, $\mathbf{S}$ the extra stress tensor and μ the dynamic viscosity. The Cauchy stress τ_1 in the tensor form is expressed as

$$\tau_1 = \begin{bmatrix} \sigma_{xx} & \tau_{xy} & \tau_{xz} \\ \tau_{yx} & \sigma_{yy} & \tau_{yz} \\ \tau_{zx} & \tau_{zy} & \sigma_{zz} \end{bmatrix}. \tag{2.8}$$

Eq. (2.7) is a vector equation and can be decomposed further into three scalar components by taking the scalar product with the basis vectors of an appropriate orthogonal coordinate system. By setting $\mathbf{g} = -g\nabla z$, where z is the distance from an arbitrary reference elevation in the direction of gravity, Eq. (2.7) can also be expressed as

$$\rho\frac{D\mathbf{V}}{Dt}=\rho\left(\frac{\partial\mathbf{V}}{\partial t}+\mathbf{V}.\left(\nabla\mathbf{V}\right)\right)=\nabla.\left(-p\mathbf{I}+\mathbf{S}\right)+\nabla\left(-\rho gz\right), \tag{2.9}$$

where D/Dt is the substantial derivative. The momentum equation then states that the acceleration of a particle following the motion is the result of a net force, expressed by the gradient of pressure, viscous and gravity forces. In Cartesian coordinates, using the velocity field $\mathbf{V}=\left[u\left(x,y,z,t\right),v\left(x,y,z,t\right),w\left(x,y,z,t\right)\right]$, the momentum equation can be expressed as

$$\left.\begin{aligned}\rho\left(\frac{\partial u}{\partial t}+u\frac{\partial u}{\partial x}+v\frac{\partial u}{\partial y}+w\frac{\partial u}{\partial z}\right)&=\frac{\partial\tau_{xx}}{\partial x}+\frac{\partial\tau_{xy}}{\partial y}+\frac{\partial\tau_{xz}}{\partial z}+\rho b_x,\\ \rho\left(\frac{\partial v}{\partial t}+u\frac{\partial v}{\partial x}+v\frac{\partial v}{\partial y}+w\frac{\partial v}{\partial z}\right)&=\frac{\partial\tau_{yx}}{\partial x}+\frac{\partial\tau_{yy}}{\partial y}+\frac{\partial\tau_{yz}}{\partial z}+\rho b_y,\\ \rho\left(\frac{\partial w}{\partial t}+u\frac{\partial w}{\partial x}+v\frac{\partial w}{\partial y}+w\frac{\partial w}{\partial z}\right)&=\frac{\partial\tau_{zx}}{\partial x}+\frac{\partial\tau_{zy}}{\partial y}+\frac{\partial\tau_{zz}}{\partial z}+\rho b_z.\end{aligned}\right\} \tag{2.10}$$

In which, $\tau_{xx},\tau_{xy},\tau_{xz},\tau_{yx},\tau_{yy},\tau_{yz},\tau_{zx},\tau_{zy}$, and τ_{zz} denote the components of Cauchy stress tensors and b_x,b_y and b_z denote the components of the body force."

2.2.2.1 Magnetohydrodynamics [91]

"In MHD, the plasma is considered as an electrically conducting fluid. Governing equations are equations of fluid dynamics and Maxwell's equations. A self-consistent set of MHD equations connects the plasma mass density ρ, the plasma velocity $\mathbf{V}$, the thermodynamic (also called kinetic) pressure P and the magnetic field $\mathbf{B}$. In strict derivation of MHD, one should neglect the motion of electrons and consider only heavy ions.

The momentum equation in the presence of magnetic field as a body force can be described as

$$\rho\left(\frac{\partial\mathbf{V}}{\partial t}+\left(\mathbf{V}\nabla\right)\mathbf{V}\right)=-\nabla P+\mathbf{j}\times\mathbf{B}. \tag{2.11}$$

The vector $\mathbf{j}$ is the electric current density which can be expressed through the magnetic field $\mathbf{B}$. Start with Ohm's law,

$$\mathbf{j}=\sigma\mathbf{E}', \tag{2.12}$$

where σ is electric conductivity (the physical quantity inversed to the resistivity) and $\mathbf{E}'$ is the electric field experienced by the fluid element in its rest frame. When the plasma is moving with respect to the external magnetic field at the velocity $\mathbf{V}$, applying the Lorentz transformation we obtain

$$\mathbf{E}' = \mathbf{E} + \mathbf{V} \times \mathbf{B}. \tag{2.13}$$

Now, Eq. 2.12 can be re-written as

$$\frac{1}{\sigma}\mathbf{j} = \mathbf{E} + \mathbf{V} \times \mathbf{B}. \tag{2.14}$$

In the case of perfect conductivity, $\sigma \to \infty$, we have

$$\mathbf{E} = -\mathbf{V} \times \mathbf{B}. \tag{2.15}$$

Calculating the curl of the electric field $\mathbf{E}$ and using one of Maxwell's equation,

$$\nabla \times \mathbf{E} = -\frac{\partial \mathbf{B}}{\partial t}, \tag{2.16}$$

we can exclude the electric field and obtain the 4-th MHD equation

$$\frac{\partial \mathbf{B}}{\partial t} = \nabla \times (\mathbf{V} \times \mathbf{B}). \tag{2.17}$$

To close the set of MHD equations, we have to express the current density $\mathbf{j}$ through the magnetic field $\mathbf{B}$. Consider the other Maxwell's equation,

$$\nabla \times \mathbf{B} = \mu_0 \mathbf{j} + \frac{1}{c^2}\frac{\partial \mathbf{E}}{\partial t}. \tag{2.18}$$

From Ohm's law, we had $\mathbf{E} = \mathbf{V} \times \mathbf{B}$. Consequently, we can estimate the electric field as $E \sim V_0 B$, where V_0 is a characteristic speed of the process. Neglecting $\frac{\partial \mathbf{E}}{\partial t}$ terms in Eq. 2.18:

$$\nabla \times \mathbf{B} = \mu_0 \mathbf{j}, \tag{2.19}$$

or

$$\mathbf{j} = \frac{1}{\mu_0} (\nabla \times \mathbf{B}) . \tag{2.20}$$

In addition, the magnetic field $\mathbf{B}$ must satisfy the condition $\nabla.\mathbf{B} = 0$. Thus, the closed set of MHD equations is

$$\rho \left(\frac{\partial \mathbf{V}}{\partial t} + (\mathbf{V}\nabla)\, \mathbf{V} \right) = -\nabla P + \frac{1}{\mu_0} (\nabla \times \mathbf{B}) \times \mathbf{B}, \tag{2.21}$$

and

$$\frac{\partial \mathbf{B}}{\partial t} = \nabla \times (\mathbf{V} \times \mathbf{B}) , \tag{2.22}$$

is the equation for magnetic induction."

2.2.3 Energy Equation (Conservation Law of Energy)

The law of conservation of energy based on the first law of thermodynamics is stated as follows:

"The conservation law for the energy equation physically describes that the total energy of the system remains constant. It is derived from the first law of thermodynamics. In mathematical form, it can be expressed as follows

$$\rho \left[\frac{\partial \mathbf{U}}{\partial t} + \mathbf{V}.\nabla \mathbf{U} \right] = [\tau_1 : \nabla \mathbf{V} + p \nabla.\mathbf{V}] + \nabla (k \nabla T) \pm \hat{H}r, \tag{2.23}$$

where $\mathbf{U}$ is the internal energy per unit mass, and $\hat{H}r$ is the heat of reaction. By invoking the definition of the internal energy, $d\mathbf{U} \equiv C_v dT$, Eq. (2.23) becomes,

$$\rho C_v \left[\frac{\partial T}{\partial t} + \mathbf{V}.\nabla T \right] = [\tau_1 : \nabla \mathbf{V} + p \nabla.\mathbf{V}] + \nabla (k \nabla T) \pm \hat{H}r. \tag{2.24}$$

For heat conduction in solids, i.e., when $\mathbf{V} = 0$, $\nabla.\mathbf{V} = 0$, and $C_v = C$, the resulting equation is

$$\rho C \frac{\partial T}{\partial t} = \nabla (k \nabla T) \pm \hat{H}r. \tag{2.25}$$

For phase change, the latent heat rate per unit volume must be added as a source term to the energy equation."

2.2.4 Equation of Mass Transport

"It describes that the total concentration of the system under observation remains constant. It is derived from Fick's second law which stated as the rate of accumulation (or depletion) of concentration within the volume as proportional to the local curvature of the concentration gradient. Mathematically, in the absence of chemical reaction, we have

$$\frac{dC}{dt} = -\nabla.\mathbf{j}. \tag{2.26}$$

In which the accumulation is $\frac{dC}{dt}$ is proportional to the diffusivity D and the second derivative (or curvature) of the concentration. From Fick's first law we have

$$\mathbf{j} = -\mathbf{D}\nabla C. \tag{2.27}$$

Thus equation of mass transport becomes

$$\frac{dC}{dt} = \mathbf{D}\nabla^2 C, \tag{2.28}$$

where C represents the concentration of specie, $\mathbf{D}$ the mass diffusivity and $\mathbf{j}$ the mass flux".

2.2.5 Boundary Layer Equation of Upper-Convected Maxwell Fluid [92]

It is a non-Newtonian fluid model and the simplest subclass of the rate type fluids which elaborates the features of the linear viscoelastic fluids having the relaxation time. This model is the generalization of Maxwell fluid model. The inclusion of Oldroyd time dependent derivative deals for the large deformation in the fluid flow. An example is the polymer solutions of low molecular weight. The extra stress tensor $\mathbf{S}$ for a Maxwell fluid is

$$\left(1 + \lambda_1 \frac{D}{Dt}\right)\mathbf{S} = \mu A_1, \tag{2.29}$$

in which λ_1 is the relaxation time, $\frac{D}{Dt}$ the covariant differentiation, μ denotes the kinematic viscosity and A_1 the first Rivlin-Erickson tensor. The first Rivlin-Erickson tensor can be defined as

$$A_1 \;=\; (grad\ \mathbf{V}) \;+\; (grad\ \mathbf{V})', \tag{2.30}$$

where $'$ (prime) denotes the matrix transpose. Here

$$A_1 = \begin{bmatrix} 2\frac{\partial u}{\partial x} & \frac{\partial u}{\partial y} + \frac{\partial v}{\partial x} & \frac{\partial u}{\partial z} + \frac{\partial w}{\partial x} \\ \frac{\partial u}{\partial y} + \frac{\partial v}{\partial x} & 2\frac{\partial v}{\partial y} & \frac{\partial v}{\partial z} + \frac{\partial w}{\partial y} \\ \frac{\partial u}{\partial z} + \frac{\partial w}{\partial x} & \frac{\partial v}{\partial z} + \frac{\partial w}{\partial y} & 2\frac{\partial w}{\partial z} \end{bmatrix}. \tag{2.31}$$

The covariant derivative for a tensor $\mathbf{S}$ of rank two, a vector a_1 and a scalar b_1, is expressed by

$$\frac{D\mathbf{S}}{Dt} = \frac{\partial \mathbf{S}}{\partial t} + (\mathbf{V}.\nabla)\,\mathbf{S} - \mathbf{S}\,(grad\ \mathbf{V})' - (grad\ \mathbf{V})\,\mathbf{S}, \tag{2.32}$$

$$\frac{Da_1}{Dt} = \frac{\partial a_1}{\partial t} + (\mathbf{V}.\nabla)\,a_1 - (grad\ \mathbf{V})\,a_1, \tag{2.33}$$

$$\frac{Db_1}{Dt} = \frac{\partial b_1}{\partial t} + (\mathbf{V}.\nabla)\,b_1. \tag{2.34}$$

Multiplying equation of motion for the Maxwell fluid by $\left(1 + \lambda_1 \frac{D}{Dt}\right)$, we have

$$\rho\left(1 \;+\; \lambda_1 \frac{D}{Dt}\right)\frac{D\mathbf{V}}{Dt} \;=\; -\left(1 \;+\; \lambda_1 \frac{D}{Dt}\right)\nabla p \;+\; \left(1 \;+\; \lambda_1 \frac{D}{Dt}\right)(\nabla.\mathbf{S}). \tag{2.35}$$

Applying

$$\frac{D}{Dt}(\nabla.) = \nabla.\frac{D}{Dt}, \tag{2.36}$$

invoking the value of $\mathbf{S}$ in Eq. (2.35) and using Eq. (2.36) we have

$$\rho\left(1 \;+\; \lambda_1 \frac{D}{Dt}\right)\frac{D\mathbf{V}}{Dt} = -\left(1 \;+\; \lambda_1 \frac{D}{Dt}\right)\nabla p \;+\; \nabla.\left(1 \;+\; \lambda_1 \frac{D}{Dt}\right)\mathbf{S}, \tag{2.37}$$

using (2.29) and ignoring the pressure gradient, the above equation can be written as

$$\rho\left(1 \;+\; \lambda_1 \frac{D}{Dt}\right)\frac{D\mathbf{V}}{Dt} \;=\; \mu\nabla.A_1, \tag{2.38}$$

Component form of the two-dimensional steady flow of Maxwell fluid can be represented by the following expression:

$$u\frac{\partial u}{\partial x} + v\frac{\partial u}{\partial y} + \lambda_1\left(u^2\frac{\partial^2 u}{\partial x^2} + v^2\frac{\partial^2 u}{\partial y^2} + 2uv\frac{\partial^2 u}{\partial x \partial y}\right) = \nu\left(\frac{\partial^2 u}{\partial x^2} + \frac{\partial^2 u}{\partial y^2}\right) \tag{2.39}$$

$$u\frac{\partial v}{\partial x} + v\frac{\partial v}{\partial y} + \lambda_1\left(u^2\frac{\partial^2 v}{\partial x^2} + v^2\frac{\partial^2 v}{\partial y^2} + 2uv\frac{\partial^2 v}{\partial x \partial y}\right) = \nu\left(\frac{\partial^2 v}{\partial x^2} + \frac{\partial^2 v}{\partial y^2}\right) \tag{2.40}$$

By employing the boundary layer assumptions, the equation of linear momentum for the three-dimensional flow of Upper-Convected Maxwell fluid is as follows:

$$u\frac{\partial u}{\partial x} + v\frac{\partial u}{\partial y} + w\frac{\partial u}{\partial z} + \lambda_1\begin{pmatrix} u^2\frac{\partial^2 u}{\partial x^2} + v^2\frac{\partial^2 u}{\partial y^2} \\ + 2uv\frac{\partial^2 u}{\partial x \partial y} + w^2\frac{\partial^2 u}{\partial z^2} \\ + 2vw\frac{\partial^2 u}{\partial y \partial z} + 2wx\frac{\partial^2 u}{\partial z \partial x} \end{pmatrix} = \nu\left(\frac{\partial^2 u}{\partial x^2} + \frac{\partial^2 u}{\partial y^2} + \frac{\partial^2 u}{\partial z^2}\right) \tag{2.41}$$

$$u\frac{\partial v}{\partial x} + v\frac{\partial v}{\partial y} + w\frac{\partial v}{\partial z} + \lambda_1\begin{pmatrix} u^2\frac{\partial^2 v}{\partial x^2} + v^2\frac{\partial^2 v}{\partial y^2} \\ + 2uv\frac{\partial^2 v}{\partial x \partial y} + w^2\frac{\partial^2 v}{\partial z^2} + \\ 2vw\frac{\partial^2 v}{\partial y \partial z} + 2wx\frac{\partial^2 v}{\partial z \partial x} \end{pmatrix} = \nu\left(\frac{\partial^2 v}{\partial x^2} + \frac{\partial^2 v}{\partial y^2} + \frac{\partial^2 v}{\partial z^2}\right) \tag{2.42}$$

2.3 Solution Methodology

We have used two different techniques to solve the non-linear ordinary differential equations. The shooting method and a MATLAB built-in function bvp4c.

2.3.1 Shooting Method [93]

"The problems formulated in this thesis are solved numerically by the shooting method with the integration scheme of Runge-Kutta method of order four. To solve the transformed non-linear ordinary differential equations with the help of the shooting method, first convert the higher order ODEs to the system of first order non-linear differential equations. To solve the system of the first order equations, their respective initial conditions are needed. In case of the boundary

value problems, their must be some missing initial conditions. In the shooting method, the missing initial conditions are assumed, and the differential equations are then integrated numerically as an initial value problem. The accuracy of the assumed missing initial condition is then checked by comparing the calculated values of the dependent variables at the terminal point with their given value there, for only those dependent variables whose values at the terminal point are known. If the difference exists, another value of the missing initial condition must be chosen systematically. This process is continued until the agreement between the calculated value and the given condition at the terminal point is within a specified degree of accuracy. Newton's method is used for the purpose of the updation of the initial guess. Due to the sensitivity of the initial guesses in the Newton's method, some time this method diverges due to the singular Jacobian matrix. There is no general hard and fast rule for the successful choice of initial guesses. All the considered problem in this thesis are easily solved and no such type of hurdle is faced because of the initial guesses. The shooting method, has been explained with the help of considering a general second order differential boundary value problem,

$$y''(x) = f\left(x, y, y'(x)\right), \tag{2.43}$$

subject to the boundary conditions

$$y\left(0\right) = 0, \quad y\left(L\right) = A. \tag{2.44}$$

By denoting y by y_1 and y_1' by y_2, Eq. (2.43) can be written as the following system of first order equations.

$$\left.\begin{aligned} y_1' &= y_2, & y_1(0) &= 0, \\ y_2' &= f\left(x, y_1, y_2\right), & y_1(L) &= A. \end{aligned}\right\} \tag{2.45}$$

Denote the missing initial condition $y_2(0)$ by s, to have

$$\left.\begin{aligned} y_1' &= y_2, & y_1(0) &= 0, \\ y_2' &= f(x, y_1, y_2), & y_2(0) &= s. \end{aligned}\right\} \tag{2.46}$$

Now the problem is to find s such that the solution of the IVP (2.46) satisfies the boundary condition $y(L) = A$. In other words, if the solutions of the initial value problem (2.46) are denoted by $y_1(x, s)$ and $y_2(x, s)$, one should search for that value of s which is an approximate root of the equation.

$$y_1(L, s) - A = \phi(s) = 0. \tag{2.47}$$

To find an approximate root of Eq. (2.47) by the Newton's method, the iteration formula is given by

$$s_{n+1} = s_n - \frac{\phi(s_n)}{\phi(s_n)/ds}, \tag{2.48}$$

or

$$s_{n+1} = s_n - \frac{y_1(L, s_n) - A}{dy_1(L, s_n)/ds}. \tag{2.49}$$

To find the derivative of y_1 with respect of s, differentiate (2.46) with respect to s. For simplification, use the following notations,

$$\frac{dy_1}{ds} = y_3, \quad \frac{dy_2}{ds} = y_4. \tag{2.50}$$

This process results in the following IVP.

$$\left.\begin{aligned} y_3' &= y_4, & y_3(0) &= 0, \\ y_4' &= \frac{\partial f}{\partial y_1} y_3 + \frac{\partial f}{\partial y_2} y_4, & y_4(0) &= 1. \end{aligned}\right\} \tag{2.51}$$

Now, solving the IVP (2.51), the value of y_3 at L can be computed. This value is actually the derivative of y_1 with respect to s computed at L. Setting the value of $y_3(L, s)$ in Eq. (2.49), the modified value of s can be achieved. This new value of s is used to solve the Eq. (2.46) and the process is repeated until the value of s is within a described degree of accuracy." The case of more than one missing initial

conditions, has been explained with the help of the following example.

Example

Consider the following fourth order boundary value problem.

$$y'''' - \left(1 - x^2\right) y''^2 + 5y^2 = 0, \tag{2.52}$$

with boundary condition

$$y\left(0\right) = 1, \quad y'\left(0\right) = 0, \quad y''\left(1\right) = -2, \quad y'''\left(1\right) = -3. \tag{2.53}$$

To convert Eq. (2.52) into a system of first order equations, the following notations has been introduced.

$$y = y_1, \quad y' = y_2, \quad y'' = y_3, \quad y''' = y_4. \tag{2.54}$$

The given BVP, is then converted to the following form.

$$\left.\begin{aligned} y_1' &= y_2, & y_1\left(0\right) &= 1, \\ y_2' &= y_3, & y_2\left(0\right) &= 0, \\ y_3' &= y_4, & y_3\left(1\right) &= -2, \\ y_4' &= \left(1 - x^2\right) y_3^2 - 5y_1^2, & y_4\left(1\right) &= -3. \end{aligned}\right\} \tag{2.55}$$

Denote the missing initial conditions $y_3(0)$ and $y_4(0)$ by s and t respectively, to have the following IVP

$$\left.\begin{aligned} y_1' &= y_2, & y_1\left(0\right) &= 1, \\ y_2' &= y_3, & y_2\left(0\right) &= 0, \\ y_3' &= y_4, & y_3\left(0\right) &= s, \\ y_4' &= \left(1 - x^2\right) y_3^2 - 5y_1^2, & y_4\left(0\right) &= t. \end{aligned}\right\} \tag{2.56}$$

Now, solving the above IVP by using the RK-4 method over the interval [0,1]. The solution obtained by the RK-4 is then analyzed for $y''(1)$ and $y'''(1)$. If these solutions meet the boundary condition given in Eq. (2.53), then the problem is

solved. However, usually this does not happen in the first go. So we have to refine the initial guesses iteratively. For this purpose we use the Newton's method to solve the following system of non-linear algebraic equations,

$$\left.\begin{aligned} y_3(x,s,t)+2=0,\\ y_4(x,s,t)+3=0, \end{aligned}\right\} \tag{2.57}$$

The iterative scheme of Newton's method for the system of non-linear equations (2.56), is given by

$$\begin{bmatrix} s_{n+1} \\ t_{n+1} \end{bmatrix} = \begin{bmatrix} s_n \\ t_n \end{bmatrix} - \begin{bmatrix} \frac{\partial}{\partial s} y_3(1,s_n,t_n) & \frac{\partial}{\partial t} y_3(1,s_n,t_n) \\ \frac{\partial}{\partial s} y_4(1,s_n,t_n) & \frac{\partial}{\partial t} y_4(1,s_n,t_n) \end{bmatrix}^{-1} \begin{bmatrix} y_3(1,s_n,t_n)+2 \\ y_4(1,s_n,t_n)+3 \end{bmatrix} \tag{2.58}$$

For simplification, use the following notations,

$$\left.\begin{aligned} \frac{\partial y_1}{\partial s}\equiv y_5, \quad \frac{\partial y_2}{\partial s}\equiv y_6, \quad \frac{\partial y_3}{\partial s}\equiv y_7, \quad \frac{\partial y_4}{\partial s}\equiv y_8,\\ \frac{\partial y_1}{\partial t}\equiv y_9, \quad \frac{\partial y_2}{\partial t}\equiv y_{10}, \quad \frac{\partial y_3}{\partial t}\equiv y_{11}, \quad \frac{\partial y_4}{\partial t}\equiv y_{12}, \end{aligned}\right\} \tag{2.59}$$

To find the Jacobian matrix, differentiating the system of Eqs. (2.56) first with respect to s and then with respect to t and using the new notations, we get

$$\left.\begin{aligned} y_5' &= y_6, & y_5(0) &= 0,\\ y_6' &= y_7, & y_6(0) &= 0,\\ y_7' &= y_8, & y_7(0) &= 1,\\ y_8' &= 2\left(1-x^2\right)y_3y_7 - 10y_1y_5, & y_8(0) &= 0,\\ y_9' &= y_{10}, & y_9(0) &= 0,\\ y_{10}' &= y_{11}, & y_{10}(0) &= 0,\\ y_{11}' &= y_{12}, & y_{11}(0) &= 0,\\ y_{12}' &= 2\left(1-x^{12}\right)y_3y_{11} - 10y_1y_9, & y_{12}(0) &= 1. \end{aligned}\right\} \tag{2.60}$$

Solve the above system of equations (2.60) by the RK-4 method and put the computed values of y_7, y_{11}, y_8 and y_{12} in (2.58). This gives new modified initial guesses. This procedure is repeated until we achieved the solutions with required

accuracy. The result obtained by the shooting method are shown in Figure. 2.3

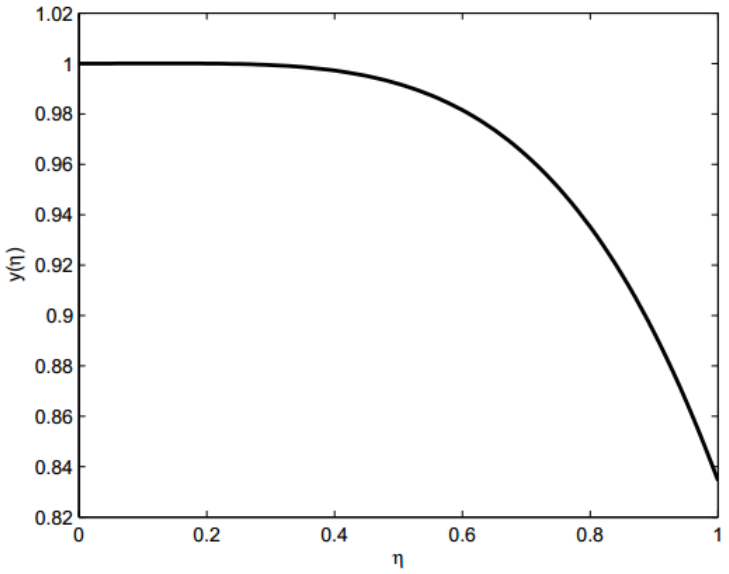

FIGURE 2.3: Solution of example

2.3.2 Matlab Solver bvp4c

"It is a MATLAB built-in function [94], which can be used to solve the system of non-linear boundary value problems. It is a finite difference code that implements the three-stage Lobatto IIIa formula. This is a collocation formula and the collocation polynomial provides a C^1-continuous solution that is fourth-order accurate uniformly in [a,b]. Mesh selection and error control are based on the residual of the continuous solution. It has the following Matlab syntax:

$$sol = bvp4c(@odefun, @bcfun, solinit, options).$$

Further details can be found in [95]". Many researchers use this package to solve the BVPs, see for example [32, 96, 97].

Chapter 3

Boundary Layer Magneto-Micropolar Nanofluid Flow with Hall and Ion-slip Effects using Variable Thermal Diffusivity

3.1 Introduction

The aim of this Chapter is to examine the effect of nanofluid on heat and mass transfer in the presence of Hall current and ion-slip effects on an electrically conducting magneto-micropolar fluid flowing on a linearly stretched sheet. Generally, two types of models are used for the simulation of the convective heat transfer of the nanofluids; the single phase and the double phase models. In the single phase modeling, a combination of the base fluid and the nanoparticles is considered as a homogenous mixture and their properties are studied collectively whereas in the two phase model, the behaviour and properties of the nanoparticles are considered separately from those of the base fluid. In the present Chapter, a single

phase model has been considered. A variable thermal diffusivity, is considered in the formation of the energy equation. The dynamics of the flow is described by the conservation laws of mass, momentum, energy and concentration. The governing set of non-linear PDEs is reduced into a system of ODEs and then solved numerically through the shooting technique. The quantities of physical significance such as velocity, concentration, temperature, Nusselt number, Sherwood number and skin-friction coefficient for various values of the emerging parameters, are computed and elaborated.

3.2 Problem Formulation

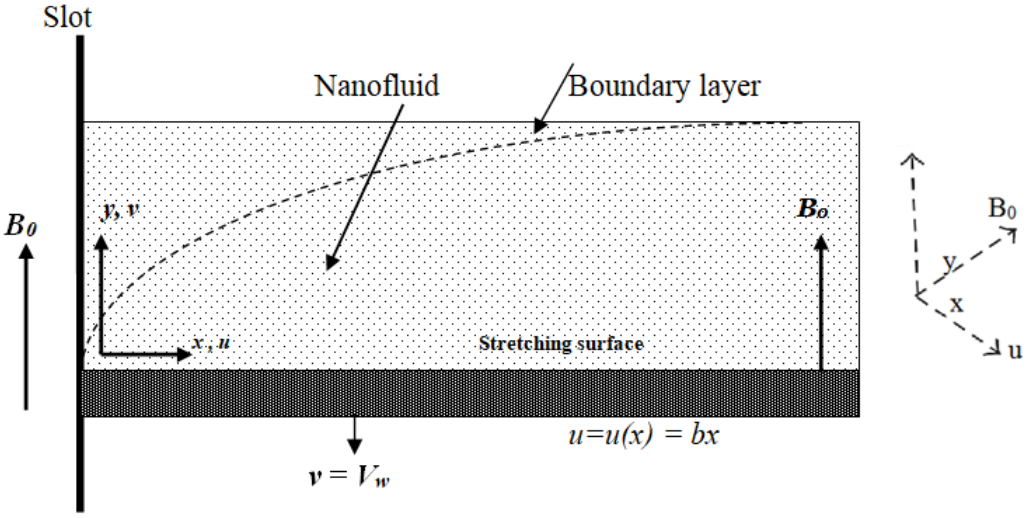

FIGURE 3.1: Geometry of the Problem.

A steady, viscous and incompressible, electrically conducting magneto-micropolar nanofluid flow over a horizontal porous plate with no slip effect stretching linearly with velocity u_x along the $x-$axis through a porous medium with the additional effects of viscous dissipation has been considered. A strong constant magnetic field of intensity B_0 in the direction along $y-$axis is also assumed. Due to this strong magnetic field strength, the electrically conducting fluid has the Hall and ion-slip effects which gives rise a force on the fluid in the z-direction and hence the flow becomes three dimensional. Further, the effects of Joule heating and thermal radiation are ignored.

Elgazery [98], generalized the Ohm's law for the Hall current in the form

$$\mathbf{J} = \frac{\sigma}{1 + (\omega/\nu_e)^2}\left(\mathbf{E} + (\mathbf{V}\times\mathbf{B}) - \frac{1}{en_e}(\mathbf{J}\times\mathbf{B})\right), \tag{3.1}$$

where ω the electron cyclotron and ν_e is the electron-atom collision frequency. When the ratio ω/ν_e is very large then the phenomena is called "ion-slip". By considering all the fluid properties constant except thermal diffusivity and applying Boussinesq approximations, the governing equations for the considered problem become [73]

$$\frac{\partial u}{\partial x} + \frac{\partial v}{\partial y} = 0, \tag{3.2}$$

$$u\frac{\partial u}{\partial x} + v\frac{\partial u}{\partial y} = \nu\frac{\partial^2 u}{\partial y^2} + \frac{K_0}{\rho}\frac{\partial N}{\partial y} - \frac{\sigma B_0^2}{\rho(\alpha_e^2 + \beta_e^2)}(\alpha_e u + \beta_e w) - \frac{\mu}{\rho k^*}u, \tag{3.3}$$

$$u\frac{\partial w}{\partial x} + v\frac{\partial w}{\partial y} = \nu\frac{\partial^2 w}{\partial y^2} + \frac{\sigma B_0^2}{\rho(\alpha_e^2 + \beta_e^2)}(\beta_e u - \alpha_e w) - \frac{\mu}{\rho k^*}w, \tag{3.4}$$

$$\frac{G_1}{K_0}\frac{\partial^2 N}{\partial y^2} - 2N - \frac{\partial u}{\partial y} = 0, \tag{3.5}$$

$$u\frac{\partial T}{\partial x} + v\frac{\partial T}{\partial y} = \frac{\partial}{\partial y}\left(\alpha\frac{\partial T}{\partial y}\right) + \frac{\mu}{\rho c_p}\left[\left(\frac{\partial u}{\partial y}\right)^2 + \left(\frac{\partial w}{\partial y}\right)^2\right] + \frac{1}{\rho c_p}\frac{\sigma B_0^2}{(\alpha_e^2 + \beta_e^2)}\left(u^2 + w^2\right) + \tau\left[D_B\left(\frac{\partial T}{\partial y}\frac{\partial C}{\partial y}\right) + \frac{D_T}{T_\infty}\left(\frac{\partial T}{\partial y}\right)^2\right], \tag{3.6}$$

$$u\frac{\partial C}{\partial x} + v\frac{\partial C}{\partial y} = D_B\frac{\partial^2 C}{\partial y^2} + \frac{D_T}{T_\infty}\frac{\partial^2 T}{\partial y^2}, \tag{3.7}$$

where ν the kinematic viscosity, u, v, and w are the velocity components along x, y and z-axis respectively, ρ the density of the fluid, K_0 the vortex velocity, N the micro-rotation component, σ the electric conductivity, β_e the Hall current parameter, μ the dynamic viscosity, B_0 the magnetic field strength, k^* the permeability of porous medium, G_1 the spin gradient viscosity, α the thermal diffusivity, C and T are the fluid concentration and temperature respectively, c_p the specific heat at constant pressure, τ the ratio of effective heat capacity of nanoparticles to the effective heat capacity of base fluid, D_B the Brownian diffusion coefficient, D_T the

thermophoresis coefficient, C_∞ and T_∞ are the ambient fluid concentration and temperature respectively. The last terms of Eq. (3.3) and (3.4) appears due to the porosity of the medium, $\frac{\partial N}{\partial y}$ in Eq. (3.3) represents the micropolar effects of particles. The corresponding boundary conditions for the governing PDEs are as follows.

$$\left.\begin{array}{l} u = u_x = bx, \quad v = -V_w, \quad N = 0, \quad w = 0, \\ T = T_w, \quad C = C_w, \text{ at } y = 0, \\ u \to 0, \quad w \to 0, \quad N \to 0, \quad T \to T_\infty, \quad C \to C_\infty. \text{ as } y \to \infty. \end{array}\right\} \tag{3.8}$$

Here, V_w is the velocity of suction (> 0) or injection (< 0), $\alpha_e = 1 + \beta_i\beta_e$, where β_i is ion-slip parameter, b is a dimensional constant with unit $(time)^{-1}$.
The dependence of thermal diffusivity on temperature is given by

$$\alpha = \alpha_0 \left(1 + \beta_2\theta\right). \tag{3.9}$$

Here, α_0 is thermal diffusivity at wall temperature. The similarity transformations which are used to convert the partial differential equations into ordinary differential equations are frequently used in many research articles [99, 100]

$$\left.\begin{array}{l} \eta = \sqrt{\frac{b}{\nu}}y, \quad u = bxf'(\eta), \quad v = -\sqrt{b\nu}f(\eta), \quad w = \sqrt{b\nu}g(\eta), \\ N = \sqrt{\frac{b^3}{\nu}}xh(\eta), \quad \theta(\eta) = \frac{T - T_\infty}{T_w - T_\infty}, \quad \phi(\eta) = \frac{C - C_\infty}{C_w - C_\infty}. \end{array}\right\} \tag{3.10}$$

Using the above mentioned similarity transformations, Eqs. (3.2) and (3.3) are derived in detail. For this purpose, we first convert the following derivatives involved in Eqs. (3.2) - (3.3) into the dimensionless form:

$$\begin{aligned} \frac{\partial u}{\partial x} &= \frac{\partial}{\partial x}\left(bxf'(\eta)\right), \\ \frac{\partial u}{\partial x} &= bf'(\eta), \\ \frac{\partial v}{\partial y} &= -\sqrt{b\nu}\frac{\partial}{\partial y}\left(f(\eta)\right) = -\sqrt{b\nu}f'(\eta)\sqrt{\frac{b}{\nu}}, \end{aligned}$$

$$\frac{\partial v}{\partial y} = -bf'(\eta),$$
$$\frac{\partial u}{\partial y} = \frac{\partial}{\partial y}(bxf'(\eta)),$$
$$\frac{\partial u}{\partial y} = bxf''(\eta)\sqrt{\frac{b}{\nu}},$$
$$\frac{\partial^2 u}{\partial y^2} = bx\sqrt{\frac{b}{\nu}}f'''(\eta)\sqrt{\frac{b}{\nu}} = \frac{b^2x}{\nu}f'''(\eta),$$
$$\frac{\partial N}{\partial y} = \sqrt{\frac{b^3}{\nu}}x\frac{\partial}{\partial y}(h(\eta)) = \sqrt{\frac{b^3}{\nu}}xh'(\eta)\sqrt{\frac{b}{\nu}},$$
$$\frac{\partial N}{\partial y} = \frac{b^2x}{\nu}h'(\eta).$$

By putting the above derivatives into the continuity equation, it is observed to be satisfied identically as follows:

$$\frac{\partial u}{\partial x} + \frac{\partial v}{\partial y} = bf'(\eta) - bf'(\eta) = 0.$$

The momentum equation is converted into the dimensionless form as follows:

$$u\frac{\partial u}{\partial x} + v\frac{\partial u}{\partial y} = \nu\frac{\partial^2 u}{\partial y^2} + \frac{K_o}{\rho}\frac{\partial N}{\partial y} - \frac{\sigma B_o^2}{\rho(\alpha_e^2+\beta_e^2)}(\alpha_e u + \beta_e w) - \frac{\mu}{\rho k^*}u,$$
$$\Rightarrow bxf'(\eta)bf'(\eta) - \sqrt{b\nu}f(\eta)bxf''(\eta)\sqrt{\frac{b}{\nu}} = \nu\frac{b^2x}{\nu}f'''(\eta) + \frac{K_o}{\rho}\frac{b^2x}{\nu}h'(\eta)$$
$$- \frac{\sigma B_o^2}{\rho(\alpha_e^2+\beta_e^2)}\left(\alpha_e bxf'(\eta) + \beta_e\sqrt{b\nu}g(\eta)\right) - \frac{\mu}{\rho k^*}bxf'(\eta),$$
$$\Rightarrow b^2xf'^2(\eta) - b^2xf(\eta)f''(\eta) = b^2xf'''(\eta) + b^2x\frac{K_o}{\nu\rho}h'(\eta)$$
$$- \frac{\sigma B_o^2 bx}{\rho(\alpha_e^2+\beta_e^2)}\left(\alpha_e f'(\eta) + \beta_e\sqrt{\frac{\nu}{bx^2}}g(\eta)\right) - \frac{\mu}{\rho k^*}bxf'(\eta),$$
$$\Rightarrow f'^2(\eta) - f(\eta)f''(\eta) = f'''(\eta) + \frac{K_o}{\nu\rho}h'(\eta) -$$
$$\frac{\sigma B_o^2}{\rho b(\alpha_e^2+\beta_e^2)}\left(\alpha_e f'(\eta) + \beta_e\sqrt{\frac{\nu}{bx^2}}g(\eta)\right) - \frac{\mu}{b\rho k^*}f'(\eta),$$
$$\Rightarrow f'^2(\eta) - f(\eta)f''(\eta) = f'''(\eta) + N_1 h'(\eta)$$
$$- \frac{M}{(\alpha_e^2+\beta_e^2)}\left(\alpha_e f'(\eta) + \frac{\beta_e}{\sqrt{Re}}g(\eta)\right) - \frac{1}{k_p}f'(\eta),$$

$$\Rightarrow f'''(\eta) - f'^2(\eta) + f(\eta) f''(\eta) + N_1 h'(\eta) - \frac{M}{(\alpha_e^2 + \beta_e^2)} \left(\alpha_e f'(\eta) + \frac{\beta_e}{\sqrt{Re}} g(\eta) \right) - \frac{1}{k_p} f'(\eta) = 0.$$

Other partial differential equations can also be transformed into the ordinary differential equations by the same manner,

$$g'' + f g' + \frac{M}{(\alpha_e^2 + \beta_e^2)} \left(\beta_e \sqrt{Re} f' - \alpha_e g \right) - \frac{1}{k_p} g = 0, \tag{3.11}$$

$$G h'' - 2h - f'' = 0, \tag{3.12}$$

$$\theta'' + \frac{\beta_2}{1 + \beta_2 \theta} \theta'^2 + \frac{Pr Ec}{1 + \beta_2 \theta} \left[f''^2 + \frac{g'^2}{Re} + \frac{M}{(\alpha_e^2 + \beta_e^2)} \left(f'^2 + \frac{g^2}{Re} \right) \right] + \frac{Pr}{1 + \beta_2 \theta} f \theta' + \frac{Pr Nb}{1 + \beta_2 \theta} \left(\theta' \phi' + \frac{Nt}{Nb} \theta'^2 \right) = 0, \tag{3.13}$$

$$\phi'' + \frac{Nt}{Nb} \theta'' + Le Pr f \phi' = 0. \tag{3.14}$$

The transformed boundary conditions are:

$$\left. \begin{array}{l} f(0) = f_w, \quad f'(0) = 1, \quad g(0) = 0, \quad h(0) = 0, \quad \theta(0) = 1, \quad \phi(0) = 1, \\ f'(\eta) \to 0, \quad g(\eta) \to 0, \quad h(\eta) \to 0, \quad \theta(\eta) \to 0, \quad \phi(\eta) \to 0. \text{ as } \eta \to \infty \end{array} \right\}. \tag{3.15}$$

Here, θ, f, h, g and ϕ are dimensionless temperature, stream functions along x & y-axis direction, micro-rotation component, dimensionless concentration of fluid. N_1, Nb, M, Re, Nt, k_p, G, β_2, Ec, Le, and Pr, are coupling constant parameter, Brownian motion parameter, Magnetic parameter, Reynolds number, thermophoresis parameter, permeability parameter, Micro rotation parameter, fluid nature dependent parameter, Eckert number, Lewis number, and Prandtl number respectively and these are defined as;

$$\left. \begin{array}{l} N_1 = \frac{K_0}{\rho \nu}, \quad M = \frac{\sigma B_0^2}{\rho b}, \quad G = \frac{G_1 b}{K_0 \nu}, \quad Pr = \frac{\nu}{\alpha}, \quad f_w = \frac{V_w}{\sqrt{b\nu}}, \\ Ec = \frac{(bx)^2}{c_p (T_w - T_\infty)}, \quad k_p = \frac{k^* b \rho}{\mu}, \quad Re = \frac{b x^2}{\nu}, \quad \gamma = \frac{k\nu}{(bx)^2}, \\ Nb = \frac{\tau D_B}{\nu} (C_w - C_\infty), \quad Nt = \frac{D_T}{T_\infty} \frac{\tau}{\nu} (T_w - T_\infty), \quad Le = \frac{\alpha}{D_B}, \quad \beta_2 = \frac{k_w - k_\infty}{k_w}. \end{array} \right\} \tag{3.16}$$

The quantities concerning the engineering purpose, such as the skin-friction coefficient in $x-$ and $z-$ directions, local Sherwood number and Nusselt number, are illustrated as

$$\left.\begin{aligned} Cf_x &= \frac{\tau_{wx}}{\rho b x\sqrt{b\nu}}, \qquad Cf_z = \frac{\tau_{wz}}{\rho b x\sqrt{b\nu}}, \\ Nu_x &= \frac{-\left(\frac{\partial T}{\partial y}\right)_{y=0}}{(T_w - T_\infty)\sqrt{\frac{b}{\nu}}}, \qquad Sh_x = \frac{-\left(\frac{\partial C}{\partial y}\right)_{y=0}}{(C_w - C_\infty)\sqrt{\frac{b}{\nu}}}. \end{aligned}\right\} \tag{3.17}$$

Here, the local wall shear stresses are defined as

$$\tau_{wz} = \left[(\mu + K_0)\left(\frac{\partial u}{\partial y}\right) + K_0 N\right]_{y=0}, \quad \tau_{wz} = \left[(\mu + K_0)\left(\frac{\partial w}{\partial y}\right)\right]_{y=0}. \tag{3.18}$$

The local Nusselt number, skin friction and Sherwood number, in the dimensionless form are:

$$\left.\begin{aligned} &Cf_x = (1 + N_1)\, f''(0)\,, \; Cf_z = (1 + N_1)\, g'(0)\,, \\ &Nu_x = -\theta'(0)\,, \; Sh_x = -\phi'(0)\,. \end{aligned}\right\} \tag{3.19}$$

3.3 Solution Methodology

The resulting system of non-linear ODEs (**??**-3.14) subject to the conditions (3.15) has been explored numerically through shooting method [93], which is used frequently by many researchers to obtain the solution of such type of problems [101–105] for numerous values of different parameters. To apply the shooting method, the system of non-linear ODEs (**??**-3.14) is converted to the following system of first order ODEs:

$$\left.\begin{aligned} y_1' &= y_2, & y_1(0) &= f_w \\ y_2' &= y_3, & y_2(0) &= 1 \\ y_3' &= y_2^2 - y_1 y_3 - N_1 y_7 + \frac{M}{\alpha_e^2 + \beta_e^2}\left(\alpha_e y_2 + \frac{\beta_e}{\sqrt{Re}} y_4\right) + \frac{1}{k_p} y_2, & y_3(0) &= \varrho_1 \\ y_4' &= y_5, & y_4(0) &= 0 \end{aligned}\right\}$$

$$\left.\begin{aligned}
y_5' &= y_1 y_5 - \frac{M}{\alpha_e^2+\beta_e^2}\left(\beta_e\sqrt{Re}y_2 - \alpha_e y_4\right) + \frac{1}{k_p}y_4, & y_5(0) &= \varrho_2\\
y_6' &= y_7, & y_6(0) &= 0\\
y_7' &= \frac{1}{G}\left(2y_6 + y_3\right), & y_7(0) &= \varrho_3\\
y_8' &= y_9, & y_8(0) &= 1\\
y_9' &= \frac{-1}{\beta y_8 + 1}\left[\begin{array}{c}\beta y_9 + PrEc\left(y_3^2 + \frac{1}{Re}y_5^2\right) + \\ \frac{PrEcM}{\alpha_e^2+\beta_e^2}\left(y_2^2 + \frac{1}{Re}y_4^2\right) + Pry_1y_9\end{array}\right] & y_9(0) &= \varrho_4\\
&\quad + \frac{PrNb}{1+\beta_2 y_8}\left(y_8 y_{11} + \frac{Nt}{Nb}y_9^2\right),\\
y_{10}' &= y_{11}, & y_{10}(0) &= 1\\
y_{11}' &= -LePry_1y_{11} - \frac{Nt}{Nb}y_9'. & y_{11}(0) &= \varrho_5
\end{aligned}\right\}$$

Here, f is denoted by y_1, g by y_4, h by y_6, θ by y_8 and ϕ by y_{10}. After choosing the five missing conditions, the above system of first order ODEs, is solved by using the Runge Kutta method of order four. To refine the missing initial conditions ϱ_1, ϱ_2, ϱ_3, ϱ_4 and ϱ_5, the Newton's iterative scheme is used which requires another system of 55 first order ODEs along with the initial conditions. This new system is then solved by using the RK-4 method. The solution of this IVP is then used to construct the Jacobian matrix involved in the Newton's iterative method. On the basis of a number of computational experiments, we are considering [0, 8] as the domain of the problem instead of [0, ∞). The stopping criteria for the iterative process is set as

$$\max\left\{\left|y_2(8)-1\right|, \left|y_4(8)\right|, \left|y_6(8)\right|, \left|y_8(8)\right|, \left|y_{10}(8)\right|\right\} < \varepsilon. \tag{3.20}$$

All the computations are made with the tolerance of $\varepsilon = 10^{-6}$, using a verified Matlab code. To strengthen the results obtained by shooting method, we have also solved this system of ODEs with MATLAB built-in function bvp4c.

3.4 Results and Discussions

This section is devoted to the detailed discussions of the numerical solutions of our problem. In Table 3.1, a comparison between the present results obtained by shooting method and bvp4c in the absence of nanofluid, with those given by Motsa and Shateyi in [73] has been presented. Motsa and Shateyi have used successive linearization method together with the Chebyshev collocation method. An excellent agreement is observed between these results, which strengthens our methodology.

To see the effect of physical parameter on skin-friction coefficient, local Nusselt and Sherwood number, numerical results are obtained and are tabulated. From Table 3.2, it is noticed that the skin friction coefficient Cf_x in x- direction increases with the increasing value of magnetic parameter M, coupling parameter N_1 and mass transfer parameter f_w, whereas it is a decreasing function for increasing values of β_e, β_i and k_p. Table 3.2 also shows the variation of parameters for skin-friction coefficient in z-direction. It is observed that Cf_z increases with the increment of magnetic parameter M, material parameter N_1, Hall current parameter β_e and permeability parameter k_p. However by increasing f_w and β_i, the skin friction decreases. In Table 3.3, the effect of magnetic parameter M, mass transfer parameter f_w, Brownian motion parameter Nb, Eckert number Ec, thermophoresis parameter Nt, Lewis number Le, ion-slip parameter β_i, Hall current parameter β_e, variable thermal diffusivity parameter β_2 and Prandtl number Pr on local Sherwood number and Nusselt number are shown. From the table it is analyzed that M, Ec, Le, Nb, Nt and β_2 have decreasing effect on Nusselt number, whereas it increases for the increasing values of f_w, Pr, β_e and β_i. Furthermore, the magnitude of local Sherwood number $-\phi'(0)$ increases when M, f_w, Ec, Le, Pr, Nb and β_2 are increased while it decreases by increasing β_i, β_e and Nt.

To see the insight impact of various emerging parameters on tangential velocity $f'(\eta)$, lateral velocity $g(\eta)$, angular velocity $h(\eta)$, temperature $\theta(\eta)$ and nanoparticle concentration profiles $\phi(\eta)$, Figures 3.2 to 3.23 are plotted. Figure 3.2 and 3.3 depict the effect of Hall parameter β_e on velocity components along $x-$ and

$z-$ directions respectively. Due to the involvement of Hall parameter, the Lorentz force which is a resistive force in nature, enforced by the magnetic field, is reduced, and therefore the effective conductivity decreases. Hence an increase in the Hall parameter will increase the velocity component but this increase in the velocity is very small. Similarly the transverse velocity also increases with the enhancing value of β_e. The temperature distribution $\theta(\eta)$ increases by increasing the variable thermal diffusivity parameter β_2 and this fact is shown in Figure 3.4.

Figure 3.5 gives the effect of permeability parameter k_p on the velocity $f'(\eta)$. As shown in figure, stream velocity $f'(\eta)$ is an increasing function of permeability parameter. This is because of the fact that the holes of the porous medium become large resulting in the reduction in the resistive force. A similar behavior is observed for the lateral and angular velocity profile against the increasing values of permeability parameter k_p as shown in Figures 3.6 and 3.7 respectively. Figures 3.8 and 3.9 show the effect of ion-slip parameter β_i on the horizontal and lateral velocity respectively. In the presence of Hall and ion-slip parameters, the velocity of the flow increases and consequently the boundary layer thickness increases. Hence the horizontal velocity $f'(\eta)$ increases with an increment in β_i. An opposite behavior is observed for the velocity across the plate as it decreases by the enhancement of ion-slip parameter. Figure 3.10 shows the effect of variation in the mass transfer parameter f_w on velocity with suction if $f_w > 0$ and injection if $f_w < 0$. It is recorded that the momentum boundary layer thickness reduces with an increase in f_w and the flow becomes more uniform within the boundary layer. Figure 3.11 shows the reverse relation between the nanoparticle concentration profile $\phi(\eta)$ and the Lewis number Le, as concentration decreases with an increase in the Lewis number. As we know that the Lewis number is inversely proportional to the Brownian diffusion coefficient, so an increase in the Lewis number will reduce the Brownian diffusion which affect the concentration of the fluid.

Figures 3.12 and 3.13 show the typical profiles of tangential and lateral velocities for the magnetic parameter M. By increasing the magnetic parameter M, a drag force known as the Lorentz force also increases which resultantly reduces the velocity of the fluid. As we are considering an electrically conducting micropolar

nanofluid with the strong magnetic field in the direction normal to the flow, so an increase in the magnetic field will increase a force in the $z-$direction, which resultantly increases the lateral velocity $g(\eta)$, as shown in Figure 3.13. To see the variation in temperature against the increasing value of Prandtl number Pr, Figure 3.14 is plotted. It is observed that for increasing value of Prandtl number, there is a thinner temperature boundary layer thickness. Fluids having larger Prandtl number have lower thermal diffusivity and hence the temperature decreases.

The coupling parameter or the material parameter N_1 has decreasing effects on velocity component as the induced velocity $g(\eta)$ decreases with the increasing value of N_1 as shown in Figure 3.15. Influence of Brownian motion parameter Nb on the temperature and concentration profile is studied in Figures 3.16 and 3.17. From these figures, we notice that an enhancement in the values of Nb gives rise to the temperature, while it decreases the nanoparticle concentration profile. The random motion of the particles produced due to the collision of the suspended nanoparticles with the particles of the base fluid is called Brownian motion. Due to the increment in Brownian motion effect, the kinetic energy of the molecules increases and hence the temperature increases. Figures 3.18 and 3.19 illustrate the effect of Nt on temperature and nanoparticles concentration profiles. One can notice that temperature and concentration fields increase with an enhancement in Nt. Thermophoresis parameter plays an important role in temperature flow. Thermophoresis force enhances when Nt is increased. This increment in Nt will tend to accelerate the nanoparticles from hot region to cold region and as a result the boundary layer thickness and temperature increase. From Figure 3.20, it is witnessed that the temperature profile is enhanced with an enhancement in the Eckert number. Increase in Ec increases the friction force between the fluid particles which resultantly stores the heat energy and hence the temperature increases. An enhancement in the micro-rotation parameter will definitely reduce the angular velocity of the fluid away from the wall, however it has an increasing effect near the surface and this phenomenon is depicted in Figure 3.21. In Figure 3.22, the influence of the material parameter N_1 on the stream velocity is portrayed. The tangential velocity is slightly reduced as we move away

from the stretching sheet for $\eta > 1$. The Reynolds number Re on lateral velocity can be seen in Figure 3.23 which shows an increase in the lateral velocity.

				-$(1+N_1)\,f''(0)$			$(1+N_1)\,g'(0)$		
				Motsa	Present		Motsa	Present	
M	β_e	βi	N_1		Shooting	bvp4c		Shooting	bvp4c
1	5	0.4	0.2	1.563229	1.563229	1.563229	0.085991	0.085989	0.085992
2				1.610774	1.610775	1.610774	0.164225	0.164221	0.164226
3				1.659723	1.659725	1.659723	0.235543	0.235536	0.235544
4				1.709225	1.709228	1.709226	0.300893	0.300882	0.300893
5				1.758729	1.758731	1.758729	0.361156	0.361143	0.361156
0.3	0			1.658124	1.658124	1.658124	0	0	0
	2			1.555081	1.555081	1.555081	0.048860	0.048859	0.048860
	4			1.535302	1.535302	1.535301	0.031719	0.031718	0.031719
	6			1.528942	1.528942	1.528941	0.022920	0.022919	0.022920
		0		1.524377	1.524377	1.524377	0.035105	0.035104	0.035105
		0.5		1.532225	1.532225	1.532224	0.024303	0.024303	0.024303
		1		1.532737	1.532737	1.532737	0.014833	0.014833	0.014833
		1.5		1.531103	1.531103	1.531103	0.009320	0.009319	0.009320
			0	1.287381	1.286723	1.286723	0.020386	0.022352	0.022352
			0.2	1.532225	1.531435	1.531435	0.024303	0.026647	0.026648
			0.5	1.891326	1.890341	1.890339	0.030063	0.032963	0.032964
			1.0	2.467535	2.466231	2.466227	0.039313	0.043106	0.043107

TABLE 3.1: Comparison of the present results with those of Motsa and Shateyi [73] for Re=1.0, G=2.0, $k_p = 2.0$, $f_w = 0.1$, $Pr = 0.72$, $Ec = 0.02$, $Le = 0.014$ and $\beta_2 = 0.5$.

						Shooting		bvp4c	
M	f_w	N_1	β_e	β_i	k_p	$(1+N_1)f''(0)$	$(1+N_1)g'(0)$	$(1+N_1)f''(0)$	$(1+N_1)g'(0)$
0.3	0.1	1.0	0.1	0.1	0.2	4.914013	0.008673	4.914014	0.008675
0.5						4.980245	0.014255	4.980249	0.014256
0.7						5.045650	0.019686	5.045653	0.019687
1.0						5.142261	0.027565	5.142264	0.027570
0.3	0.2					5.017363	0.008657	5.017367	0.008660
	0.3					5.122830	0.008638	5.122833	0.008640
	0.4					5.230402	0.008613	5.230405	0.008617
	0.1	0.5				3.756071	0.006500	3.756072	0.006504
		0.8				4.456686	0.007801	4.456690	0.007806
		1.0				4.914012	0.008672	4.914014	0.008675
		1.0	0.2			4.912004	0.017002	4.912008	0.017006
			0.3			4.908831	0.024690	4.908836	0.024692
			0.4			4.904715	0.031510	4.904722	0.031511
			0.1	3.0		4.906403	0.007410	4.906409	0.007412
				4.0		4.899860	0.006403	4.899865	0.006405
				5.0		4.894167	0.005586	4.894174	0.005590
				0.1	0.1	6.636182	0.006348	6.636183	0.006349
					0.2	4.914012	0.008673	4.914014	0.008675
					0.3	4.191970	0.010273	4.191973	0.010276

TABLE 3.2: Numerical values of Cf_x, Cf_z, when $Re = 1.0$, $G = 0.8$, $Le = 2.0$, $Ec = 0.02$, $Pr = 0.72$, $Nb = 0.3$, $Nt = 0.7$, $\beta_2 = 0.8$.

										Shooting		bvp4c	
M	f_w	Ec	Le	Pr	Nb	Nt	β_e	β_i	β_2	$-\theta'(0)$	$-\phi'(0)$	$-\theta'(0)$	$-\phi'(0)$
0.3	0.1	0.02	2.0	0.72	0.3	0.7	0.1	2.0	0.8	0.151872	0.462619	0.151872	0.462620
0.5										0.150651	0.462813	0.150653	0.462815
0.7										0.149471	0.463007	0.149472	0.463009
1.0										0.147762	0.463295	0.147765	0.463297
	0.2									0.174790	0.497349	0.174793	0.497351
	0.3									0.199190	0.533777	0.199192	0.533779
	0.4									0.224815	0.573860	0.224820	0.573862
		0.05								0.136794	0.496608	0.136799	0.496611
		0.1								0.111673	0.553274	0.111676	0.553276
		0.2								0.061412	0.666653	0.061414	0.666655
			1.0							0.154774	0.224936	0.154777	0.224938
			1.5							0.153114	0.341616	0.153121	0.341618
			2.0							0.151868	0.462617	0.151872	0.462620
				1.0						0.173673	0.563014	0.173677	0.563017
				1.5						0.205772	0.773660	0.205775	0.773662
				2.0						0.225211	1.024993	0.225215	1.024995
					0.5					0.141812	0.528838	0.141816	0.528841
					0.7					0.132350	0.556662	0.132353	0.556664
					0.9					0.123450	0.571710	0.123451	0.571711
						0.6				0.155107	0.471947	0.155111	0.471949
						0.8				0.148688	0.456202	0.148692	0.456204
						1.0				0.142498	0.451987	0.142501	0.451989
							0.2			0.152195	0.462487	0.152197	0.462489
							0.3			0.152432	0.462407	0.152434	0.462411
							0.4			0.152611	0.462360	0.152613	0.462362
								3.0		0.152032	0.462546	0.152036	0.462547
								4.0		0.152177	0.462490	0.152179	0.462491
								5.0		0.152290	0.462446	0.152292	0.462448
									0.6	0.163807	0.425330	0.163811	0.425332
									0.8	0.151869	0.462619	0.151872	0.462620
									1.0	0.142231	0.494938	0.142235	0.494941

TABLE 3.3: Numerical values of Nu_x and Sh_x for various values of Pr, f_w, k_p, Re, G, Ec, M, β_e, β_i, N_1.

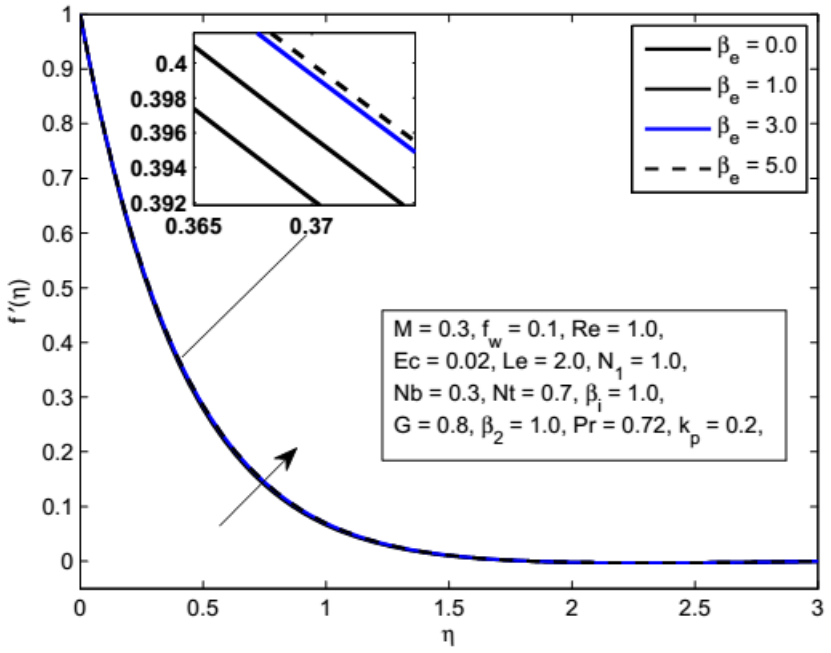

FIGURE 3.2: Influence of β_e on $f'(\eta)$.

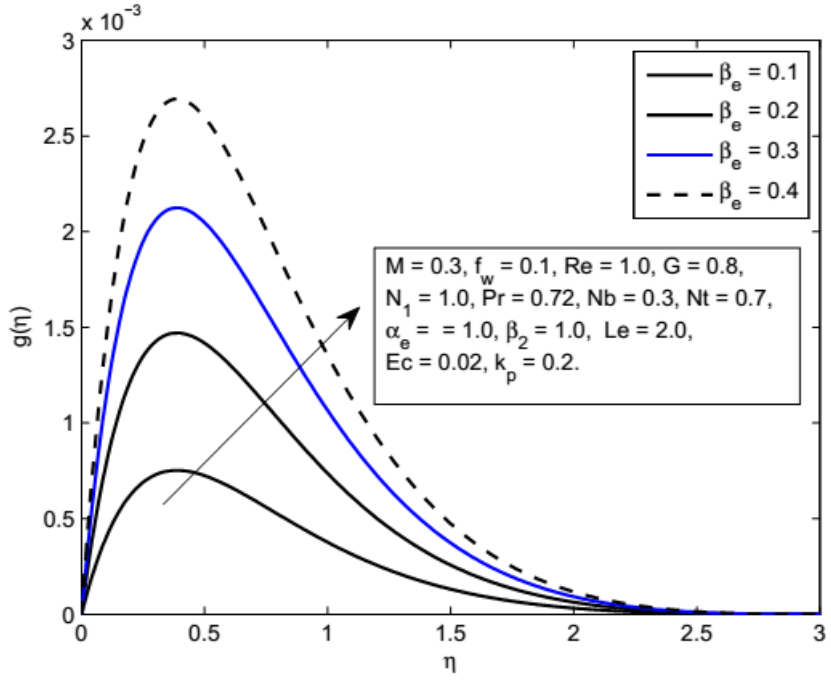

FIGURE 3.3: Influence of β_e on $g(\eta)$.

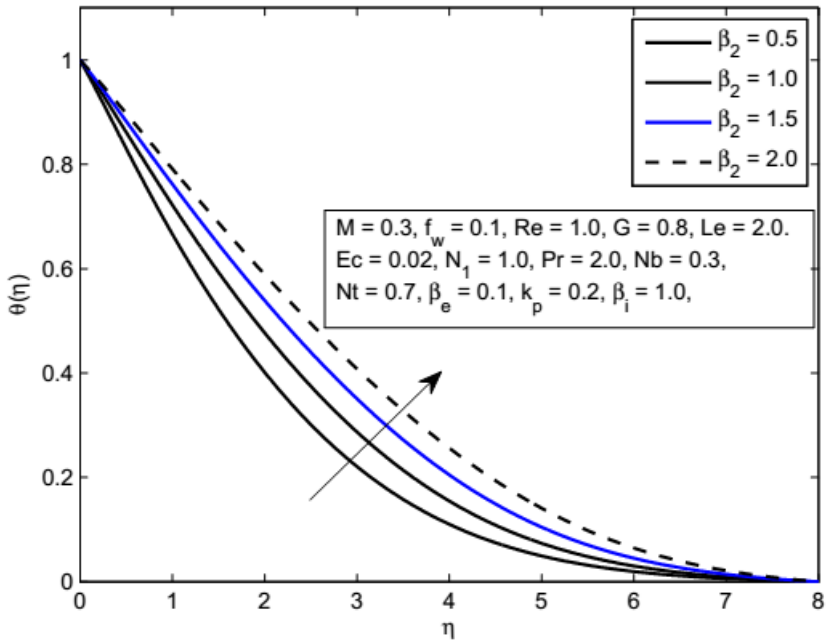

FIGURE 3.4: Influence of β_2 on $\theta(\eta)$.

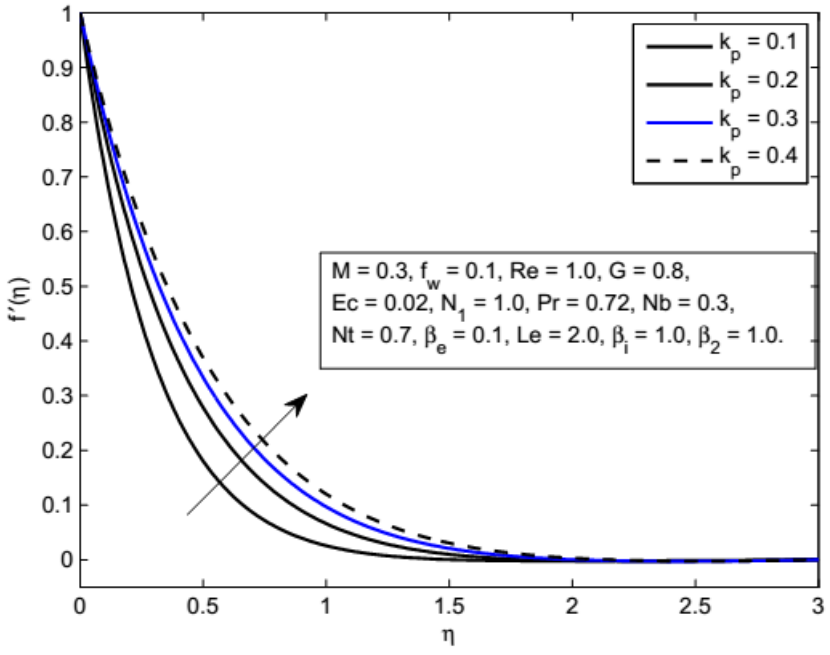

FIGURE 3.5: Influence of k_p on $f'(\eta)$.

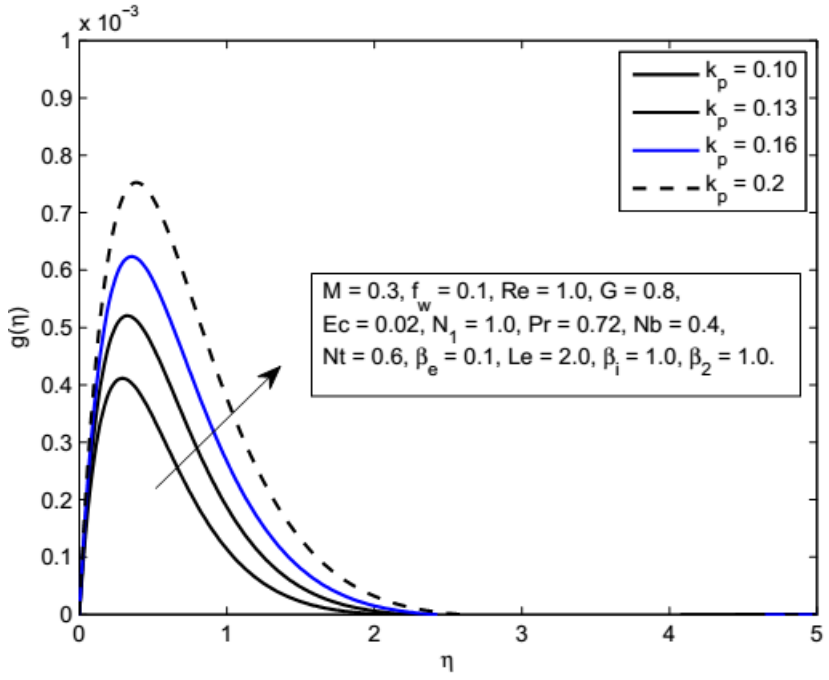

FIGURE 3.6: Influence of k_p on $g(\eta)$.

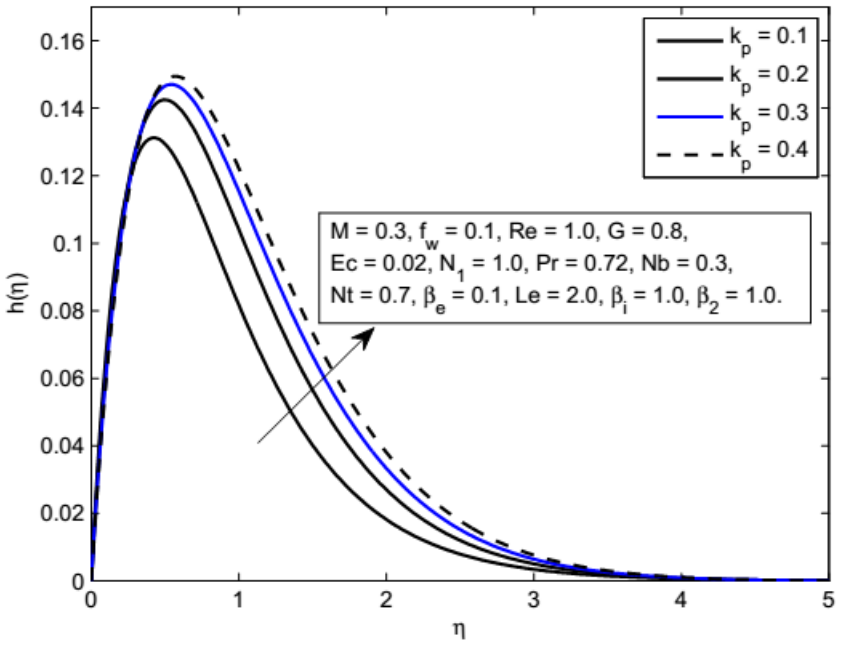

FIGURE 3.7: Influence of k_p on $h(\eta)$.

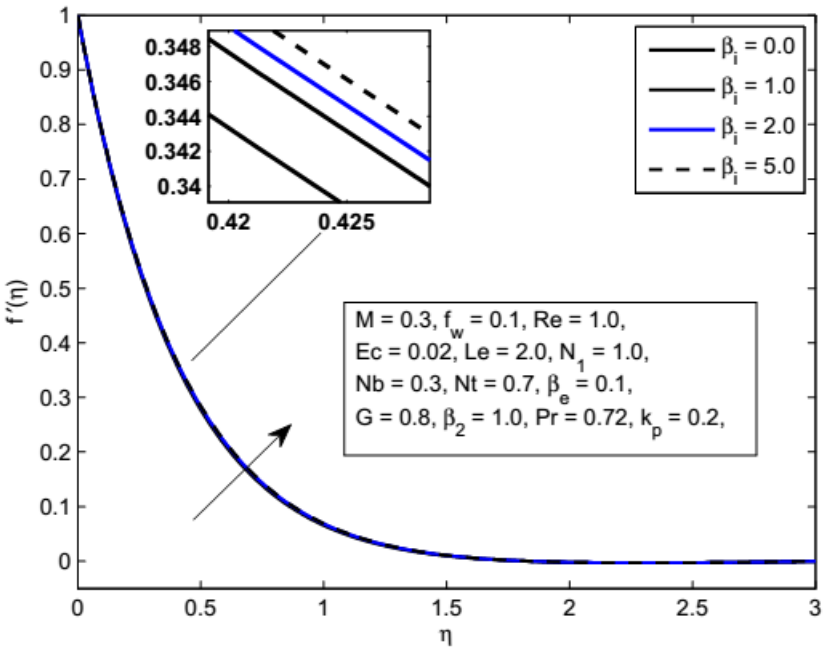

FIGURE 3.8: Influence of β_i on $f'(\eta)$.

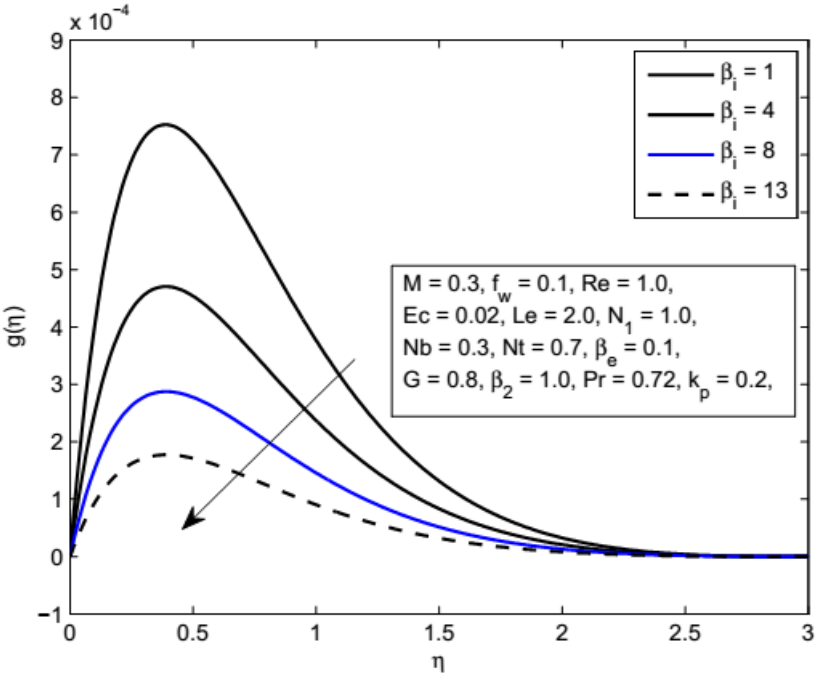

FIGURE 3.9: Influence of β_i on $g(\eta)$.

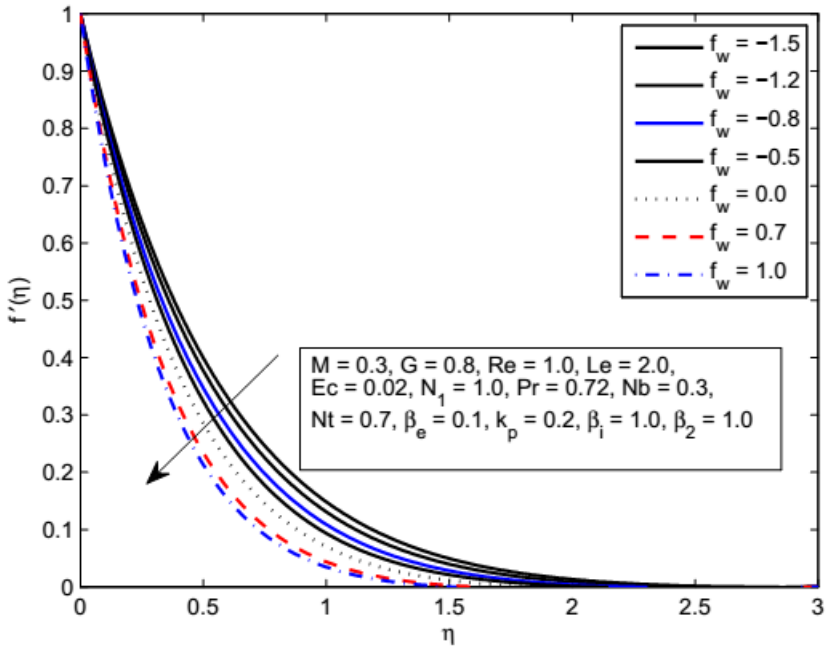

FIGURE 3.10: Influence of f_w on $f'(\eta)$.

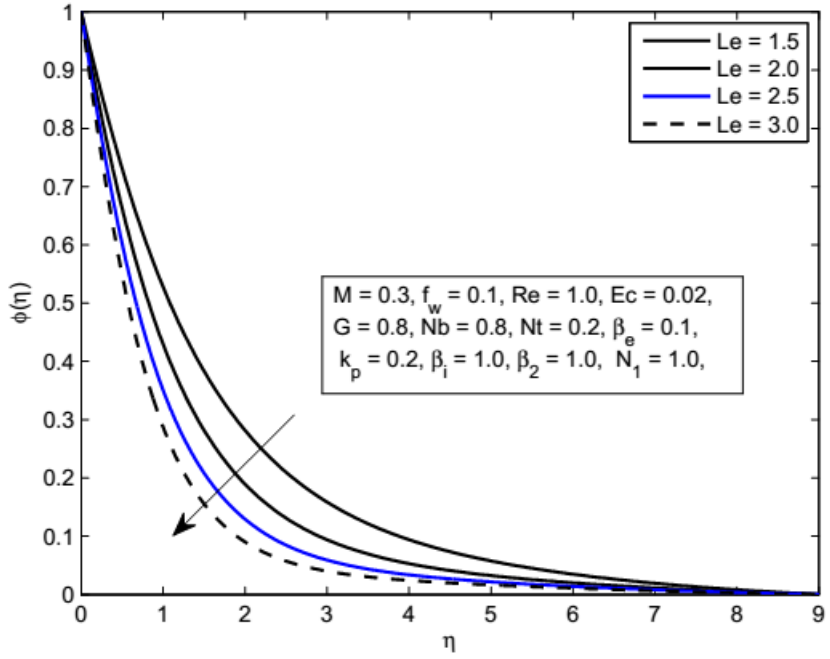

FIGURE 3.11: Influence of Le on $\phi(\eta)$.

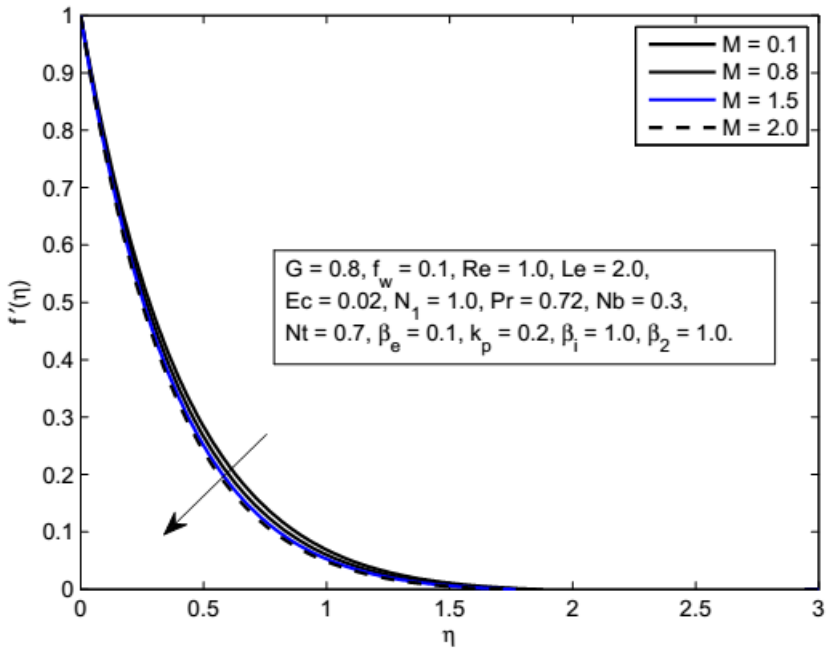

FIGURE 3.12: Influence of M on $f'(\eta)$.

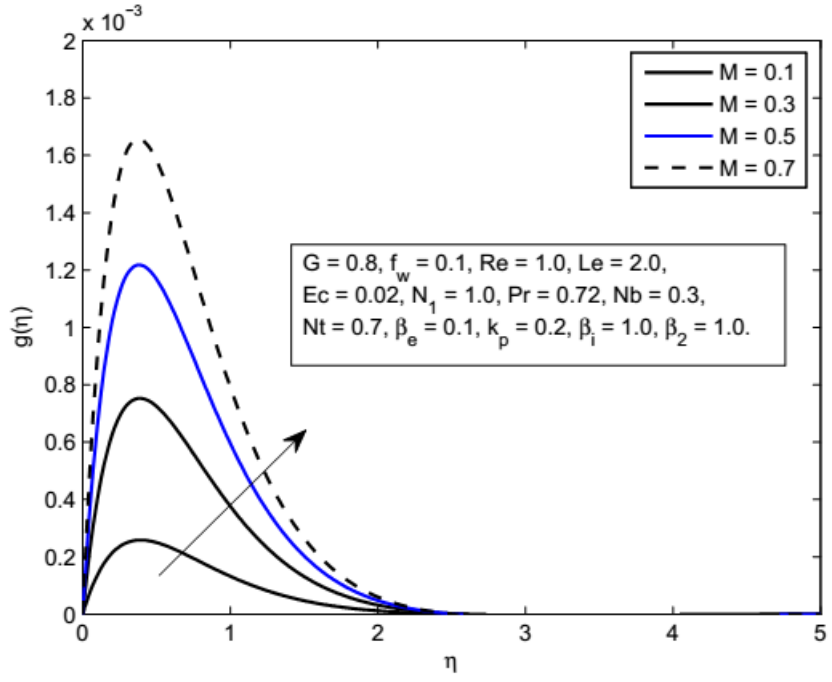

FIGURE 3.13: Influence of M on $g(\eta)$.

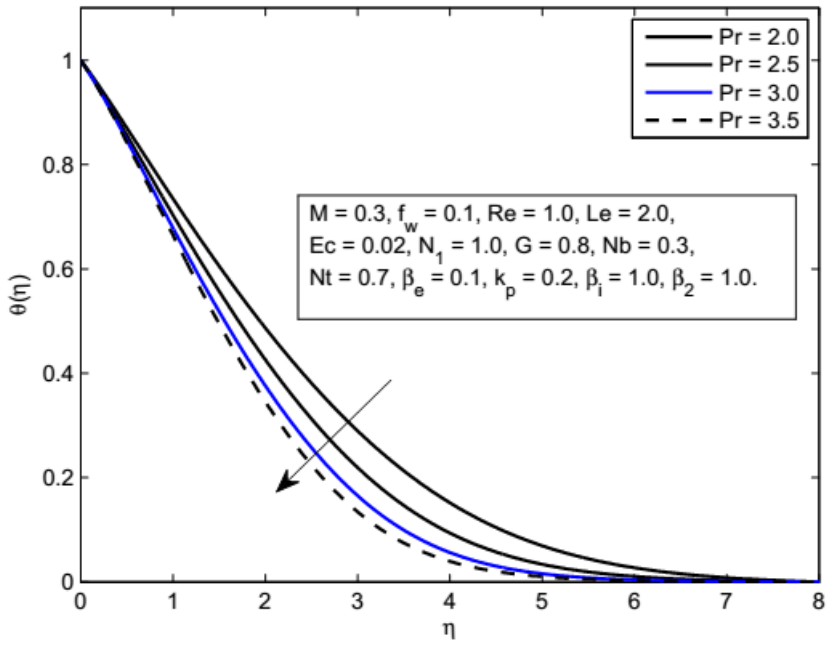

FIGURE 3.14: Influence of Pr on $\theta(\eta)$.

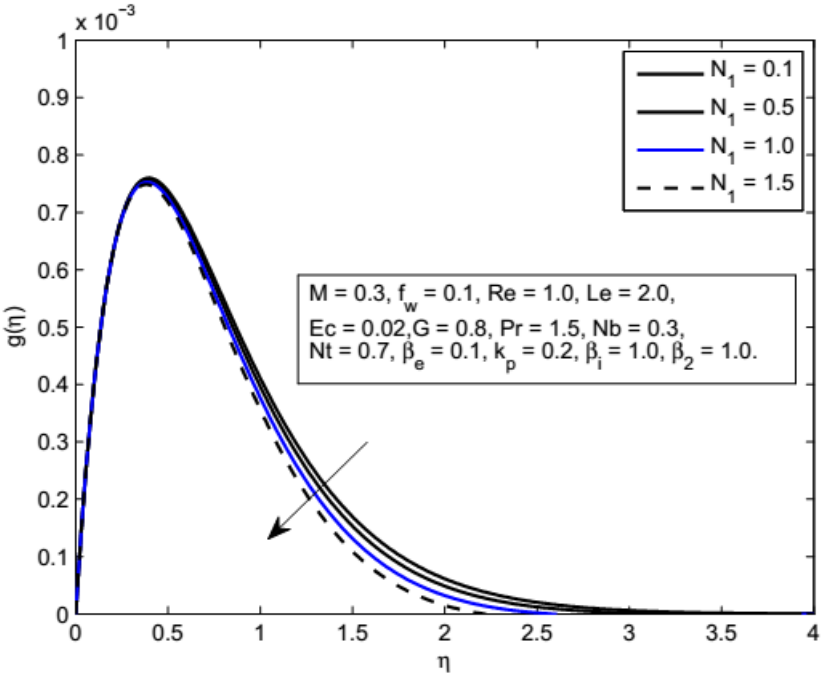

FIGURE 3.15: Influence of N_1 on $g(\eta)$.

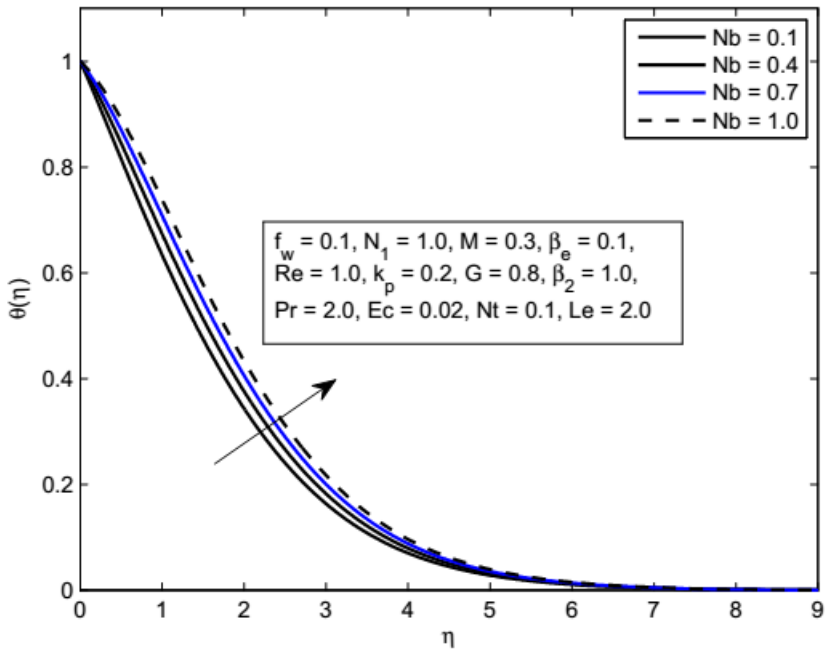

FIGURE 3.16: Influence of Nb on $\theta(\eta)$.

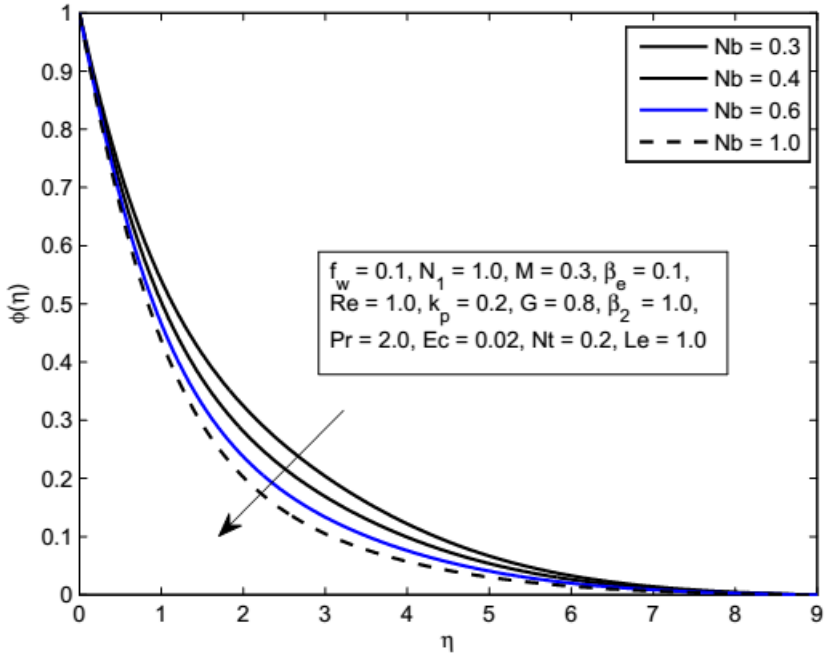

FIGURE 3.17: Influence of Nb on $\phi(\eta)$.

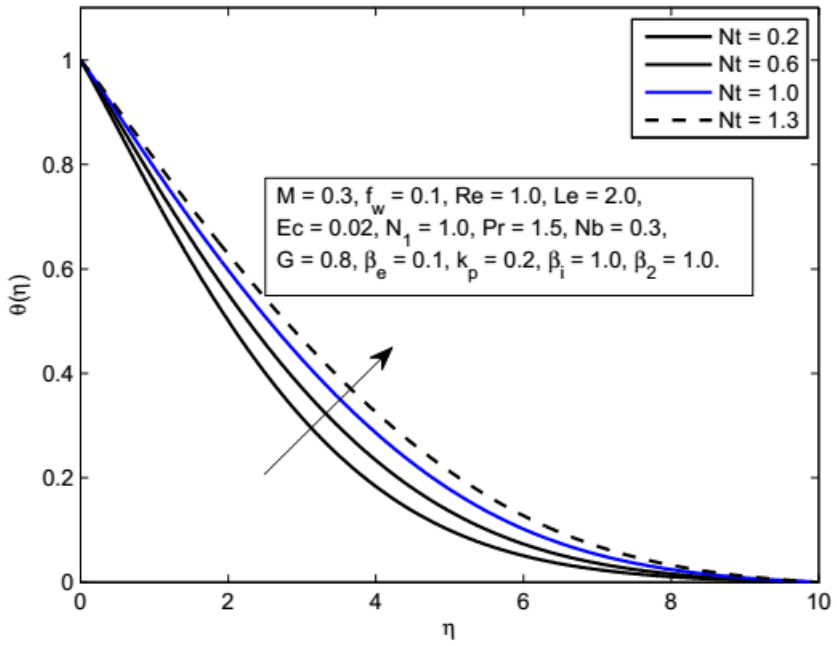

FIGURE 3.18: Influence of Nt on $\theta(\eta)$.

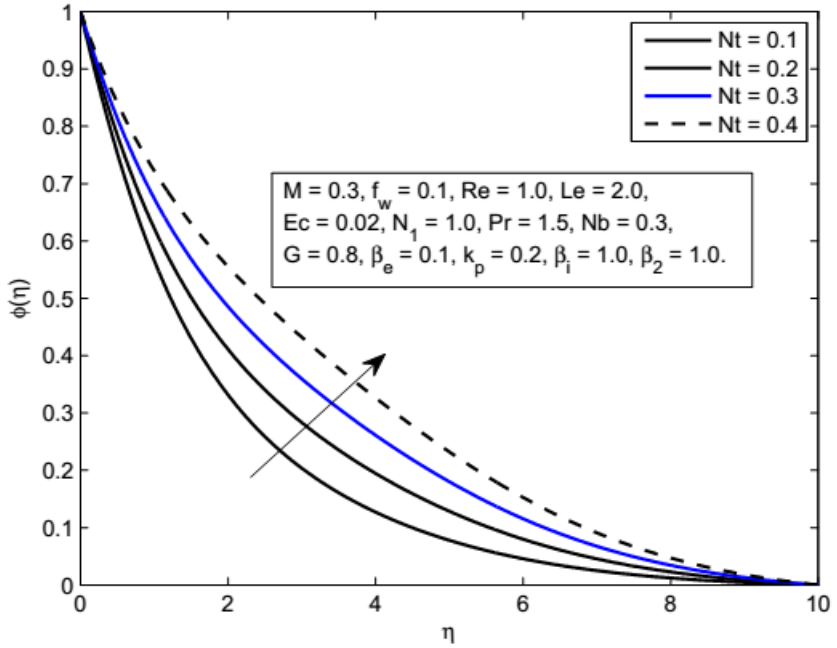

FIGURE 3.19: Influence of Nt on $\phi(\eta)$.

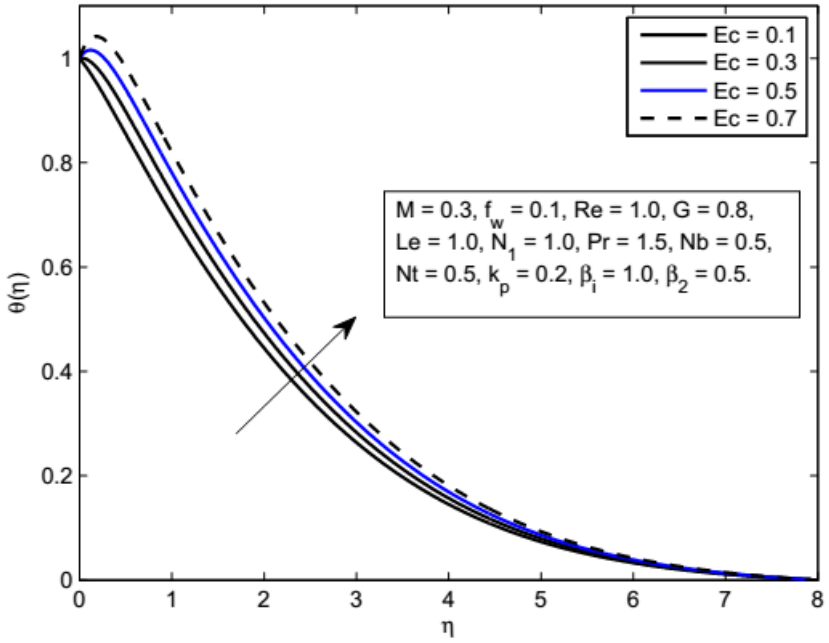

FIGURE 3.20: Influence of Ec on $\theta(\eta)$.

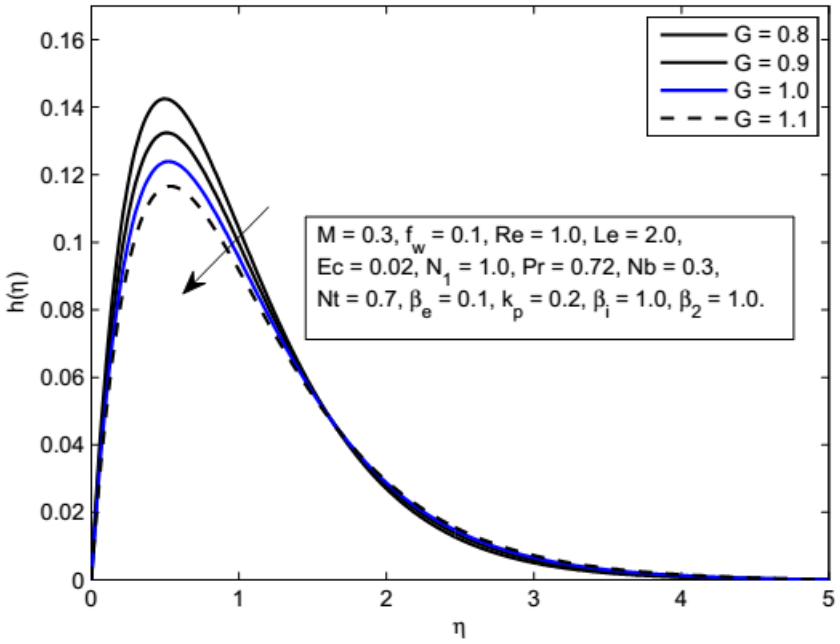

FIGURE 3.21: Influence of G on $h(\eta)$.

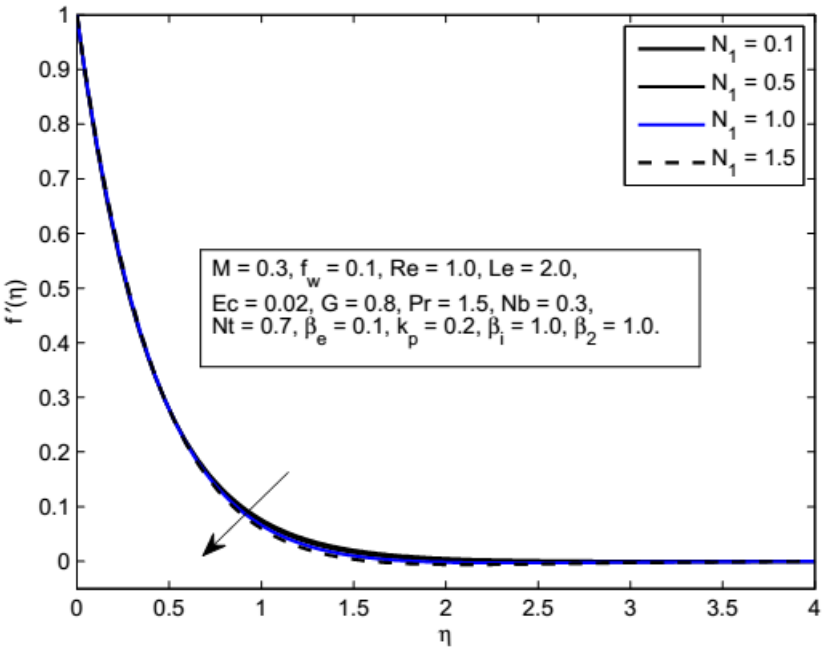

FIGURE 3.22: Influence of $N1$ on $f'(\eta)$.

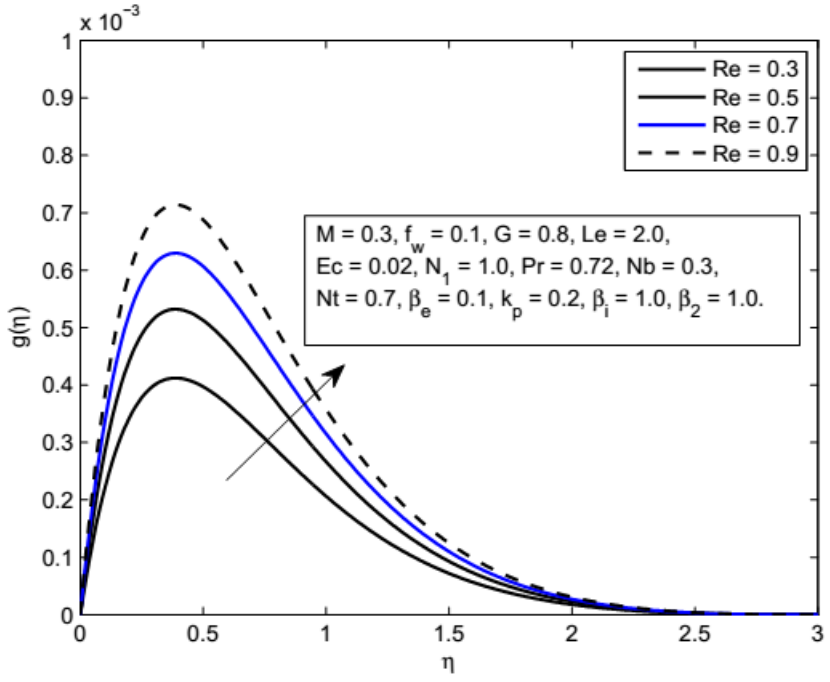

FIGURE 3.23: Influence of Re on $g(\eta)$.

3.5 Concluding Remarks

In this Chapter, the effect of Hall current and ion-slip effects with variable thermal diffusivity on magneto-micropolar nanofluid on a stretching porous medium is numerically and graphically analyzed by using the shooting method which has been frequently used to calculate the solutions in many fluid mechanics problems and related fields. The main points are summarized as follows.

- Thermal and concentration boundary layer thickness increase with the increase in thermophoresis parameter.
- Brownian motion parameter has opposite effect on temperature and concentration fields.
- Stronger magnetic parameter M results an increase in temperature, concentration and decrease in stream and lateral velocity.
- Velocity components such as stream velocity, velocity distribution along the stretching sheet and angular velocity all are increased by the enhancement in the permeability parameter.
- Minor increase of the velocity along the $x-$direction is observed for the increasing values of ion-slip and Hall current parameter.

Chapter 4

Hall Current and Non-linear Heat Generation Effects on MHD Nanofluid

4.1 Introduction

In this chapter, the impact of Hall current on an electrically conducting nanofluid flow past a continuously stretching surface with heat generation/absorption has been explored. Transverse magnetic field with the assumption of small Reynolds number is implemented vertically. Appropriate similarity transformations are utilized to transform the governing partial differential equations into the non-linear ordinary differential equations. Numerical solutions for the dimensionless velocity, temperature and nanoparticle concentration are computed with the help of the shooting method. Results are further supported with the results obtained by bvp4c, a MATLAB built-in function. Both these methods show the excellent agreement. The impact of each of the Hall current parameter, Brownian motion parameter, Prandtl number, thermophoresis parameter and magnetic parameter on velocity, concentration and temperature, is discussed through graphs. The

skin friction coefficient along the $x-$ and $z-$ directions, the local Nusselt number and the Sherwood number are calculated numerically to look into the inside behavior of the emerging parameters.

4.2 Problem Formulation

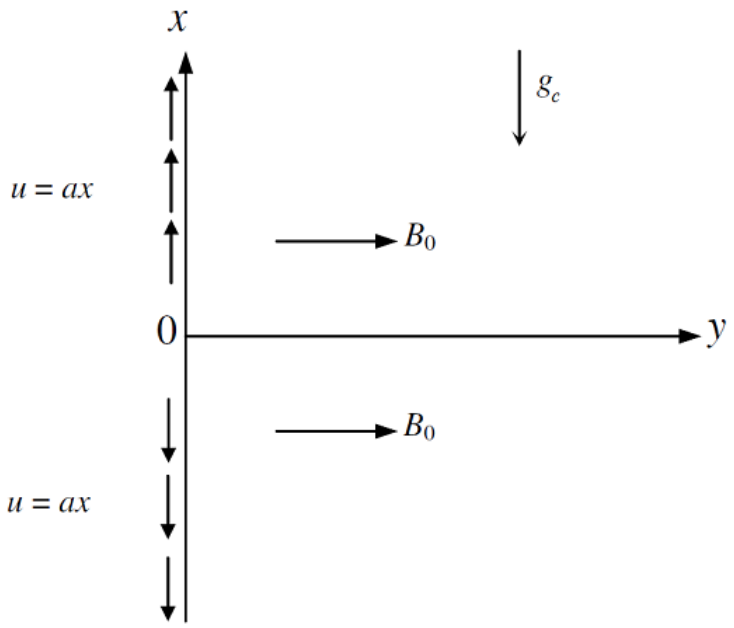

FIGURE 4.1: Geometry of the Problem.

Here, steady heat and mass transfer of an incompressible hydromagnetic nanofluid flow along a vertical stretching sheet coinciding with the plane $y = 0$, has been considered in the presence of the Hall current effects. By keeping the origin fixed, two opposite and equal forces are assumed to employ along the x-axis so that the sheet stretches linearly in both positive and negative direction (see Figure 4.1). With the assumption that the Newtonian nanofluid be electrically conducting and heat generating/absorbing, a strong magnetic field has been imposed normal to the direction of flow. Moreover, no electric field has been assumed to apply and the frequency of atom-electron collision has also been considered high for the generation of Hall current effect [106]. Due to the strong magnetic flux density B_0, the Hall current effect is taken into consideration, however the small magnetic

Reynolds number is employed and the induced magnetic field is ignored. Hall current effect is strong enough to give rise to a force in the $z-$direction and a cross flow is induced in the same direction which causes a three dimensional flow. It is further assumed that there are no variations in the flow, heat and mass transfer in the z-direction. This assumption can be achieved by taking the sheet of infinite width. Non-conducting plate is considered so that the generalized Ohm's law [107] gives $J_y = 0$ in the flow field. Brownian motion and thermophoresis effects are considered using the Buongiorno model [29] for the nanofluid. Further, the effects of viscous dissipation and Joule heating are ignored. By the above mentioned assumptions and Boussinesq approximation, the mathematical form of the problem is

$$\frac{\partial u}{\partial x} + \frac{\partial v}{\partial y} = 0, \tag{4.1}$$

$$u\frac{\partial u}{\partial x} + v\frac{\partial u}{\partial y} = \nu\frac{\partial^2 u}{\partial y^2} - \frac{\sigma B_0^2}{\rho\left(1+\beta_e^2\right)}\left(u+\beta_e w\right) + g_c\beta_T\left(T-T_\infty\right) + g_c\beta_C\left(C-C_\infty\right), \tag{4.2}$$

$$u\frac{\partial w}{\partial x} + v\frac{\partial w}{\partial y} = \nu\frac{\partial^2 w}{\partial y^2} + \frac{\sigma B_0^2}{\rho\left(1+\beta_e^2\right)}\left(\beta_e u - w\right), \tag{4.3}$$

$$u\frac{\partial T}{\partial x} + v\frac{\partial T}{\partial y} = \frac{k}{\rho c_p}\frac{\partial^2 T}{\partial y^2} + \frac{q^m}{\rho c_p} + \tau\left(D_B\frac{\partial C}{\partial y}\frac{\partial T}{\partial y} + \frac{D_T}{T_\infty}\left(\frac{\partial T}{\partial y}\right)^2\right), \tag{4.4}$$

$$u\frac{\partial C}{\partial x} + v\frac{\partial C}{\partial y} = D_B\frac{\partial^2 C}{\partial y^2} + \frac{D_T}{T_\infty}\frac{\partial^2 T}{\partial y^2}. \tag{4.5}$$

Here, q^m indicates the coefficient of internal heat absorption (or generation). From [108, 109], it follows that

$$q^m = \left(\frac{ka}{\nu}\right)\left[A^*\left(T_w - T_\infty\right)e^{-\eta} + B^*\left(T - T_\infty\right)\right]. \tag{4.6}$$

When both A^* and B^* are positive, we have the heat generation case whereas for the negative values of both of them, there is the internal heat absorption. The corresponding boundary conditions for the governing PDEs are

$$\left.\begin{aligned} u &= ax, \quad v = 0, \quad w = 0, \quad T = T_w, \quad C = C_w \ \ at \ \ y = 0, \\ u &\to 0, \quad v \to 0, \quad w \to 0 \quad T \to T_\infty, \quad C \to C_\infty \ \ as \ \ y \to \infty. \end{aligned}\right\} \tag{4.7}$$

Now, propose the following dimensionless variables to non-dimensionalize the PDEs.

$$\left.\begin{aligned} \eta &= \sqrt{\frac{a}{\nu}}y, \quad \psi(x,y) = \sqrt{a\nu}xf(\eta), \quad w = axg(\eta), \\ \phi(\eta) &= \frac{C - C_\infty}{C_w - C_\infty}, \quad \theta(\eta) = \frac{T - T_\infty}{T_w - T_\infty}, \end{aligned}\right\} \tag{4.8}$$

where $\psi(x,y)$ represents the stream function with $u = \frac{\partial \psi}{\partial y}$ and $v = -\frac{\partial \psi}{\partial x}$. The resulting ordinary differential equations are

$$f''' + ff'' - f'^2 + Gr_x\theta + Gr_c\phi - \frac{M}{1+\beta_e^2}(f' + \beta_e g) = 0, \tag{4.9}$$

$$g'' + fg' - f'g + \frac{M}{1+\beta_e^2}(\beta_e f' - g) = 0, \tag{4.10}$$

$$\theta'' + Prf\theta' + PrNb\left(\theta'\phi' + \frac{Nt}{Nb}\theta'^2\right) + A^*e^{-\eta} + B^*\theta = 0, \tag{4.11}$$

$$\phi'' + PrLef\,\phi' + \frac{Nt}{Nb}\theta'' = 0. \tag{4.12}$$

The transformed boundary conditions are

$$\left.\begin{aligned} f'(0) &= 1, \quad f(0) = 0, \quad g(0) = 0, \quad \theta(0) = 1, \quad \phi(0) = 1, \\ f'(\eta) &\to 0, \quad \theta(\eta) \to 0, \quad g(\eta) \to 0, \quad \phi(\eta) \to 0. \text{ as } \eta \to \infty. \end{aligned}\right\} \tag{4.13}$$

Different dimensionless parameters appearing in equations (4.9-4.13) are defined as

$$\left.\begin{aligned} Gr_x &= \frac{g_c\beta_T(T_w - T_\infty)}{a^2x}, \quad Pr = \frac{\nu}{\alpha} = \frac{\nu\rho c_p}{k}, \quad Nb = \frac{\tau D_B}{\nu}(C_w - C_\infty), \\ Nt &= \frac{D_T\tau}{T_\infty\nu}(T_w - T_\infty), \quad Le = \frac{\alpha}{D_B}, \quad M = \frac{\sigma B_0^2}{\rho a} \quad Gr_c = \frac{g_c\beta_C(C_w - C_\infty)}{a^2x}, \end{aligned}\right\} \tag{4.14}$$

The important quantities of interest are the coefficients of skin-friction in $x-$ and $z-$ directions, local Nusselt number and Sherwood number. These are defined as

$$\left.\begin{aligned} C_{fx} &= \frac{2\tau_{wx}}{\rho\,(ax)^2}, \qquad C_{fz} = \frac{2\tau_{wz}}{\rho\,(ax)^2}, \\ Nu_x &= \frac{xq_w}{k\,(T_w - T_\infty)}, \qquad Sh_x = \frac{xj_w}{D_B\,(C_w - C_\infty)}. \end{aligned}\right\} \tag{4.15}$$

Here, the local skin-friction, heat and mass fluxes are defined as

$$\left.\begin{aligned} \tau_{wx} &= \mu \left.\frac{\partial u}{\partial y}\right|_{y=0}, \quad \tau_{wz} = \mu \left.\frac{\partial w}{\partial y}\right|_{y=0}, \\ q_w &= -k \left.\frac{\partial T}{\partial y}\right|_{y=0}, \quad j_w = -D_B \left.\frac{\partial C}{\partial y}\right|_{y=0}. \end{aligned}\right\} \tag{4.16}$$

The dimensionless forms of skin-friction, local Nusselt number and Sherwood number are:

$$\left.\begin{aligned} C_{fx}Re_x^{1/2} &= 2f''(0), \quad C_{fz}Re_x^{1/2} = 2g'(0), \\ Nu_xRe_x^{-1/2} &= -\theta'(0), \quad Sh_xRe_x^{-1/2} = -\phi'(0). \end{aligned}\right\} \tag{4.17}$$

4.3 Solution Methodology

The resulting non-linear system of ODEs can be solved by a number of analytical and numerical techniques such as homotopy perturbation method [110], homotopy analysis method [111], optimized homotopy analysis method [112], adomian decomposition method [113], finite difference method [114], finite element method [61], etc. We have opted the well known numerical technique shooting method [93] which is considered to be an efficient scheme in the sense of computational time.

The system of non-linear ODEs (4.9-4.12) subject to the boundary conditions 4.13 has been solved by the shooting method for various values of the involved parameters. We observed through graphs that for $\eta > 8$, there is no significant variation in the behavior of solutions. Therefore, on the basis of such computational experiments, we are pondering [0, 8] as the domain of the problem instead of [0, ∞). We denote f by y_1, g by y_4, θ by y_6 and ϕ by y_8 for converting the boundary value

problem (4.9-4.13) to the following initial value problem consisting of 9 first order differential equations.

$$\left.\begin{aligned}
y_1' &= y_2, & y_1(0) &= 0,\\
y_2' &= y_3, & y_2(0) &= 1,\\
y_3' &= y_2^2 - y_1 y_3 - Gr_x y_6 - Gr_c y_8 + \frac{M}{1+\beta_e^2}\left(y_2 + \beta_e y_4\right), & y_3(0) &= \varrho_1,\\
y_4' &= y_5, & y_4(0) &= 0,\\
y_5' &= y_2 y_4 - y_1 y_5 - \frac{M}{1+\beta_e^2}\left(\beta_e y_2 - y_4\right), & y_5(0) &= \varrho_2,\\
y_6' &= y_7, & y_6(0) &= 1,\\
y_7' &= -Pr y_1 y_7 - PrNb\left(y_7 y_9 + \frac{Nt}{Nb} y_7^2\right) - A^* e^{-\eta} - B^* y_6, & y_7(0) &= \varrho_3,\\
y_8' &= y_9, & y_8(0) &= 1,\\
y_9' &= -LePr y_1 y_9 - \frac{Nt}{Nb} y_7', & y_9(0) &= \varrho_4.
\end{aligned}\right\} \tag{4.18}$$

To solve the above initial value problem with RK4 method, we have to take some initial guesses for ϱ_1, ϱ_2, ϱ_3, and ϱ_4. Newton's method is utilized to improve these original estimates of ϱ_1, ϱ_2, ϱ_3, ϱ_4 until the following benchmark is achieved

$$\max\{|y_2\{8\}|,\ |y_4\{8\}|,\ |y_6\{8\}|,\ |y_8\{8\}\} < \varepsilon, \tag{4.19}$$

where $\varepsilon > 0$ is a small positive real number. All the numerical results in this chapter are attained with $\varepsilon = 10^{-6}$.

4.4 Results and Discussions

For the validation of our MATLAB code, a comparison reflecting a convincing agreement between the present results and those of Salem and Aziz [115], is presented in Table. 4.1. It is valuable to mention here that Salem and Aziz have also used the shooting technique with Runge-Kutta integration algorithm. To perceive

the impact of the various physical parameters on the local Sherwood number, skin-friction coefficient and local Nusselt number, mathematical results are achieved and are enumerated. From Table 4.2, it is viewed that the skin-friction coefficient in $x-$ direction decreases with an increase in the thermal Grashof number and the mass Grashoff number and increases with an increase in the magnetic parameter M and Prandtl number Pr. The coefficient of the local skin-friction in $z-$ direction increases with an increase in Gr_x, M, and Gr_c and decreases when Pr increases. Nusselt number increases when Gr_x, Pr and Gr_c increase whereas it is reduced by increasing the value of M. Sherwood number has increasing behavior for Gr_x and M while it has decreasing behavior for Pr and Gr_c.

Table 4.3 shows the impact of Hall current parameter β_e, Brownian motion parameter Nb and thermophoresis parameter Nt on the skin friction, Nusselt number and Sherwood number for $Pr = 0.71, Le = 0.6, M = 0.5, Gr_x = 0.5, Gr_c = 0.5, A^* = 0.01, B^* = 0.01$. It is clear that Cf_x decreases for the increasing value of β_e and Nt while it increases for the increasing value of Nt. A completely opposite behavior is recorded for the coefficient of the skin-friction in the z-direction. With the enhancement of Hall current parameter β_e, the value of the Nusselt number increases while the Sherwood number decreases, though this reduction is very small. Brownian motion parameter Nb and thermophoresis parameter Nt both cause a decreasing trend in the Nusselt number and increasing in the Sherwood number. In Table 4.4, the effect of the space-dependent heat generation/absorption parameter A^*, the temperature dependent heat generation/absorption parameter B^* and the Lewis number Le on the skin friction coefficient, local Nusselt and Sherwood numbers, is discussed. The skin-friction coefficient in the x-direction increases when A^*, B^* and Le are increased whereas skin-friction coefficient in the z-direction decreases for Le and increases for A^* and B^*. For A^* and B^*, Nusselt number increases whereas an opposite behavior is seen in Sherwood number, however in case of Lewis number both the Nusselt and Sherwood numbers decrease.

The effect of Hall current parameter β_e on shear wall stress $f''(0)$ for different parameters is shown in Table 4.5. We have considered $\beta_e = 0$, (i.e., without Hall current effect), $\beta_e = 0.2$ and $\beta_e = 0.5$. From the table, it is observed that the

wall shear stress in the direction of flow decreases when β_e increases. It is also observed that this decrement in the skin friction is enhanced when the impact of Hall current increases.

To envision the effect of various physical parameters on tangential velocity $f'(\eta)$, transverse velocity $g(\eta)$, nanoparticle concentration $\phi(\eta)$ and temperature $\theta(\eta)$ profiles, Figures 4.2-4.26 are plotted. In all these computations, unless mentioned, otherwise we have considered $Nb = 0.3,\ Nt = 0.7,\ Pr = 0.71,\ Le = 0.6,\ M = 0.5,\ \beta_e = 0.2,\ Gr_x = 0.5,\ Gr_c = 0.5,\ A^* = 0.01,\ B^* = 0.01$. The impact of spatial-dependent internal heat generation parameter $A^* > 0$ and the heat absorption parameter $A^* < 0$ on the temperature field is presented in Figure 4.2. It is evident from this figure that as $A^* > 0$ increases, the temperature of the fluid also increases, because in the presence of heat source, energy is generated which results in the rise of the temperature. Due to the temperature rise, velocity of the fluid also increases and this phenomenon can be observed in Figure 4.3. An opposite effect i.e., cooling, is observed in the case of heat sink $A^* < 0$. Velocity of the fluid is also found to decrease for the heat sink case.

From Figures 4.4 and 4.5, it is evident that temperature as well as the tangential velocity grow while enhancing the temperature dependent heat source $B^* > 0$. Figures 4.6−4.9 show the typical profiles of the tangential and lateral velocities, temperature and concentration profiles for the magnetic parameter M. By increasing the magnetic parameter M, a drag force known as the Lorentz force is increased which resultantly reduces the velocity of the fluid and hence the rate of heat and mass transfer is reduced and this leads to an increment in the temperature and concentration profiles. Influence of Brownian motion parameter Nb on the temperature and concentration profiles is studied in Figures 4.10 and 4.11. From these figures, we notice that an enhancement in the values of Nb gives rise to the temperature, while it causes a decrease in the nanoparticle concentration profile. Brownian motion is the random motion of nanoparticles suspended in the fluid, caused by the collision of nanoparticles with the fluid particles. An increment in the thermophoretic effect causes an increment in the Brownian motion effect which results in the rise of the temperature due to the increment in the

kinetic energy. Figures 4.12 and 4.13 illustrate the effect of thermophoresis parameter Nt on the temperature and the nanoparticles concentration profile. One can observe that temperature and concentration fields increase with an enhancement in Nt. Thermophoresis parameter plays an important role in the heat transfer flow. Thermophoresis force enhances when Nt is increased which tends to move the nanoparticles from the hot region to the cold and as a result the temperature and the boundary layer thickness increase.

Effect of Prandtl number Pr on the temperature and the concentration profiles is shown in Figures 4.14 and 4.15. These figures show a decreasing trend in these profiles when Pr is increased. Reduction in the thermal boundary layer is encountered when Pr is increased. Larger the Prandtl number results lower the thermal diffusivity. Thus a rise in Pr reduces diffusivity and conduction and hence the thermal characteristics increase. A minor increase is seen, in Figure 4.16, in the fluid velocity when the Hall current parameter is increased. The magnetic damping on $f'(\eta)$ decreases as β_e increases and the magnetic field seems to have a propelling effect on $f'(\eta)$. An increase in the values of M (consequently the Hall parameter β_e) greatly affects the lateral direction cross flow due to the Hall current. The inclusion of the Hall parameter decreases the resistive force imposed by the magnetic field, which resultantly rises the tangential velocity component, but this increase in the velocity is very small. Similarly the transverse velocity also increases with the increasing values of β_e as clearly seen in Figure 4.17. Figures 4.18 and 4.19 show the impact of the Lewis number Le on temperature and nanoparticle concentration profiles respectively. It is observed that the temperature increases by increasing Le while concentration decreases with an increase in the Lewis number.

In Figures 4.20−4.23 the effects of the thermal Grashof Gr_x and concentration Grashof Gr_c numbers on the tangential velocity $f'(\eta)$ and the lateral velocity $g(\eta)$ are displayed. As the Grashof number is a ratio of the buoyancy force to the viscous force and it appears due to the natural convection flow, so an increase in the tangential velocity as well as the lateral velocity of the fluid is observed when the thermal and the concentration Grashof numbers are increased. It happens because of the fact that higher the Grashof number implies higher the buoyancy force which

means higher the movement of the flow. However in Figure 4.23, away from the plate a reverse relation i.e. a decrease in the lateral velocity is observed. Figures 4.24 and 4.25 depict the influence of the solutal Grashof number on the temperature and the concentration profile respectively. An increase in the solutal Grashof number means a decrease in the viscous force which reduces the temperature and the concentration of the fluid. Similarly temperature is reduced when the thermal Grashof number is enhanced and this phenomenon can be observed in Figure 4.26.

			[115]	Present	[115]	Present	[115]	Present
M	β_e	A^*	$-2f''(0)$	$-2f''(0)$	$-2g'(0)$	$-2g'(0)$	$-\theta'(0)$	$-\theta'(0)$
0.0	0.2	0.01	0.870809	0.870247	0	0	0.536486	0.536477
0.5			1.358619	1.358236	0.115852	0.115933	0.503496	0.503336
1.0			1.786271	1.785839	0.191908	0.191998	0.474604	0.474244
1.5			2.167098	2.166598	0.247956	0.248055	0.449427	0.448809
1.0	0.2		1.786271	1.785839	0.191908	0.191998	0.474604	0.474244
	0.6		1.623616	1.623231	0.473443	0.473690	0.483100	0.482784
	1.3		1.312373	1.312085	0.592181	0.601313	0.502332	0.502116
	1.5		1.248158	1.247886	0.600892	0.592634	0.506818	0.506625
	1.7		1.194659	1.194397	0.575677	0.576154	0.510692	0.510518
	2.0		1.131002	1.130745	0.543739	0.544241	0.515457	0.515309
	0.2	0.01	1.786271	1.785839	0.191908	0.191998	0.474604	0.474244
		0.5	1.709803	1.709259	0.197192	0.197301	0.106995	0.106322
		1.0	1.635663	1.635064	0.201996	0.202113	-0.261874	-0.262738
		2.0	1.496325	1.495686	0.210345	0.210467	-0.985212	-0.986259

TABLE 4.1: Comparison of the present results for the wall shear stress $C_{fx}Re_x^{1/2} = 2f''(0)$ and $C_{fz}Re_z^{1/2} = 2g'(0)$ and Nusselt number $Nu_xRe_z^{-1/2} = -\theta'(0)$ for various values of M, β_e and A^* when $B^* = 0.01$, $Pr = 0.71, Sc = 0.6$, $Gr_x = 0.5, Gr_c = 0.5$ and $\gamma = 0.1$.

Gr_x	M	Pr	Gr_c	$-2f''(0)$	$-2g'(0)$	$-\theta'(0)$	$-\phi'(0)$
0.5	0.5	0.71	0.5	0.995469	0.133782	0.448254	0.194116
0.4				1.092577	0.132638	0.444418	0.192656
0.5				0.995469	0.133782	0.448254	0.194116
0.6				0.899398	0.134886	0.451958	0.195504
	0.6			1.097146	0.153870	0.448254	0.194741
	0.7			1.196273	0.172299	0.438634	0.195234
	0.8			1.292930	0.189256	0.433933	0.195592
		0.8		1.017091	0.132157	0.465032	0.183197
		0.9		1.040024	0.130492	0.480201	0.166163
		1.0		1.061794	0.128966	0.492292	0.144968
			0.5	0.995469	0.133782	0.448254	0.194116
			0.6	0.844106	0.136940	0.457292	0.188976
			0.7	0.696075	0.139809	0.465553	0.184431

TABLE 4.2: Numerical values of $C_{fz}Re_z^{1/2}$, $C_{fx}Re_z^{1/2}$, $Nu_xRe_z^{-1/2}$ and $Sh_xRe_z^{-1/2}$ when $A^* = 0.01, B^* = 0.01, Le = 0.6, \beta_e = 0.2,\ Nb = 0.3, Nt = 0.7$

m	Nb	Nt	$-2f''(0)$	$-2g'(0)$	$-\theta'(0)$	$-\phi'(0)$
0.2	0.3	0.7	0.995469	0.133782	0.448254	0.194116
0.1			1.008624	0.068468	0.447697	0.194130
0.2			0.995469	0.133782	0.448254	0.194116
0.3			0.974886	0.193261	0.449131	0.194084
	0.4		1.062111	0.131188	0.427629	0.025649
	0.5		1.101593	0.129513	0.410054	0.074239
	0.6		1.127173	0.128352	0.394269	0.140229
		0.6	1.032373	0.132274	0.453247	0.124867
		0.7	0.995469	0.133782	0.448254	0.194116
		0.8	0.960115	0.135186	0.442973	0.258732

TABLE 4.3: Numerical values of $C_{fz}Re_z^{1/2}$, $C_{fx}Re_x^{1/2}$, $Nu_xRe_z^{-1/2}$ and $Sh_xRe_z^{-1/2}$ when $A^* = 0.01,\ B^* = 0.01, Le = 0.6,\ M = 0.5,\ Pr = 0.71,\ Gr_x = 0.5, Gr_c = 0.5$

B^*	A^*	Le	$-2f''(0)$	$-2g'(0)$	$-\theta'(0)$	$-\phi'(0)$
0.01	0.01	0.6	0.995469	0.133782	0.448254	0.194116
0.1			1.005849	0.133973	0.364631	0.023924
0.2			1.020086	0.134254	0.254466	0.197742
0.3			1.039068	0.134646	0.114194	0.475945
	0.1		1.002399	0.133890	0.387820	0.068761
	0.2		1.010132	0.134003	0.320517	0.070879
	0.3		1.017901	0.134114	0.253049	0.210898
		0.7	1.028049	0.131963	0.438410	0.124009
		0.8	1.056744	0.130394	0.429851	0.060449
		0.9	1.082308	0.129029	0.422338	0.002216

TABLE 4.4: Numerical values of $C_{fx}Re_x^{1/2}$, $C_{fz}Re_z^{1/2}$, $Nu_xRe_z^{-1/2}$ and $Sh_xRe_z^{-1/2}$ when $\beta_e = 0.2, Nb = 0.3, Nt = 0.7, M = 0.5$, $Pr = 0.71, Gr_x = 0.5, Gr_c = 0.5$

						$-2f''(0)$		
M	Gr_x	Gr_c	Pr	Nt	Nb	$\beta_e = 0.0$	$\beta_e = 0.2$	$\beta_e = 0.5$
0.5	0.5	0.5	0.71	0.7	0.3	1.013153	0.995469	0.918411
0.6						1.117358	1.097146	1.008663
0.7						1.218783	1.196273	1.097339
0.8						1.317542	1.292930	1.184399
	0.4					1.110164	1.092577	1.015915
	0.5					1.013153	0.995469	0.918411
	0.6					0.917178	0.899398	0.821953
		0.5				1.013153	0.995469	0.918411
		0.6				0.862144	0.844106	0.765536
		0.7				0.714439	0.696075	0.616110
			0.8			1.034592	1.017091	0.940876
			0.9			1.057344	1.040024	0.964644
			1.0			1.078952	1.061794	0.987159
				0.6		1.049876	1.032373	0.956119
				0.7		1.013154	0.995469	0.918411
				0.8		0.977972	0.960115	0.882295
					0.4	1.079482	1.062111	0.986429
					0.5	1.118769	1.101593	1.026774
					0.6	1.144217	1.127173	1.052938

TABLE 4.5: Numerical values of $C_{fx}Re_x^{1/2} = 2f''(0)$ when $A^* = 0.01, B^* = 0.01, Le = 0.6, \beta_e = 0.$

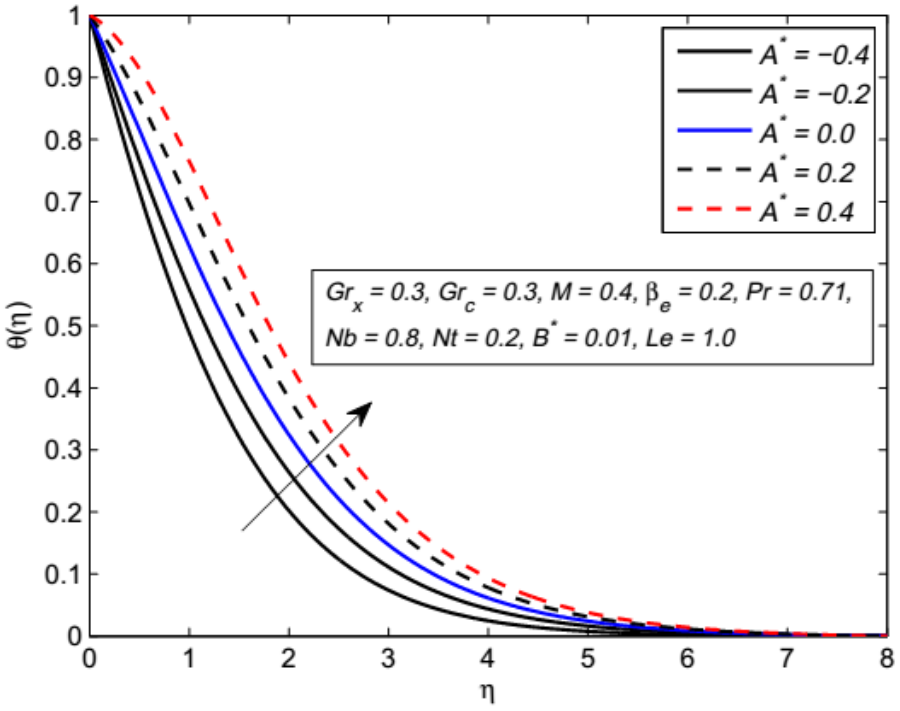

FIGURE 4.2: Influence of A^* on $\theta(\eta)$.

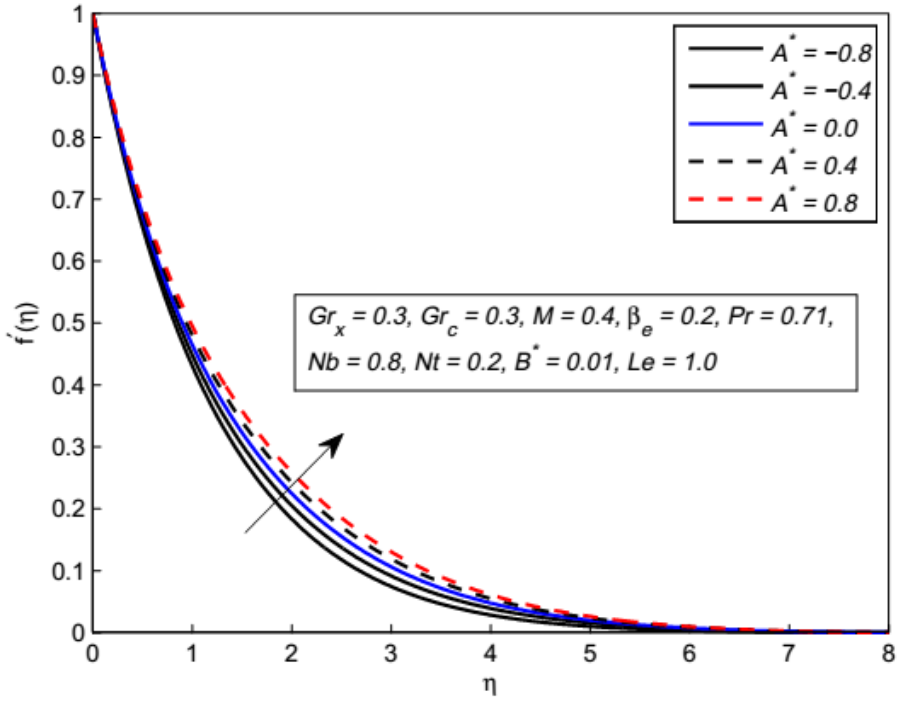

FIGURE 4.3: Influence of A^* on $f'(\eta)$.

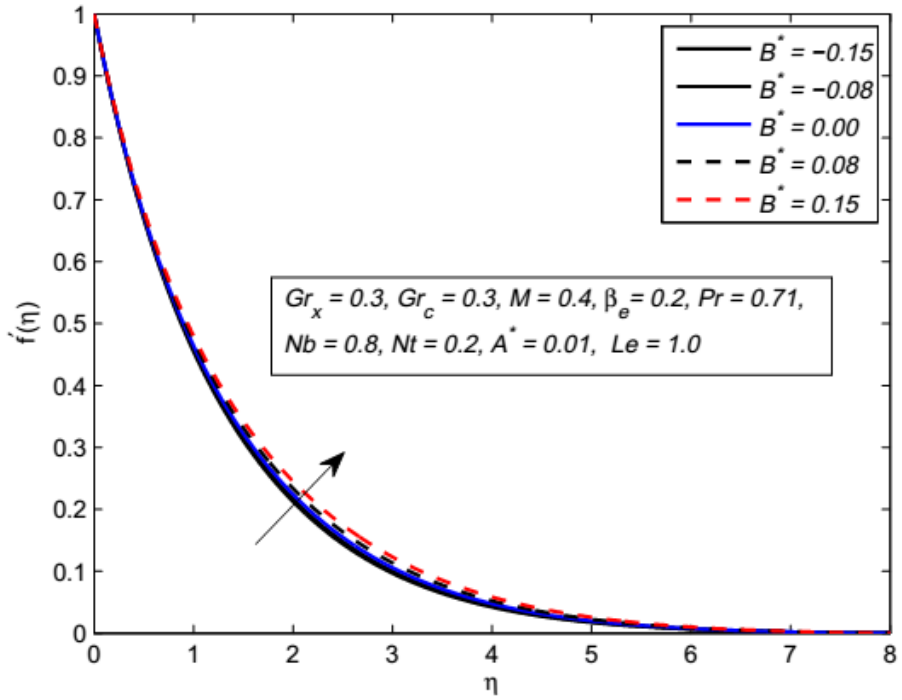

FIGURE 4.4: Influence of B^* on $f'(\eta)$.

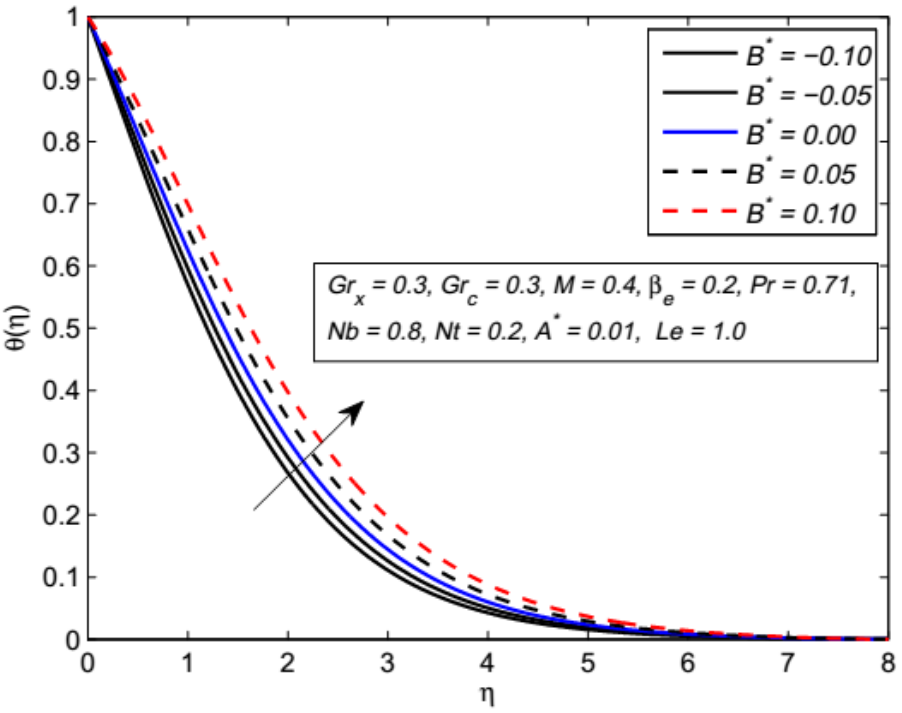

FIGURE 4.5: Influence of B^* on $\theta(\eta)$.

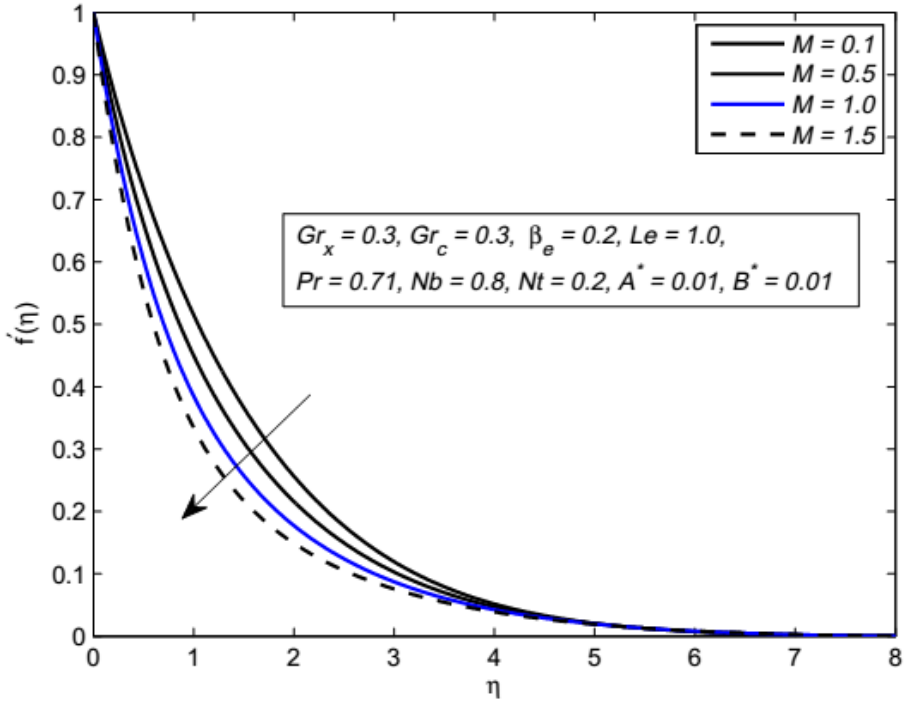

FIGURE 4.6: Influence of M on $f'(\eta)$.

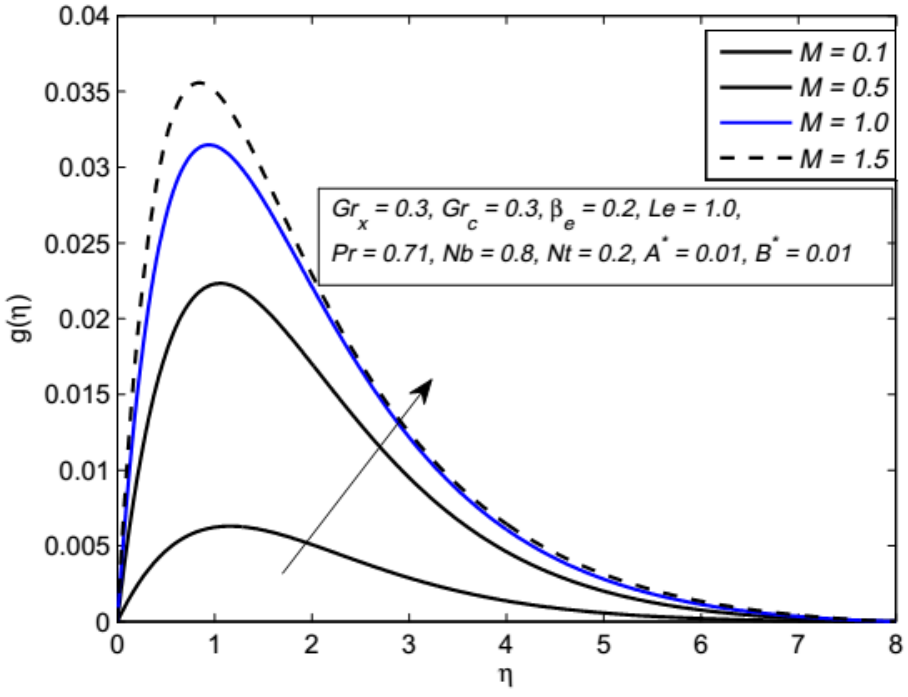

FIGURE 4.7: Influence of M on $g(\eta)$.

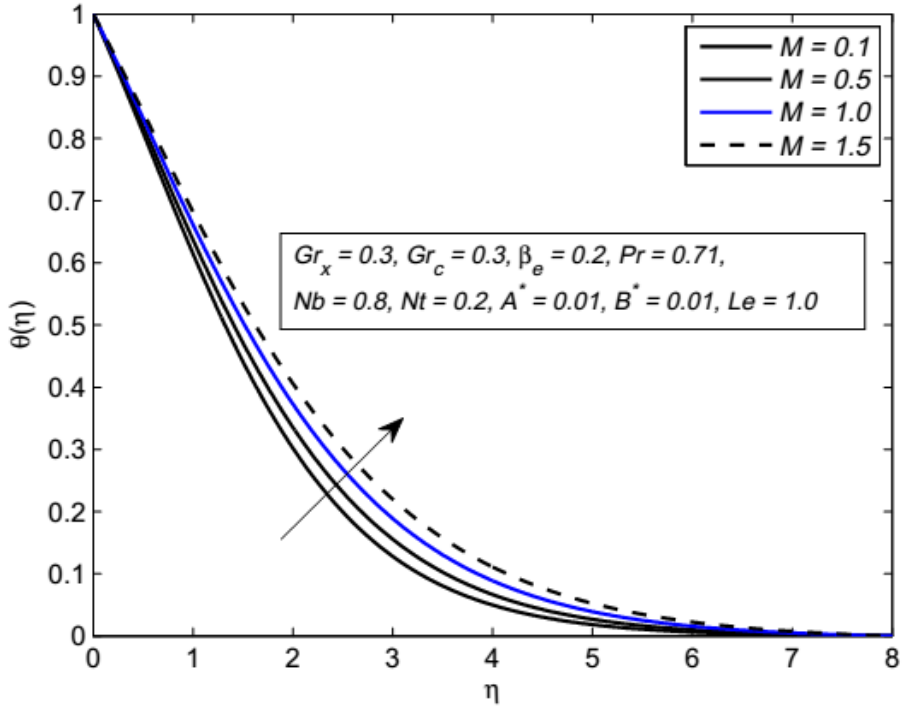

FIGURE 4.8: Influence of M on $\theta(\eta)$.

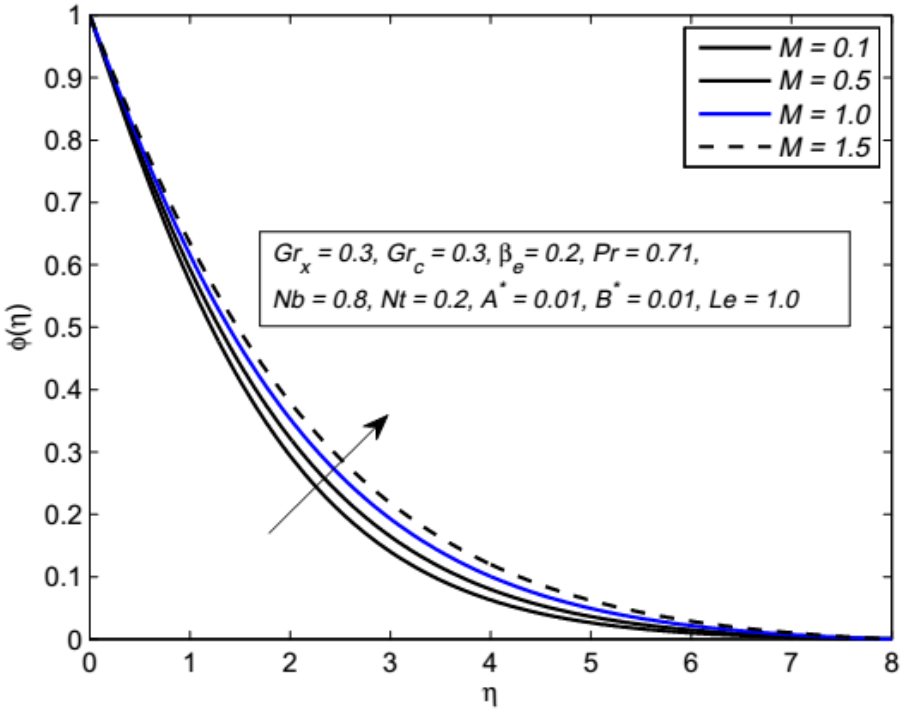

FIGURE 4.9: Influence of M on $\phi(\eta)$.

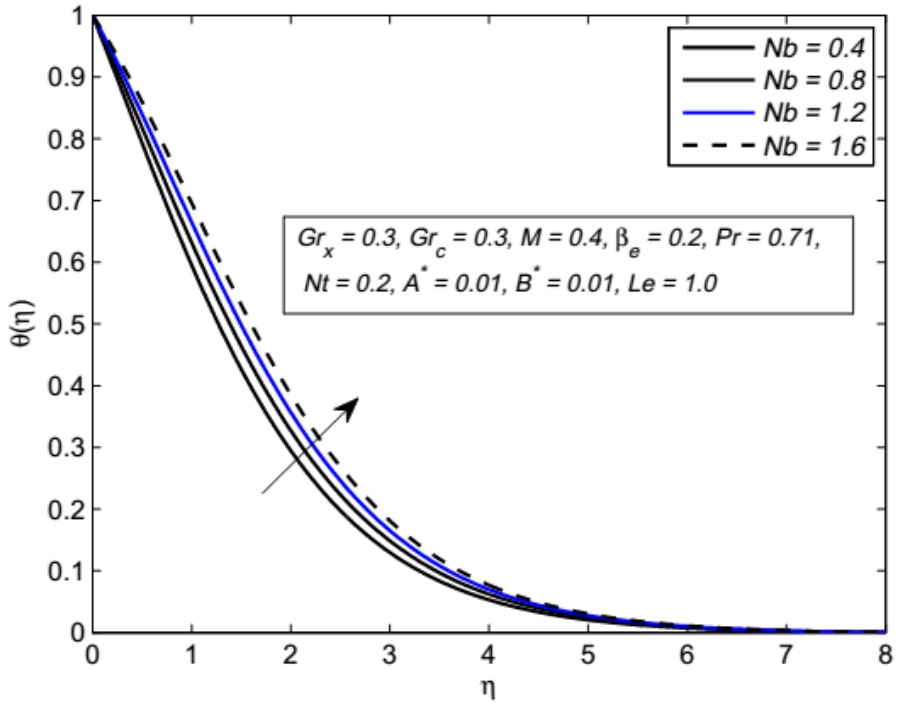

FIGURE 4.10: Influence of Nb on $\theta(\eta)$.

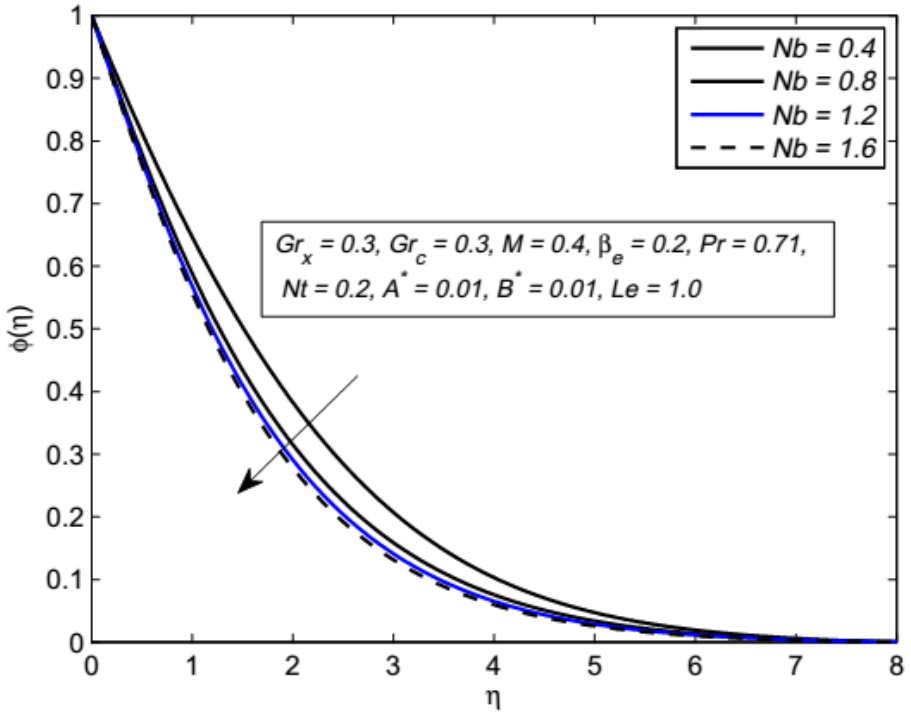

FIGURE 4.11: Influence of Nb on $\phi(\eta)$.

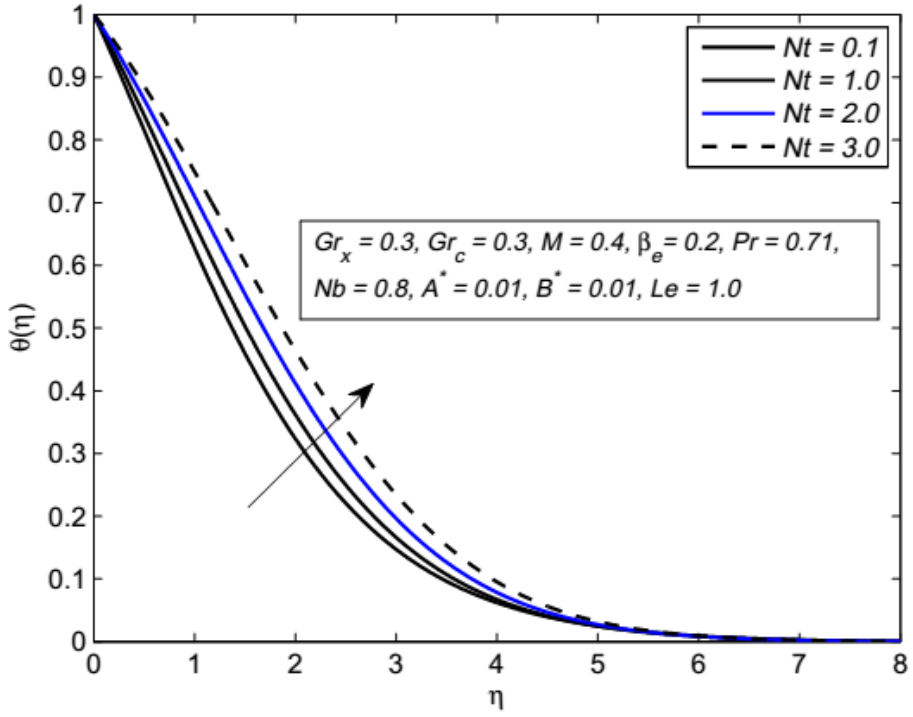

FIGURE 4.12: Influence of Nt on $\theta(\eta)$.

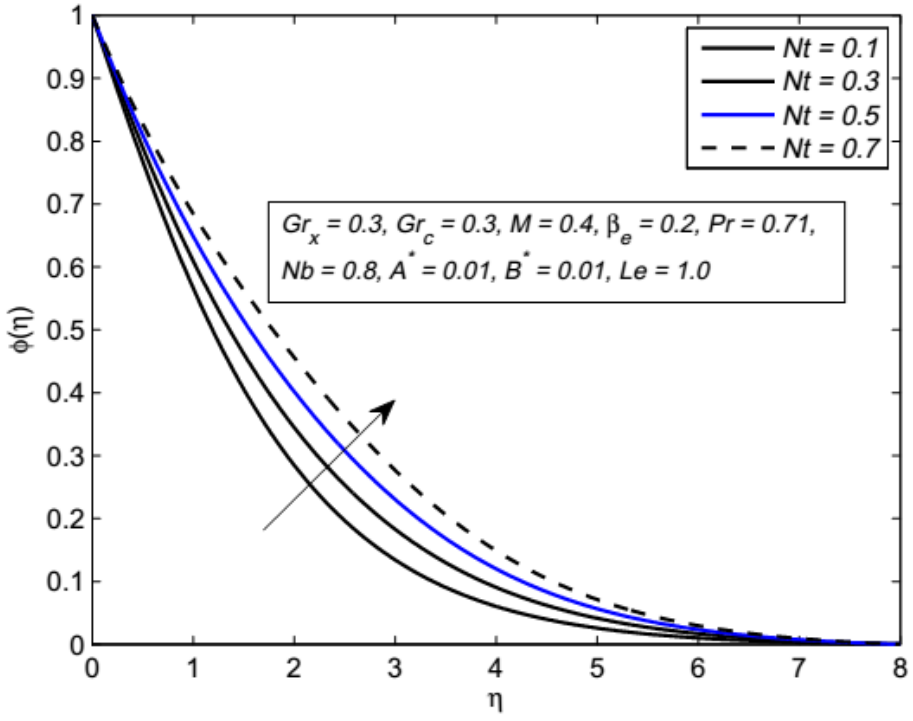

FIGURE 4.13: Influence of Nt on $\phi(\eta)$.

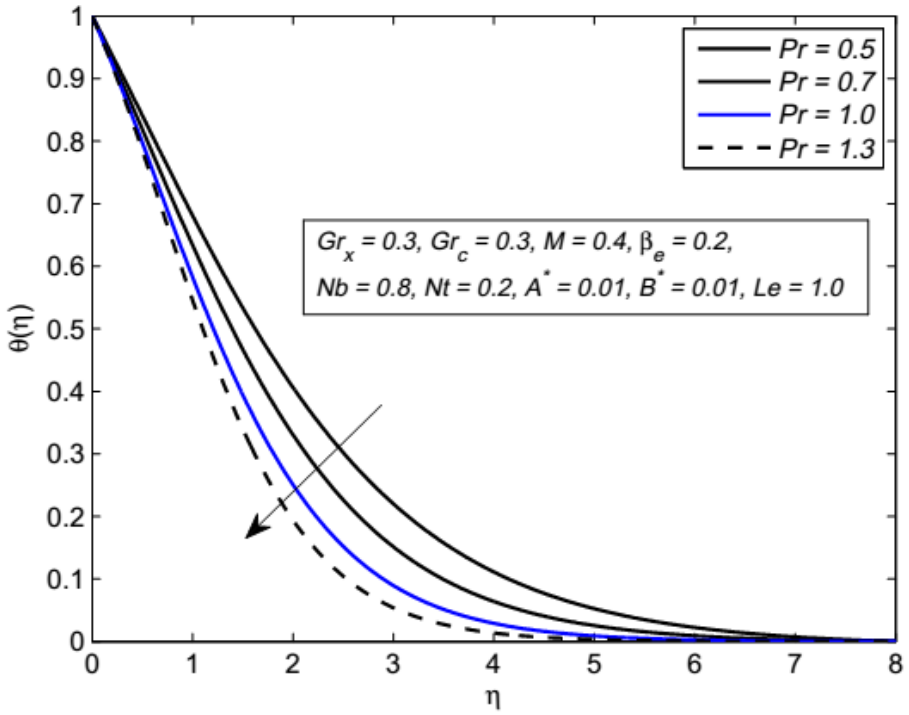

FIGURE 4.14: Influence of Pr on $\theta(\eta)$.

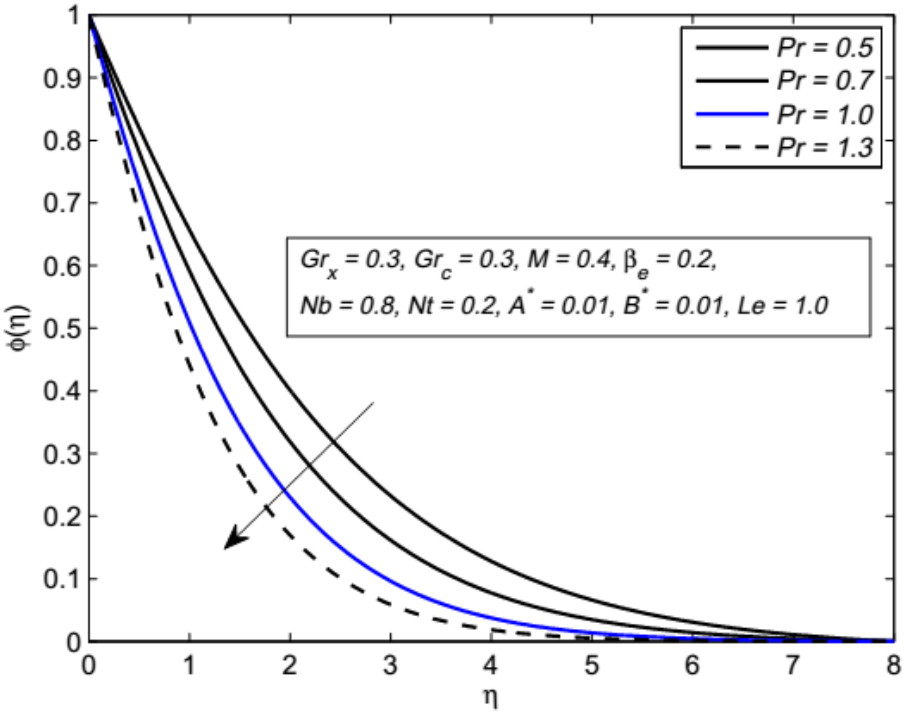

FIGURE 4.15: Influence of Pr on $\phi(\eta)$.

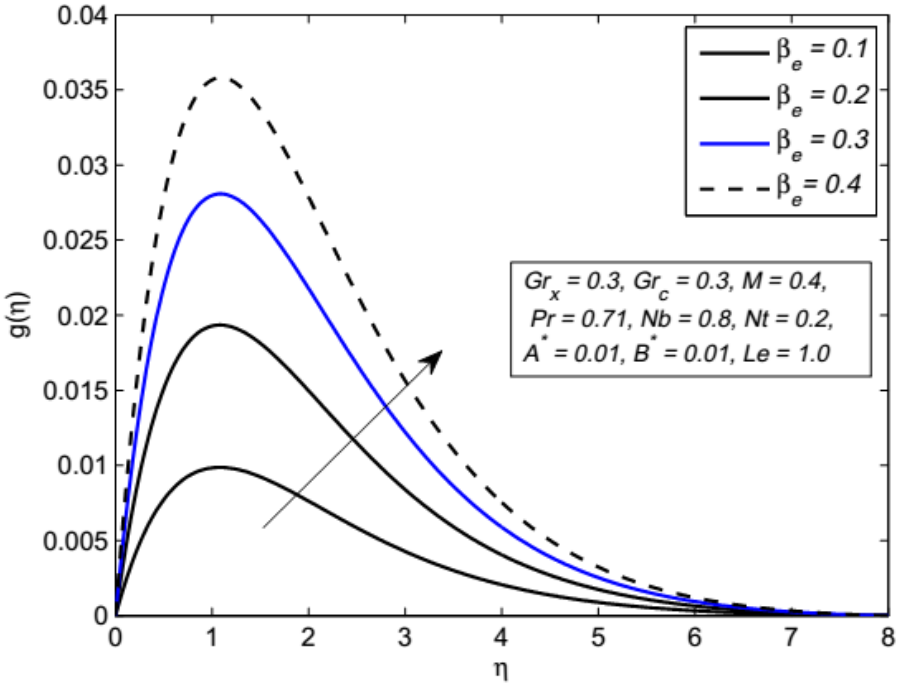

FIGURE 4.16: Influence of β_e on $f'(\eta)$.

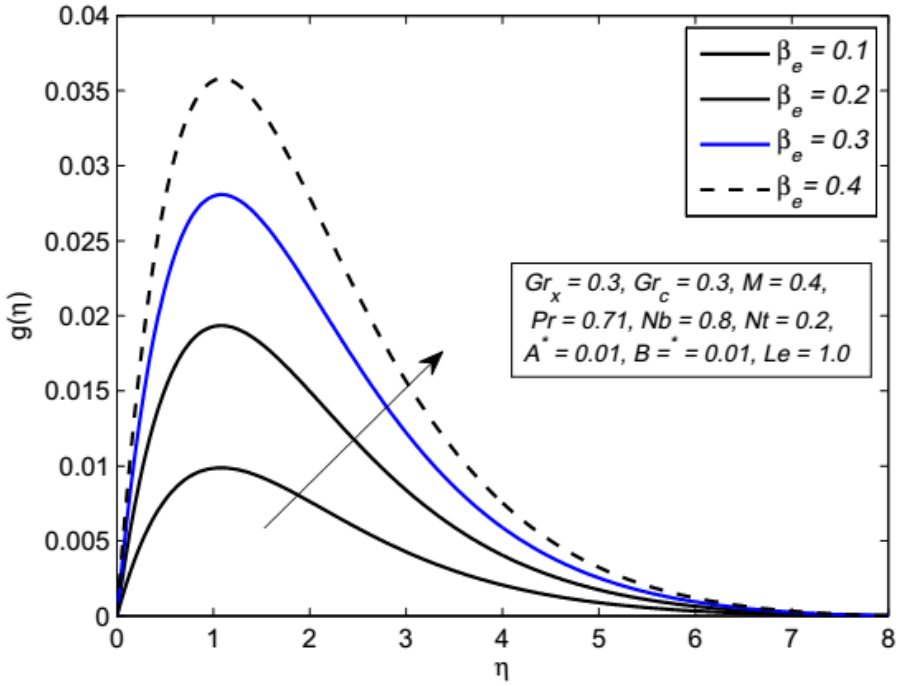

FIGURE 4.17: Influence of β_e on $g(\eta)$.

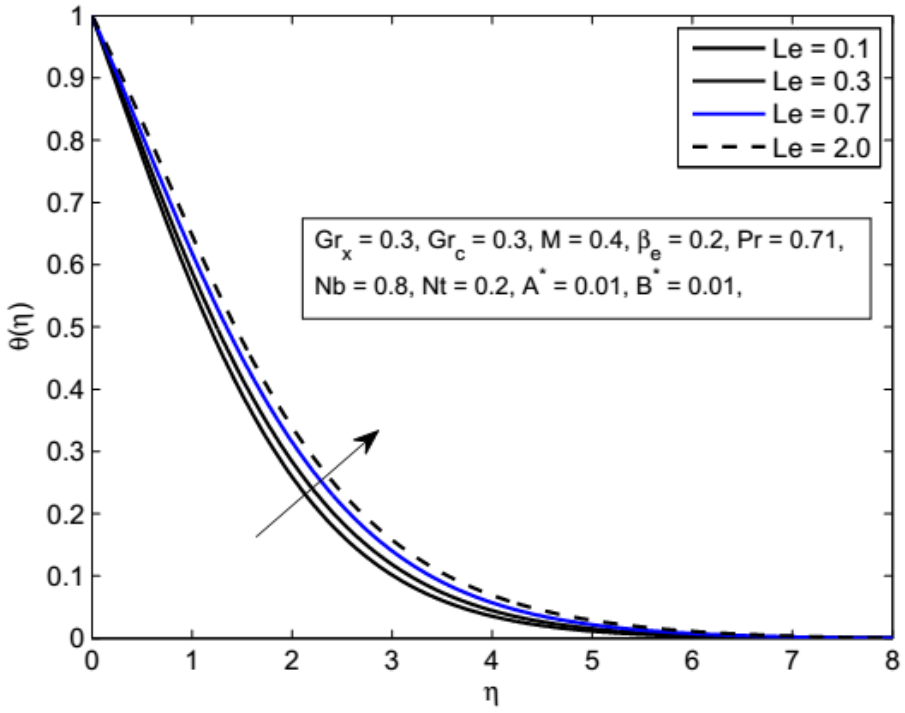

FIGURE 4.18: Influence of Le on $\theta(\eta)$.

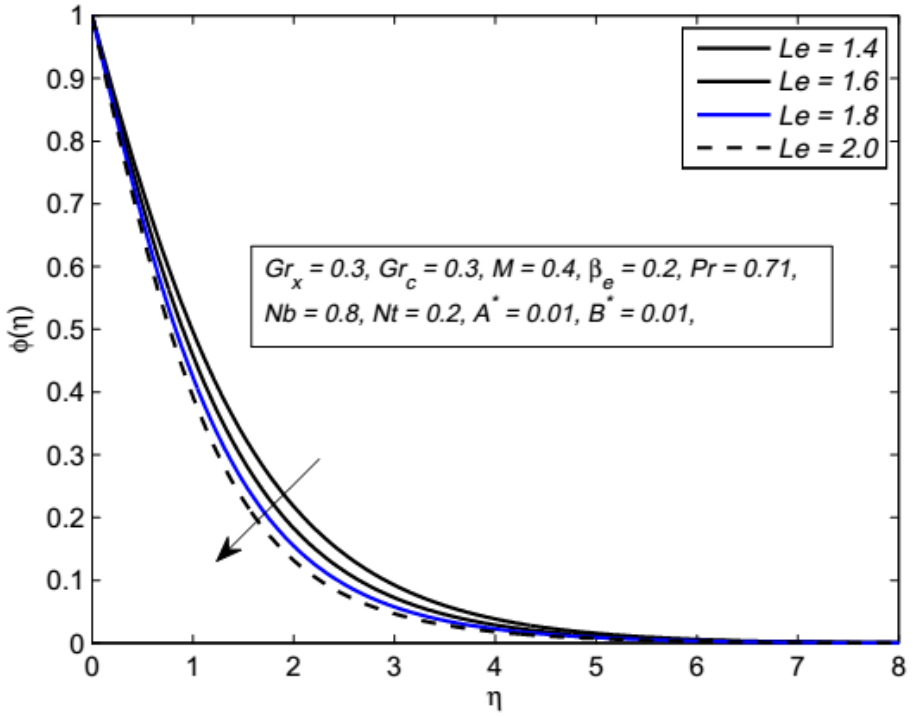

FIGURE 4.19: Influence of Le on $\phi(\eta)$.

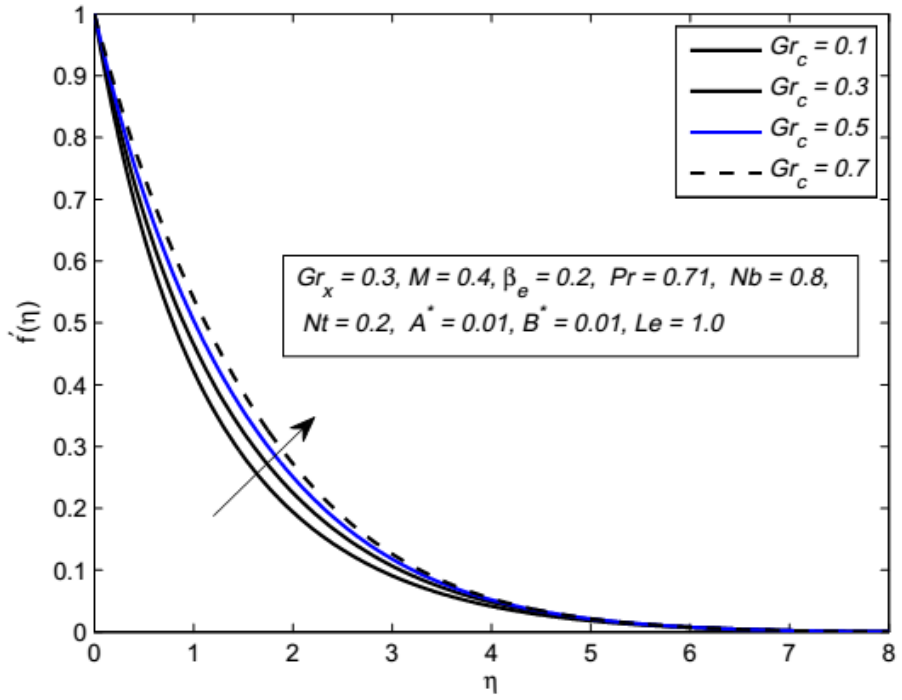

FIGURE 4.20: Influence of Gr_c on $f'(\eta)$.

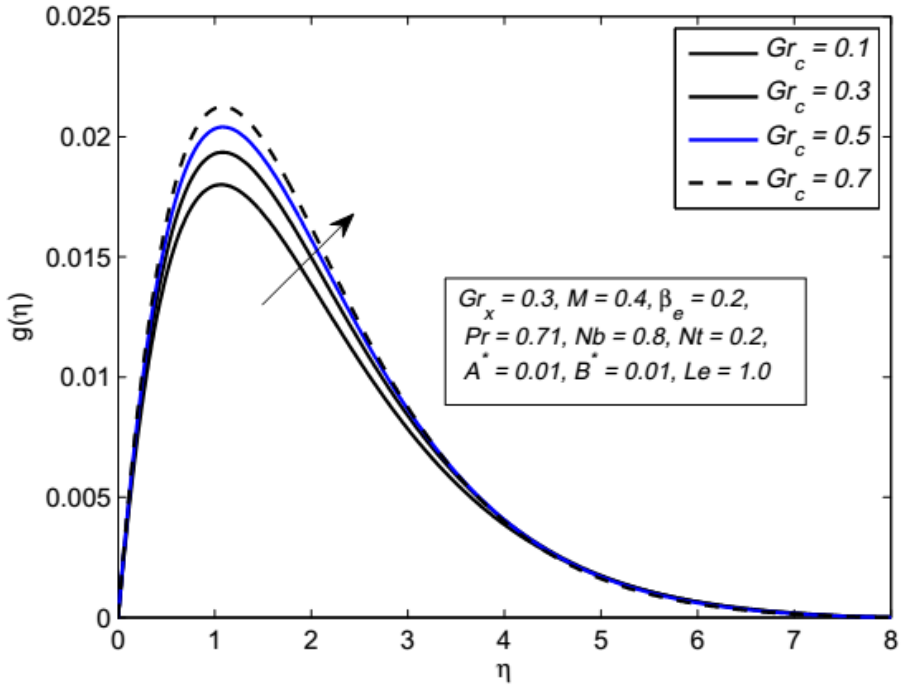

FIGURE 4.21: Influence of Gr_c on $g(\eta)$.

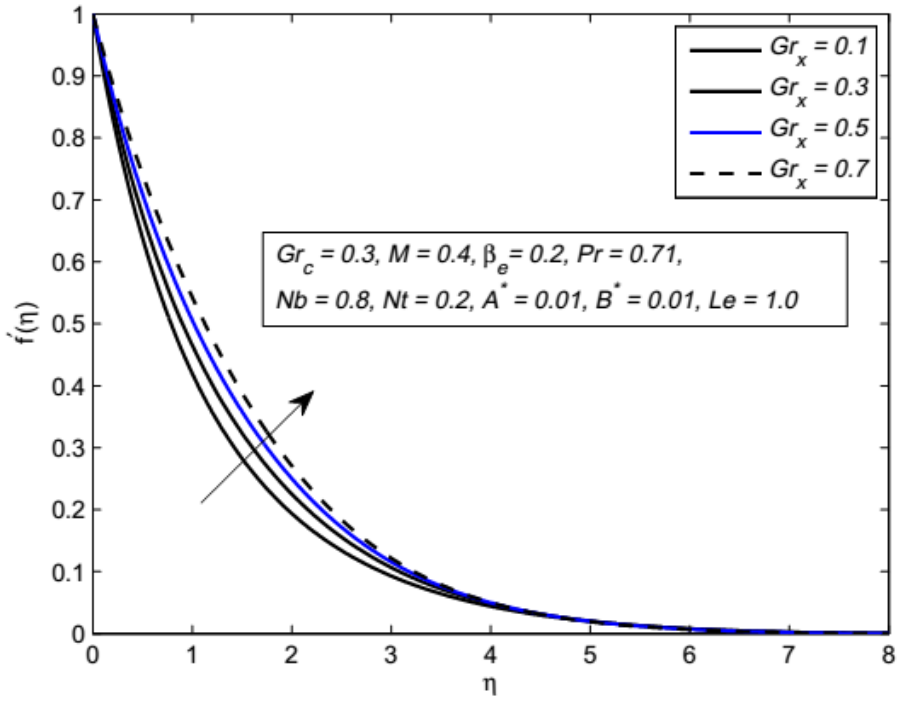

FIGURE 4.22: Influence of Gr_x on $f'(\eta)$.

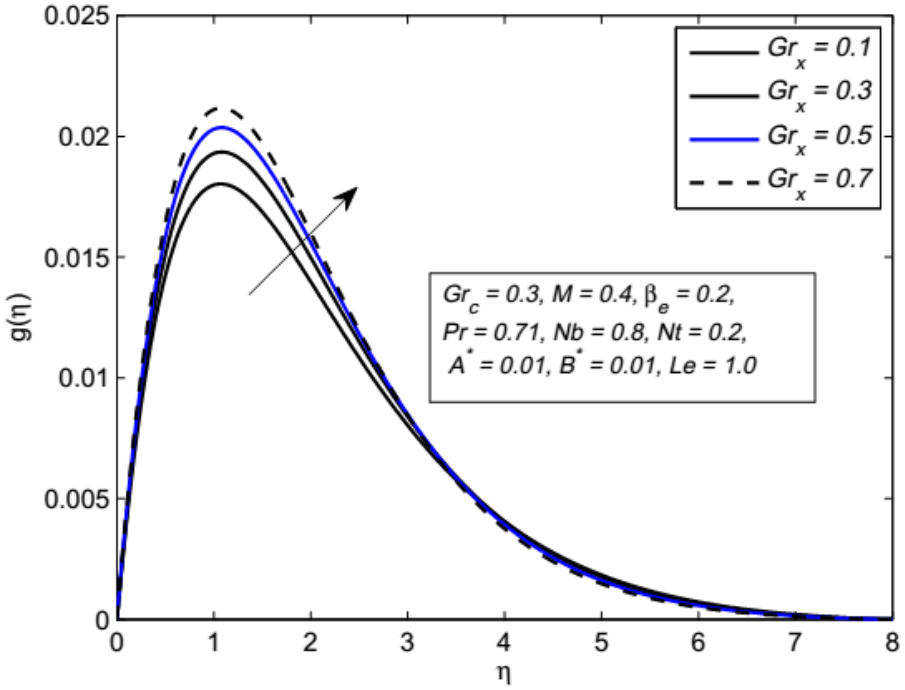

FIGURE 4.23: Influence of Gr_x on $g(\eta)$.

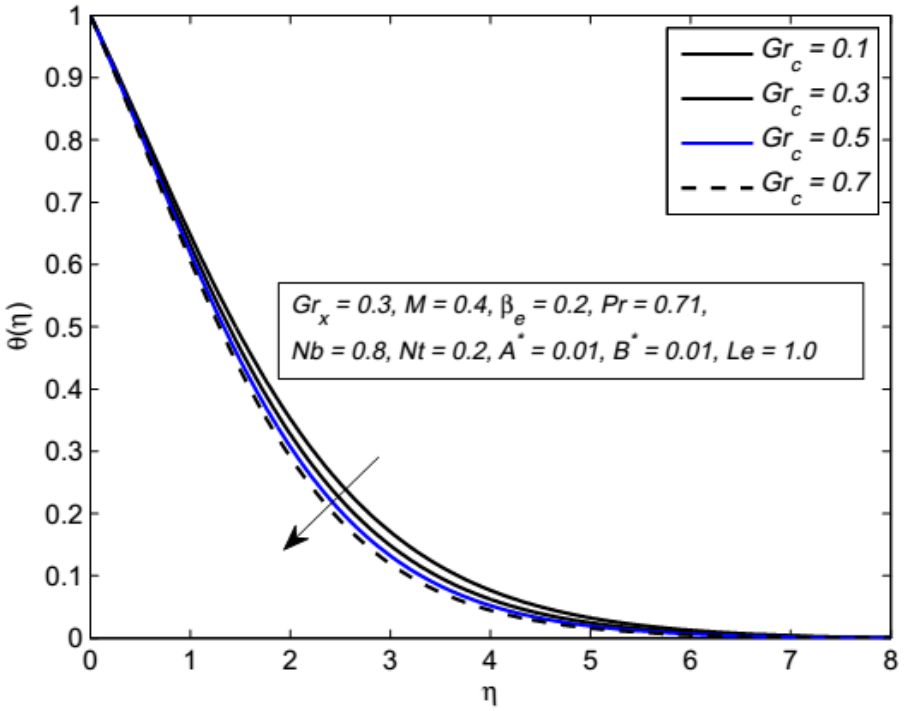

FIGURE 4.24: Influence of Gr_c on $\theta(\eta)$.

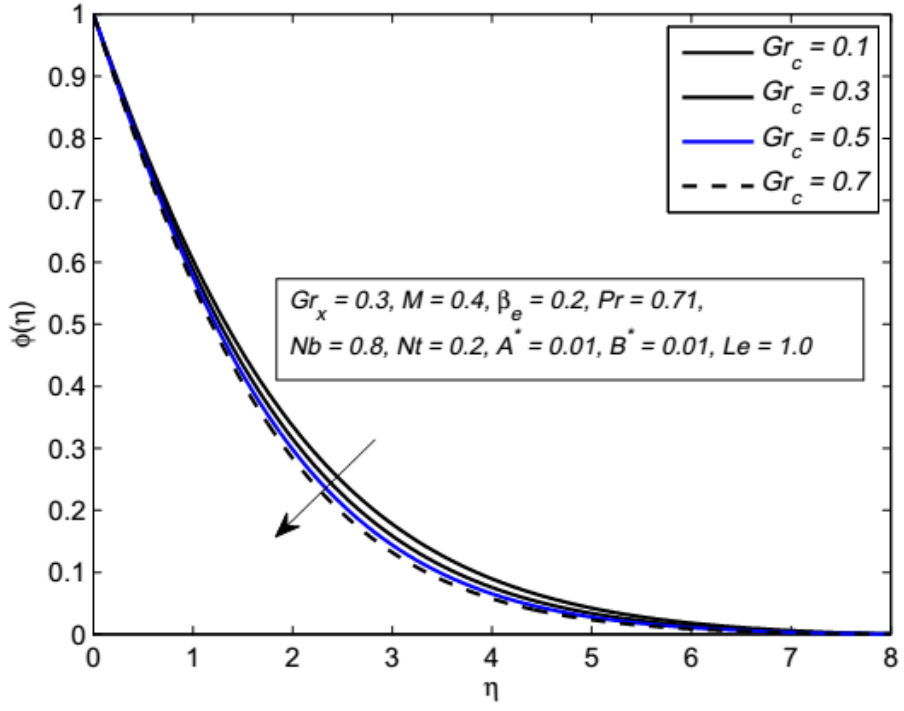

FIGURE 4.25: Influence of Gr_c on $\phi(\eta)$.

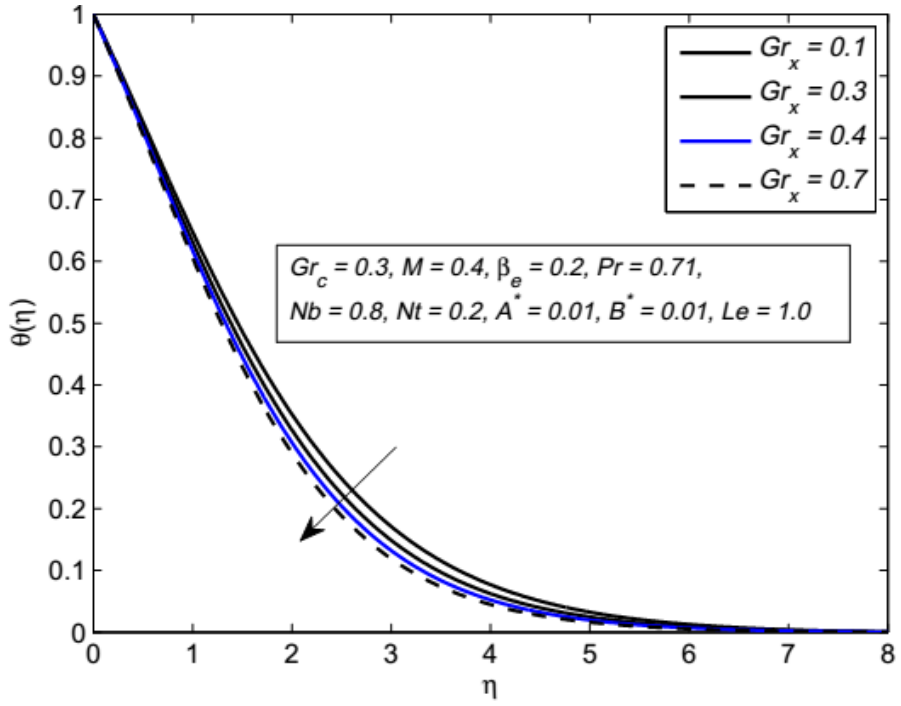

FIGURE 4.26: Influence of Gr_x on $\theta(\eta)$.

4.5 Concluding Remarks

In the present chapter, the impact of the Hall current on heat and mass transfer of nanofluid flowing over a linearly stretching sheet, is addressed. The main achievements have been summarized as follows.

- Prandtl number has a decreasing effect on the temperature and concentration profiles.
- The temperature $\theta(\eta)$ of the fluid is enhanced while increasing the thermophoresis parameter Nt and the Brownian motion parameter Nb.
- A stronger magnetic parameter M results in an increase in the temperature, concentration and transverse velocity.
- The boundary layer thickness increases when the space and the temperature dependent heat generation parameters A^* and B^* respectively, are increased.

- Increasing values of the Lewis number have the tendency to increase the temperature $\theta(\eta)$ and reduce the mass transfer.

- Wall shear stress decreases when the Hall current parameter β_e increases.

Chapter 5

Three Dimensional MHD Upper-Convected Maxwell Nanofluid Flow with Non-linear Radiative Heat Flux

5.1 Introduction

In this chapter, a three dimensional upper-convected Maxwell (UCM) nanofluid flow over a stretching surface, has been considered to examine the effects of nanoparticles and magnetohydrodynamics (MHD) on the heat and mass transfer. A non-linear radiative heat flux is incorporated in the formulation of the energy equation. Similarity transformation reduces the non-linear partial differential equations of the problem to the ordinary differential equations, which are then solved by the well known shooting technique through Runge-Kutta integration procedure of order four. To strengthen the reliability of our results, the MATLAB built-in function bvp4c is also used. The effects of some prominent parameters such as Brownian motion parameter, Prandtl number, thermophoresis parameter, magnetic parameter on the velocity, temperature and concentration

profiles are discussed graphically and numerically. It is witnessed that the flow velocity is a diminishing function of the linear and non-linear thermal radiation parameter. Moreover, mounting values of Brownian motion parameter reduce the nanoparticle concentration profile.

5.2 Problem Formulation

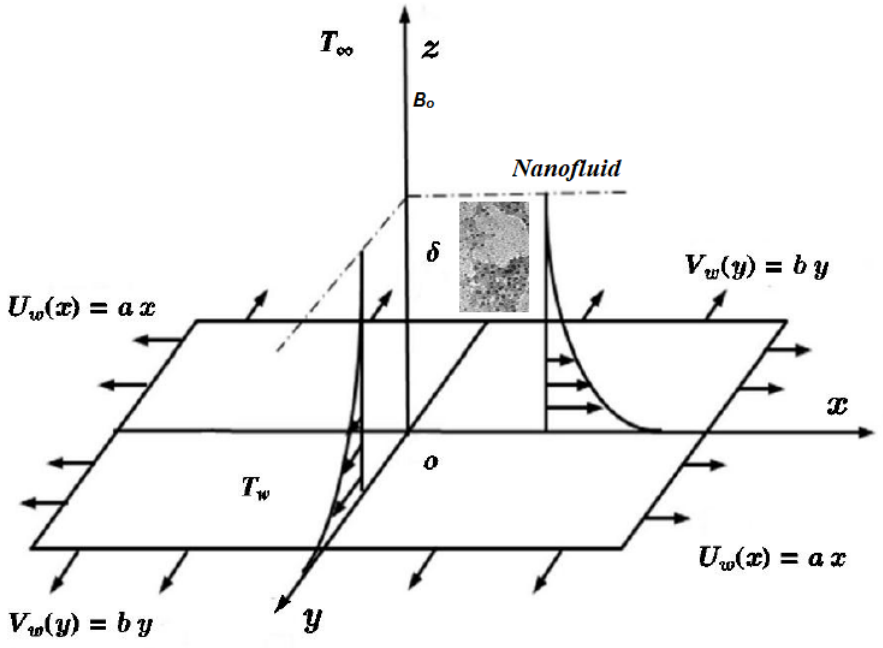

FIGURE 5.1: Geometry of the Problem.

A steady incompressible upper convected Maxwell nanofluid over a bilinear stretching surface in the positive xy-plane is considered to investigate the behavior of temperature and concentration. A uniform magnetic field of strength B_0 is applied normal to the flow i.e. in the $z-$direction. The induced magnetic field is ignored because of the assumption of the small Reynolds number. Applied magnetic field drags the magnetic field lines in the direction of the flow which interact with the induced current density to give rise a force known as the Lorentz force. Further, a non-linear thermal radiation is taken into account during the formulation of the energy equation. The stretching surface velocities in the x and y plane are considered as $U_w(x) = ax$ and $V_w(y) = by$ respectively as shown in Figure 5.1. The basic equations of the described problem for the velocity, temperature and

the nanoparticle concentration in the absence of viscous dissipation, Joule heating, mixed convection and chemical reaction [116–119] can be expressed as :

$$\frac{\partial u}{\partial x} + \frac{\partial v}{\partial y} + \frac{\partial w}{\partial z} = 0, \tag{5.1}$$

$$u\frac{\partial u}{\partial x} + v\frac{\partial u}{\partial y} + w\frac{\partial u}{\partial z} + \lambda\begin{pmatrix} u^2\frac{\partial^2 u}{\partial x^2} + v^2\frac{\partial^2 u}{\partial y^2} + w^2\frac{\partial^2 u}{\partial z^2} + \\ 2uv\frac{\partial^2 u}{\partial x\partial y} + 2uw\frac{\partial^2 u}{\partial x\partial z} + 2vw\frac{\partial^2 u}{\partial y\partial z} \end{pmatrix}$$
$$= \upsilon\frac{\partial^2 u}{\partial z^2} - \frac{\sigma B_0^2}{\rho}\left(u + \lambda w\frac{\partial u}{\partial z}\right), \tag{5.2}$$

$$u\frac{\partial v}{\partial x} + v\frac{\partial v}{\partial y} + w\frac{\partial v}{\partial z} + \lambda\begin{pmatrix} u^2\frac{\partial^2 v}{\partial x^2} + v^2\frac{\partial^2 v}{\partial y^2} + w^2\frac{\partial^2 v}{\partial z^2} + \\ 2uv\frac{\partial^2 v}{\partial x\partial y} + 2uw\frac{\partial^2 v}{\partial x\partial z} + 2vw\frac{\partial^2 v}{\partial y\partial z} \end{pmatrix}$$
$$= \upsilon\frac{\partial^2 v}{\partial z^2} - \frac{\sigma B_0^2}{\rho}\left(v + \lambda w\frac{\partial v}{\partial z}\right), \tag{5.3}$$

$$u\frac{\partial T}{\partial x} + v\frac{\partial T}{\partial y} + w\frac{\partial T}{\partial z} = \alpha\frac{\partial^2 T}{\partial z^2} - \frac{1}{\rho c_p}\frac{\partial q_r}{\partial z}$$
$$+ \tau\left(D_B\frac{\partial C}{\partial z}\frac{\partial T}{\partial z} + \frac{D_T}{T_\infty}\left(\frac{\partial T}{\partial z}\right)^2\right), \tag{5.4}$$

$$u\frac{\partial C}{\partial x} + v\frac{\partial C}{\partial y} + w\frac{\partial C}{\partial z} = D_B\frac{\partial^2 C}{\partial z^2} + \frac{D_T}{T_\infty}\frac{\partial^2 T}{\partial z^2}. \tag{5.5}$$

The corresponding boundary conditions for the governing PDEs are

$$\left.\begin{aligned} &u = u_w = ax,\ v = v_w = by,\ w = 0,\ T = T_w,\ C = C_w \text{ at } z = 0, \\ &u \to 0,\ v \to 0,\ T \to T_\infty,\ C \to C_\infty \text{ as } z \to \infty. \end{aligned}\right\} \tag{5.6}$$

In Eq. (5.4), Rosseland radiative heat flux q_r, is defined as [111, 120]:

$$q_r = \frac{4\sigma^*}{3\aleph}\frac{\partial T^4}{\partial z}. \tag{5.7}$$

For the conversion of the system of governing non-linear PDEs to system of ODEs, we use the following dimensionless variables [121]:

$$\left.\begin{aligned} &u = axf'(\eta), \quad v = ayg'(\eta), \quad w = -\sqrt{a\nu}\,(f(\eta) + g(\eta)), \\ &\theta(\eta) = \frac{T - T_\infty}{T_w - T_\infty}, \quad \phi(\eta) = \frac{C - C_\infty}{C_w - C_\infty}, \quad \eta = \sqrt{\frac{a}{\nu}}z. \end{aligned}\right\} \tag{5.8}$$

As we are considering non-linear thermal radiation, so T in (5.8) can be expressed as [120]:

$$T = T_\infty \left((\theta_w - 1)\, \theta + 1 \right). \tag{5.9}$$

Using Eq. (5.9) into Eq. (5.7), we obtain

$$q_r = -\frac{16\sigma^*}{3\aleph} T_\infty^3 \left((\theta_w - 1)\, \theta + 1 \right)^3 \frac{\partial T}{\partial z}, \tag{5.10}$$

where, $\theta_w = \frac{T_w}{T_\infty}$ is the temperature ratio parameter.
Eq. (5.1) is identically satisfied while Eqs. (5.2) to (5.5) are converted to the ordinary differential equations:

$$\begin{aligned} & f''' - f'^2 + \left(M^2\Lambda + 1\right)(f + g)f'' + 2\Lambda f'(f + g)\, f'' \\ & - \Lambda(f + g)^2 f''' - M^2 f' = 0, \end{aligned} \tag{5.11}$$

$$\begin{aligned} & g''' - g'^2 + \left(M^2\Lambda + 1\right)(f + g)g'' + 2\Lambda g'(f + g)\, g'' \\ & - (f + g)^2 g''' - M^2 g' = 0, \end{aligned} \tag{5.12}$$

$$\begin{aligned} & \theta'' + (4/3)\, Rd \left[(1 + (\theta_w - 1)\, \theta)^3 \theta'' + 3(\theta_w - 1)(1 + (\theta_w - 1)\, \theta)^2 \theta'^2 \right] \\ & + Pr\,(f + g)\, \theta' + PrNt\, \theta'^2 + PrNb\, \theta' \phi' = 0, \end{aligned} \tag{5.13}$$

$$\phi'' + \frac{Nt}{Nb}\, \theta'' + PrLe\,(f + g)\, \phi' = 0, \tag{5.14}$$

The transformed boundary conditions are:

$$\left.\begin{aligned} & f(0) = 0, \quad f'(0) = 1, \quad g(0) = 0, \quad g'(0) = c, \quad \theta(0) = 1, \quad \phi(0) = 1, \\ & f'(\eta) \to 0, \; g'(\eta) \to 0, \; \theta(\eta) \to 0, \; \phi(\eta) \to 0, \text{ as } \eta \to \infty, \end{aligned}\right\} \tag{5.15}$$

Different dimensionless parameters appearing in Eqs. (5.11)-(5.15) are defined as

$$\left.\begin{aligned} & \Lambda = \lambda a, \quad M = \frac{\sigma B_0^2}{\rho a}, \quad Pr = \frac{\nu}{\alpha} = \frac{\rho c_p \nu}{k}, \quad Rd = \frac{4\sigma^* T_\infty^3}{k\aleph}, \quad \theta_w = \frac{T_w}{T_\infty} \\ & Nb = \frac{\tau D_B}{\nu}(C_w - C_\infty), \quad Nt = \frac{D_T}{T_\infty}\frac{\tau}{\nu}(T_w - T_\infty), \quad Le = \frac{\alpha}{D_B}, \quad c = \frac{b}{a}. \end{aligned}\right\} \tag{5.16}$$

The important quantities of interest, local Nusselt and Sherwood numbers, are defined as

$$Nu_z = \frac{xq_w}{k\left(T_w - T_\infty\right)}, \qquad Sh_z = \frac{x\ j_w}{D_B\left(C_w - C_\infty\right)}. \tag{5.17}$$

Here, heat and mass fluxes are defined as

$$q_w = -k\left(\frac{\partial T}{\partial z}\right)_{z=0}, \qquad j_w = -D_B\left(\frac{\partial C}{\partial z}\right)_{z=0}. \tag{5.18}$$

The dimensionless form of Local Nusselt number and Sherwood number are:

$$Re_z^{-1/2}Nu_z = -[1 + 4/3Rd\theta_w^3]\theta'(0), \qquad Re_z^{-1/2}Sh_z = -\phi'(0). \tag{5.19}$$

5.3 Solution Methodology

The resulting system of non-linear ODEs (5.11) - (5.14) along with boundary conditions (5.15) is solved iteratively by the shooting method [93] for various values of different parameters. The results are validated by using MATLAB built-in function bvp4c. After performing numerous computational trials, we are taking [0, 7] as the domain of the problem rather than [0, ∞), as there are no substantial changes in the results after $\eta > 7$. We denote f by y_1, g by y_4, θ by y_7 and ϕ by y_9 for converting the boundary value problem (5.11) - (5.14) to the following initial value problem (IVP) consisting of 10 first order ordinary differential equations.

$$\left.\begin{aligned}
y_1' &= y_2 & y_1(0) &= 0,\\
y_2' &= y_3 & y_2(0) &= 1,\\
y_3' &= \tfrac{1}{1-K(y_1+y_4)^2}(y_2^2 - (M^2\Lambda+1)(y_1+y_4)y_3 \\
&\quad +2\Lambda y_2 y_3(y_1+y_4) + M^2 y_2) & y_3(0) &= \varrho_1,\\
y_4' &= y_5 & y_4(0) &= 0,\\
y_5' &= y_6 & y_5(0) &= c,\\
y_6' &= \tfrac{1}{1-K(y_1+y_4)^2}(y_5^2 - (M^2\Lambda+1)(y_1+y_4)y_6 \\
&\quad -2\Lambda y_5 y_6(y_1+y_4) + M^2 y_5) & y_6(0) &= \varrho_2,
\end{aligned}\right\}$$

$$\left.\begin{aligned}
y_7' &= y_8 && y_7(0) &&= 1\ , \\
y_8' &= \tfrac{-3y_8}{3+4Rd(1+(\theta_w-1)y_7)^3}\left(4Rd\left(\theta_w-1\right)\left(1+\left(\theta_w-1\right)y_7\right)^2 y_8\right. \\
&\quad \left.+Pr((y_1+y_4)+Nty_8+Nby_{10})\right. && y_8(0) &&= \varrho_3, \\
y_9' &= y_{10} && y_9(0) &&= 1, \\
y_{10}' &= -PrLe\left(y_1+y_4\right)y_{10}-\tfrac{Nt}{Nb}y_8' && y_{10}(0) &&= \varrho_4.
\end{aligned}\right\} \tag{5.20}$$

To solve the above initial value problem arising in the shooting method, Runge Kutta method of order four is used. Classical Newton method is applied for the refinement of initial guesses ϱ_1, ϱ_2, ϱ_3 and ϱ_4 subject to the tolerance of $\varepsilon = 10^{-7}$. The stoping criteria for the iterative process is set as

$$\max\left\{\left|y_2(7)-0\right|,\left|y_5(7)-0\right|,\left|y_7(7)-0\right|,\left|y_9(7)-0\right|\right\} < \varepsilon. \tag{5.21}$$

5.4 Results and Discussions

The results obtained by the shooting method and bvp4c are almost the same but still for more satisfaction, we feel a need to validate our MATLAB code by implementation on some published work of similar nature. For this purpose, we reproduced the numerical values of the Nusselt number for the model investigated by Mushtaq et al. [14]. They have incorporated the shooting method with RK-4 integration scheme. An impressively convincing agreement of our results with those of Mushtaq et al. can be seen in Table 5.1. Numerical results of the local Nusselt and Sherwood numbers for various values of different parameters are tabulated in Table 5.2. From Table 5.2, it is observed that the rate of heat flux decreases for the increasing values of Deborah number Λ and magnetic parameter M. It happens due to the fact that an increase in the magnetic parameter will enhance the Lorentz force which slows down the motion of the fluid and resultantly the rate of heat flux is reduced. The same phenomenon is observed for the increasing value of Λ and M for the case of Sherwood number $\phi'(0)$. An increment is observed in the rate of the heat flux for the thermal radiation parameter Rd, the temperature ratio

parameter θ_w and the stretching ratio c. Similarly for temperature ratio parameter θ_w, thermal radiation parameter Rd and stretching ratio c, a decreasing trend is noticed for the mass transfer rate. The influence of the thermophoresis parameter Nt, Brownian motion parameter Nb, Prandtl number Pr, and the Lewis number Le on the rate of heat and mass transfer is also shown in Table 5.2. From the numerical values, it is noticeable that Nt, Nb and Le have a decreasing effect on Nusselt number while this increases for the increasing values of Prandtl number. On the other hand, Sherwood number decreases for the increasing thermophoresis parameter Nt, however the rate of mass transfer enhances for the increasing values of Nb, Pr and Le.

To visualize the effect of different physical parameters on velocity $f'(\eta)$, temperature $\theta(\eta)$ and nanoparticle concentration profiles $\phi(\eta)$, Figures 5.2–5.21 are plotted. Figures 5.2 and 5.3 reflect the impact of the Deborah number Λ, which is a ratio of the fluid relaxation time to its characteristic time scale on the velocity profiles. When the shear stress is applied on the fluid, the time in which it gains its equilibrium position is called relaxation time. This time is higher for the fluids having high viscosity. So an increase in the Deborah number may increase the viscosity of the fluid and hence the velocity decreases as shown in Figures 5.2 and 5.3. The fluid becomes Newtonian if we consider $\Lambda = 0$ and its viscosity gradually increases with an increase in the Deborah number Λ. From Figure 5.3, it is also concluded that boundary layer thickness reduces for the upper convected Maxwell fluid. When Λ is increased, the hydrodynamic boundary layer thickness decreases. In Figures 5.4 and 5.5, the effect of the variation in the Deborah number on the temperature $\theta(\eta)$ and the nanoparticle concentration $\phi(\eta)$ is displayed respectively. It is observed that the temperature and the concentration increase with an increase in the relaxation time. From this observation, we can conclude that the elastic force promotes the heat and the mass transfer in the upper-convected Maxwell nanofluid.

Figures 5.6 and 5.7 depict the typical profiles of velocity and temperature for the magnetic parameter M. By increasing the magnetic parameter M, a drag force known as the Lorentz force also increases which resultantly reduces the velocity

of the fluid and hence the rate of heat transfer is reduced and this leads to an increment in the temperature. To see the variation in the temperature profile against the increasing values of the Prandtl number Pr, Figure 5.8 is plotted in which the increasing values of Prandtl number result in a thinner temperature boundary layer thickness. Fluids having larger Prandtl number have lower thermal diffusivity, and hence the temperature decreases. The same decreasing trend of Pr number on the mass concentration profile is observed in Figure 5.9.

Figure 5.10 shows the influence of the thermal radiation parameter Rd on the velocity profile for linear and non-linear radiation. From this figure, it is seen that flow decreases with the increasing value of Rd. Here it is noticeable that there is no variation in the flow velocity for the linear radiation ($\theta_w = 1.0$) and the non-linear radiation ($\theta_w = 1.3$). In Figures 5.11 and 5.12, the effect of the thermal radiation parameter Rd on the temperature and nanoparticle concentration profiles, both for linear and non-linear radiation, is displayed. It is observed that $\theta(\eta)$ and $\phi(\eta)$ both have decreasing trend for the increasing values of Rd. It is also observed that a decrease in the temperature and concentration is lower in non-linear radiation case ($\theta_w = 1.3$) as compared to the linear radiation case ($\theta_w = 1.0$). In Figure 5.13, the variation of θ_w is studied for the temperature profile. From the figure, it is analyzed that the temperature moves upward for the increasing values of the temperature ratio parameter θ_w. Figure 5.14 shows the effect of the Lewis number Le on the concentration profile. A decrement in the concentration profile is analyzed against the higher values of the Lewis number and as a result a minor molecular diffusivity and emaciated concentration boundary layer is observed. Figures 5.15 and 5.16 demonstrate the influence of the stretching ratio parameter c on the velocity profiles f' and g' respectively. The displayed sketch shows that f' diminishes and g' enhances when the stretching ratio parameter c escalates. It can be validated from the relation $c = \frac{b}{a}$ that increasing the value of c implies the stretching along the $y-$axis is more rapid as compared to $x-$axis. So the velocity along the $y-$axis seems to be increasing whereas it decreases along the $x-$axis. In Figure 5.17, temperature of the fluid reduces with the increasing value of the stretching ratio parameter c.

Temperature is enhanced when the Brownian motion parameter Nb is increased. Larger the Brownian motion parameter, lower the viscous force and higher the Brownian diffusion coefficient which results an enhancement in the thermal boundary layer thickness and temperature and this phenomenon can be observed in Figure 5.18. From Figure 5.19, it is observed that the nanoparticle concentration decreases with an increment in Nb. The effect of thermophoresis parameter Nt on the temperature and the nanoparticle concentration is displayed in Figures 5.20 and 5.21 respectively. Thermophoresis parameter depends on the thermal diffusion coefficient and the viscous force. This viscous force is inversely proportional to Nt, so an enhancement in the thermophoresis parameter Nt implies a reduction in the viscous force and increment in the thermal diffusion coefficient which resultantly enhances the temperature and the nanoparticle concentration.

			$Rd = 0.0$		$Rd = 1.0$					
			$\theta_w = 0$		$\theta_w = 0$		$\theta_w = 1.1$		$\theta_w = 1.5$	
Λ	c	Pr	Ref. [14]	Present	Ref. [14]	Present	Ref.[14]	Present	Ref.[14]	Present
1	0.5	2	1.01695	1.01694	0.61177	0.61271	0.53932	0.53950	0.31686	0.31709
		4	1.60165	1.60165	1.01695	1.01694	0.90348	0.90348	0.55107	0.55106
		7	2.24393	2.24392	1.47271	1.47270	1.31435	1.31435	0.82083	0.82083
		10	2.75508	2.75507	1.83692	1.83692	1.64284	1.64283	1.03739	1.03739
1	0	7	1.82603	1.82602	1.20254	1.20253	1.07372	1.07371	0.67255	0.67254
	0.3		2.09403	2.09402	1.37824	1.37823	1.23051	1.23050	0.77013	0.77013
	0.6		2.31293	2.31292	1.51544	1.51543	1.35219	1.36099	0.84341	0.84340
	1		2.55918	2.55918	1.66440	1.66441	1.48361	1.48362	0.92038	0.92040
0	0.5	7	2.35436	2.35435	1.59321	1.59225	1.42760	1.42759	0.91088	0.91087
0.5			2.29665	2.29664	1.53021	1.53020	1.36840	1.36840	0.86380	0.86380
1.0			2.24393	2.24392	1.47271	1.47270	1.31435	1.31435	0.82083	0.82083
1.5			2.19501	2.19500	1.41998	1.42007	1.26482	1.26492	0.78170	0.78182

TABLE 5.1: Comparison of the presently computed values of wall temperature gradient $-\theta'(0)$ with those of Mushtaq et al. [14]

									$Nu_z Re_z^{-1/2}$		$Sh_z Re_z^{-1/2}$	
Λ	M	Rd	θ_w	c	Nt	Nb	Pr	Le	shooting	bvp4c	shooting	bvp4c
1.0	0.2	1.0	1.5	0.5	0.8	0.2	2.0	1.0	1.15466	1.15467	0.60558	0.60557
0									1.48631	1.48631	0.71205	0.71205
0.4									1.32518	1.32517	0.64011	0.64011
0.6									1.25997	1.25997	0.62158	0.62158
	0.4								1.12955	1.12955	0.60388	0.60388
	0.7								1.06936	1.06935	0.60331	0.60332
	1.0								0.99669	0.99669	0.60910	0.60910
		0.4							0.88525	0.88525	0.27462	0.27463
		0.6							0.99209	0.99210	0.40982	0.40981
		1.0							1.15466	1.15467	0.60558	0.60557
			1.1						0.93546	0.93546	0.22320	0.22320
			1.3						1.04641	1.04642	0.43067	0.43067
			1.5						1.15466	1.15467	0.60558	0.60557
				0.2					1.07374	1.07373	0.58254	0.58254
				0.3					1.10441	1.10441	0.59053	0.59054
				0.4					1.13110	1.13110	0.59824	0.59823
					0.5				1.22537	1.22536	0.73009	0.73010
					0.6				1.20118	1.20117	0.68494	0.68495
					0.7				1.17761	1.17761	0.64346	0.64345
						0.3			1.11733	1.11734	0.75525	0.75525
						0.4			1.08121	1.08122	0.82974	0.82973
						0.5			1.04625	1.04625	0.87416	0.87416
							1.0		0.82197	0.82197	0.51519	0.51519
							1.5		0.98939	0.98939	0.54706	0.54705
							2.0		1.15466	1.15467	0.60558	0.60557
								0.8	1.16125	1.16125	0.43720	0.43720
								1.0	1.15466	1.15467	0.60558	0.60557
								1.2	1.14992	1.14993	0.76043	0.76043

TABLE 5.2: Numerical values of local Nusselt number and Local Sherwood number

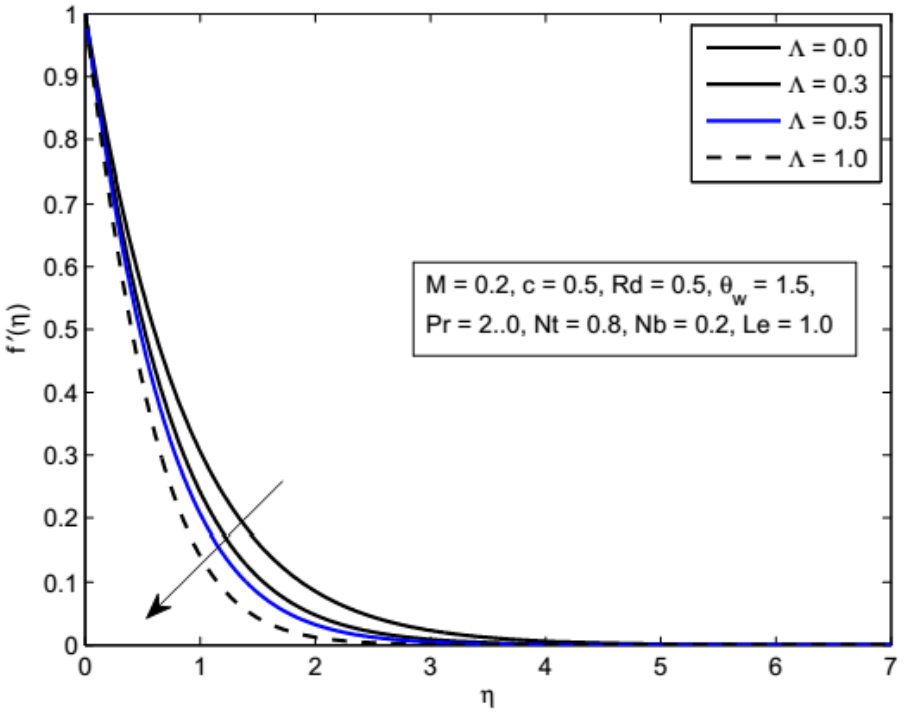

FIGURE 5.2: Influence of Λ on $f'(\eta)$.

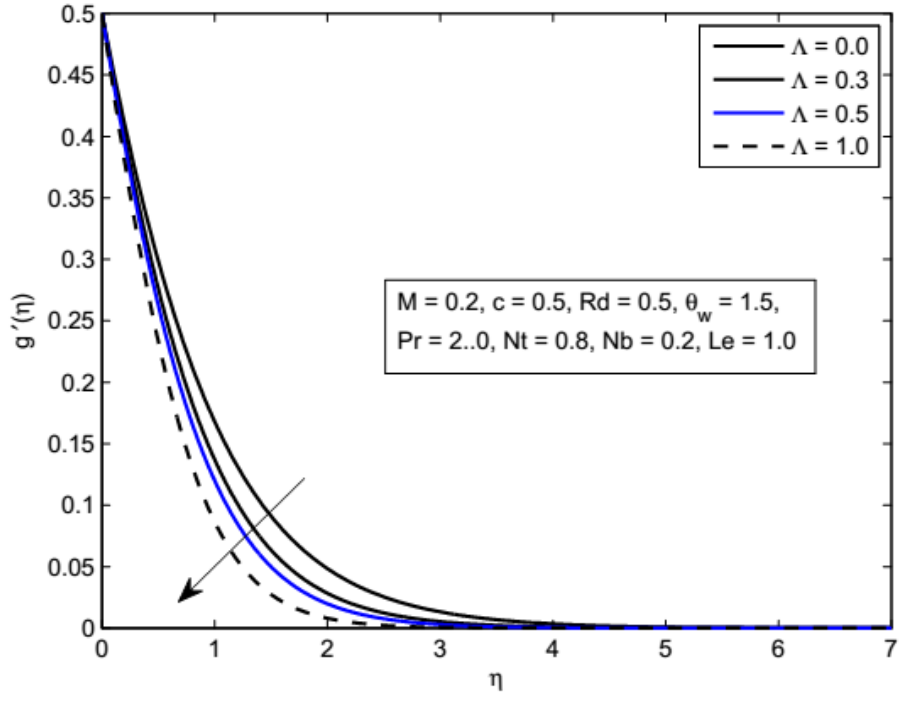

FIGURE 5.3: Influence of Λ on $g'(\eta)$.

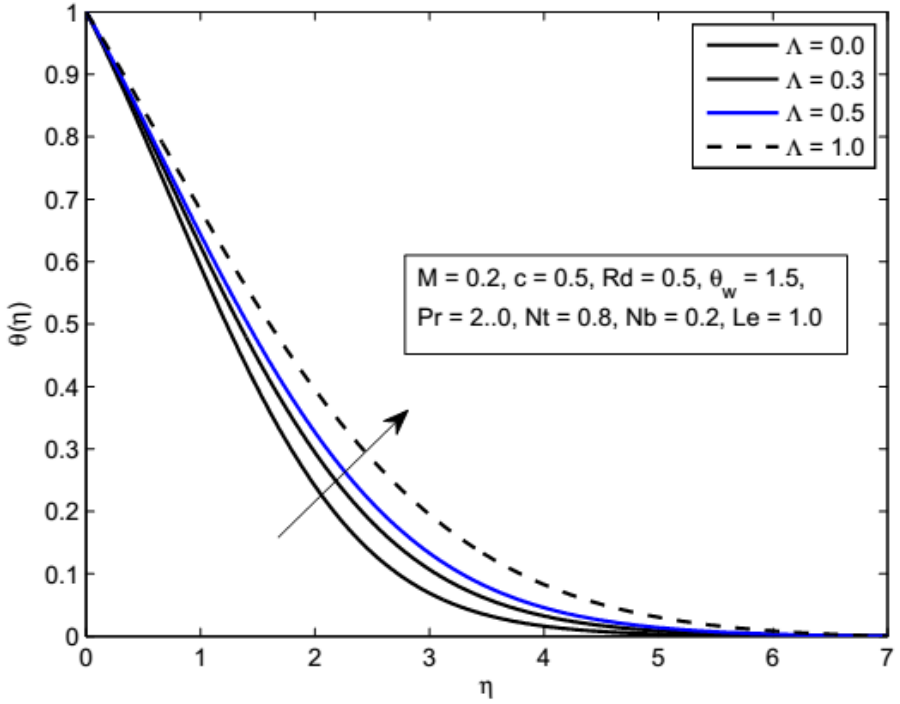

FIGURE 5.4: Influence of Λ on $\theta(\eta)$.

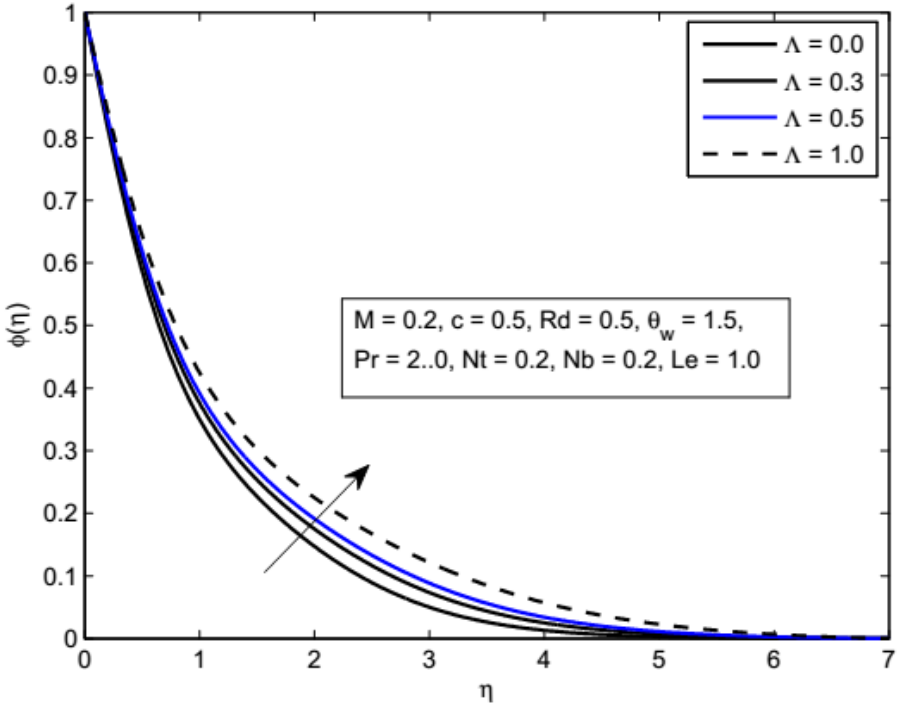

FIGURE 5.5: Influence of Λ on $\phi(\eta)$.

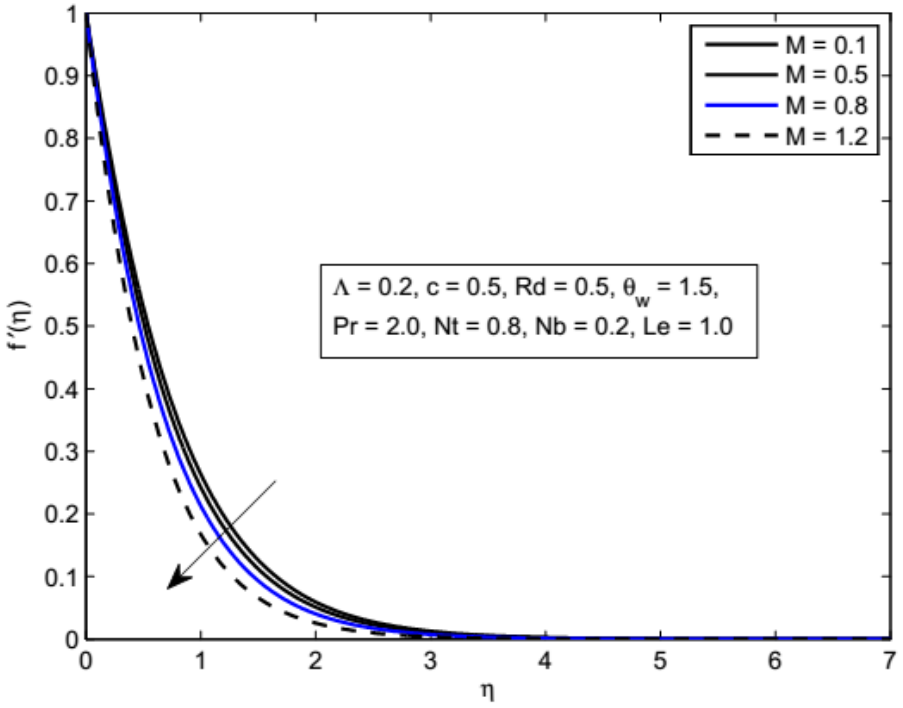

FIGURE 5.6: Influence of M on $f'(\eta)$.

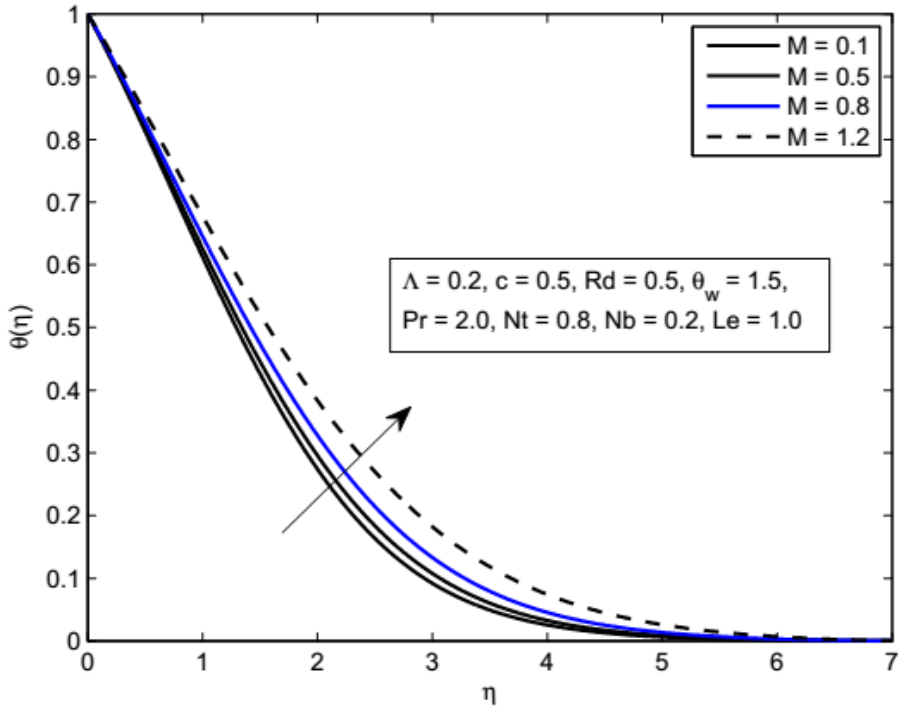

FIGURE 5.7: Influence of M on $\theta(\eta)$.

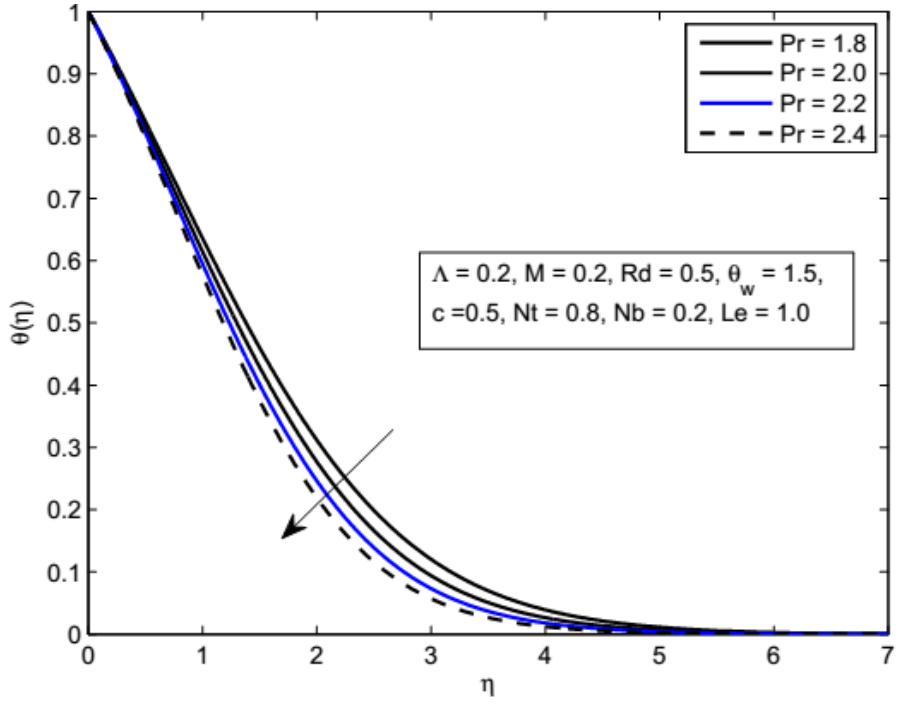

FIGURE 5.8: Influence of Pr on $\theta(\eta)$.

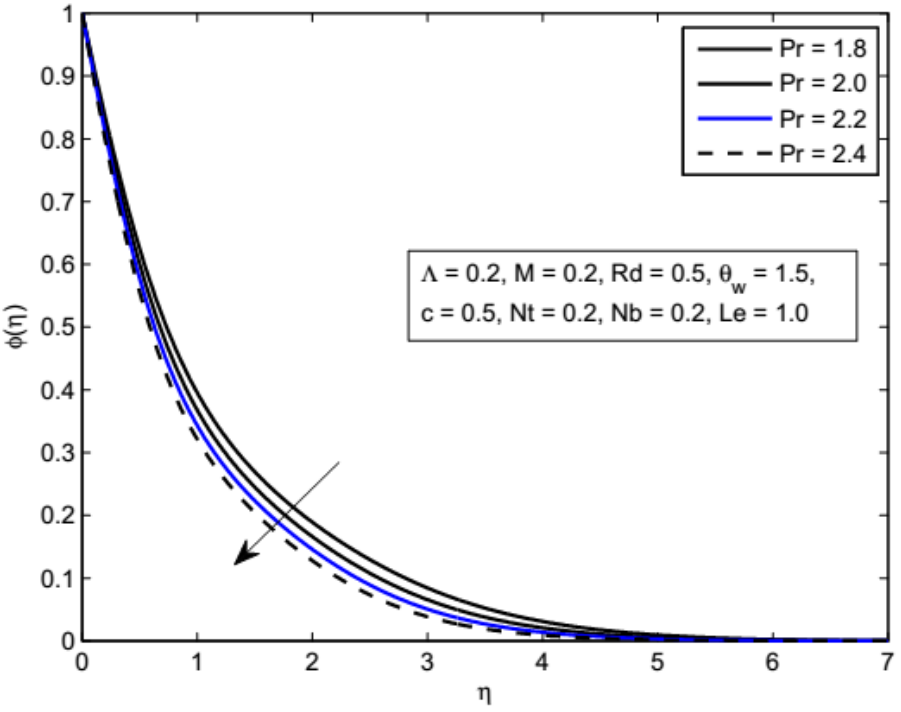

FIGURE 5.9: Influence of Pr on $\phi(\eta)$.

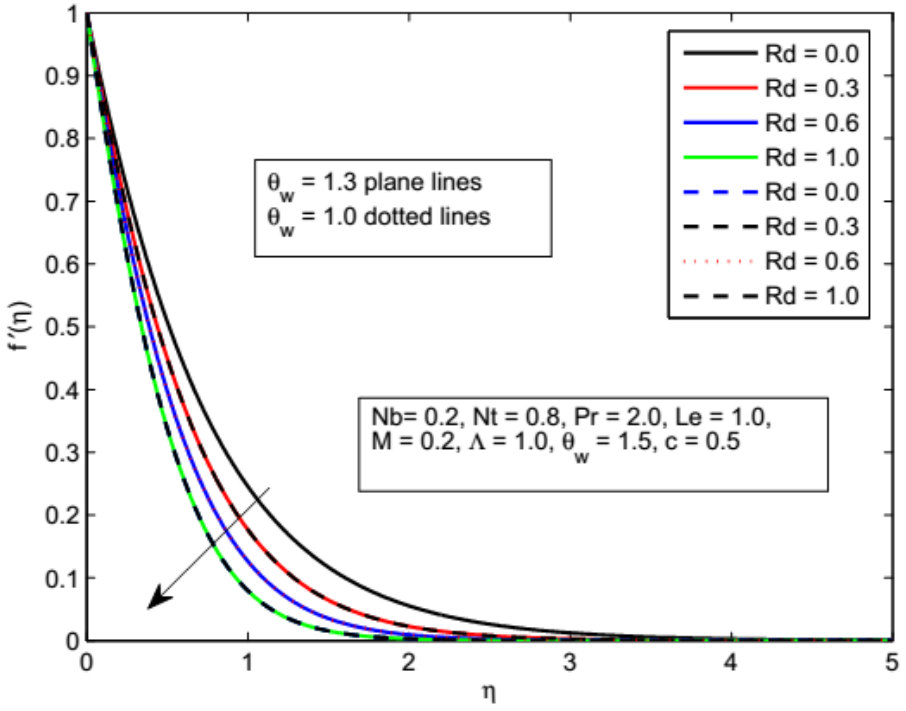

FIGURE 5.10: Influence of Rd on $f'(\eta)$.

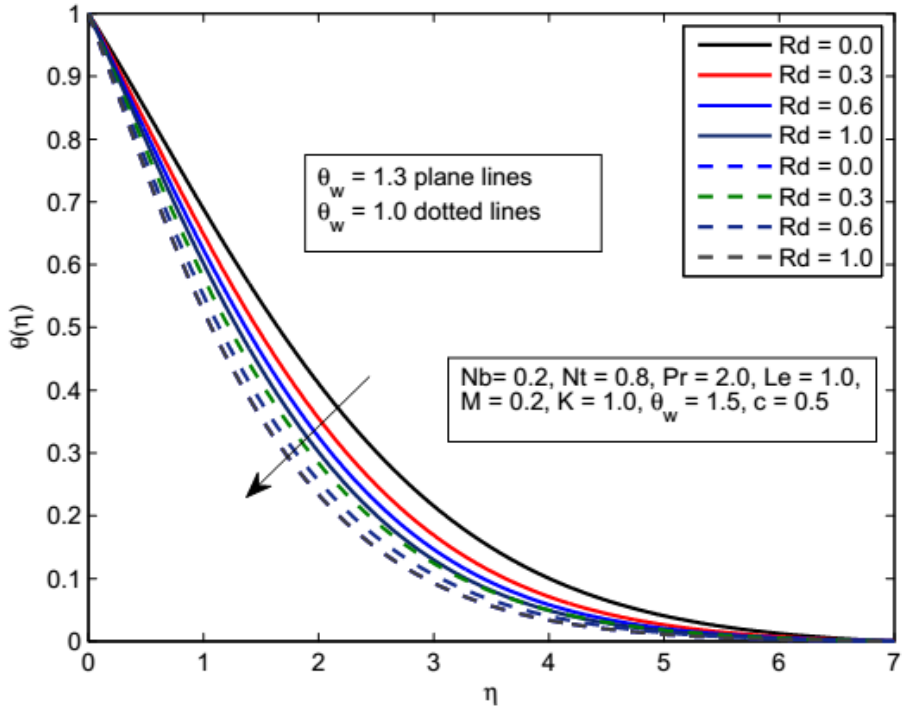

FIGURE 5.11: Influence of Rd on $\theta(\eta)$.

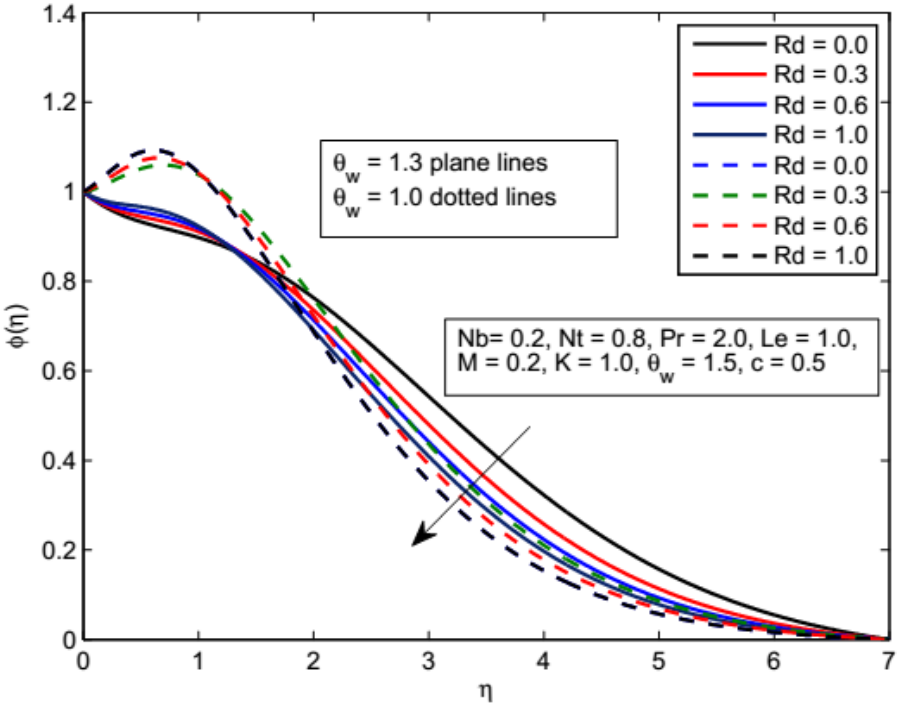

FIGURE 5.12: Influence of Rd on $\phi(\eta)$.

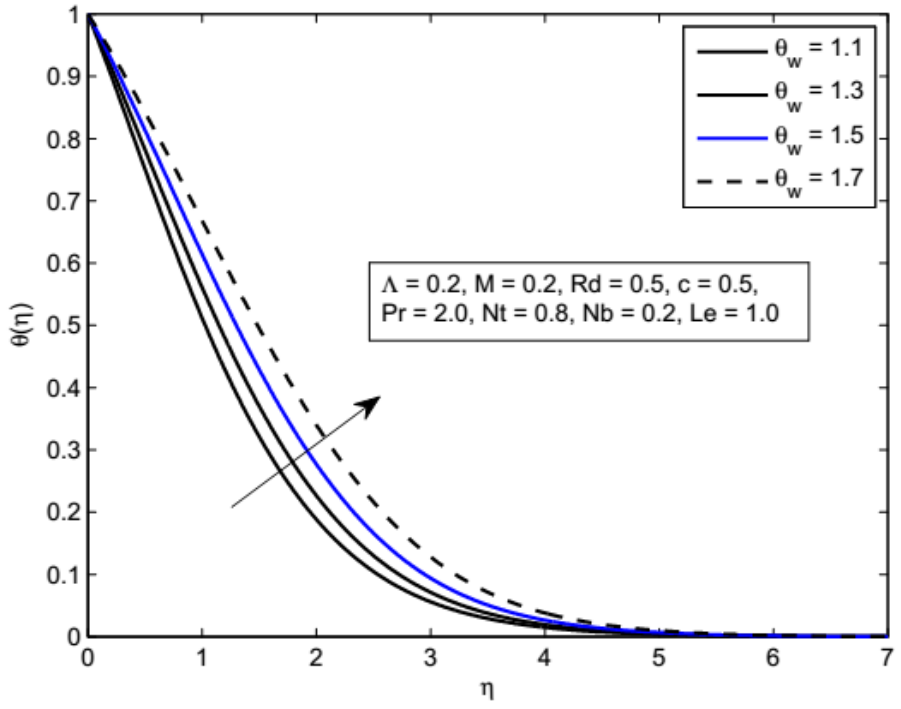

FIGURE 5.13: Influence of θ_w on $\theta(\eta)$.

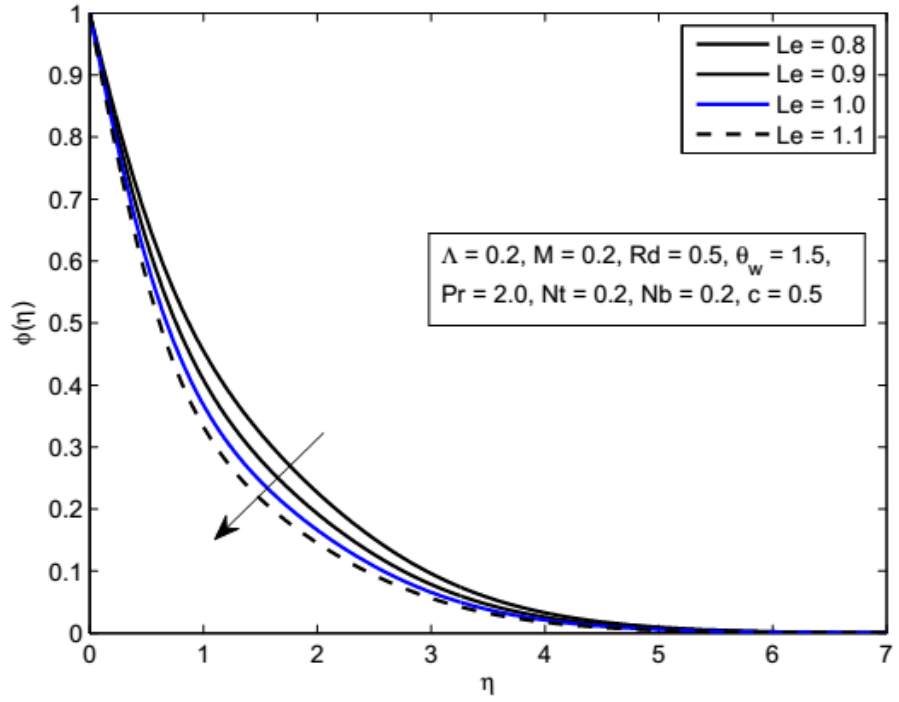

FIGURE 5.14: Influence of Le on $\phi(\eta)$.

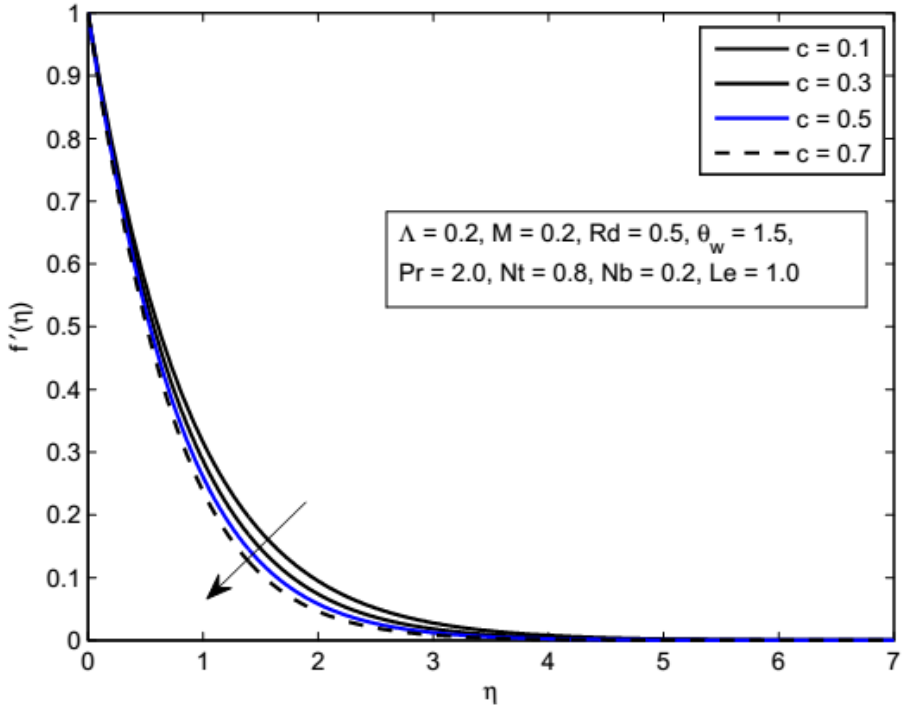

FIGURE 5.15: Influence of c on $f'(\eta)$.

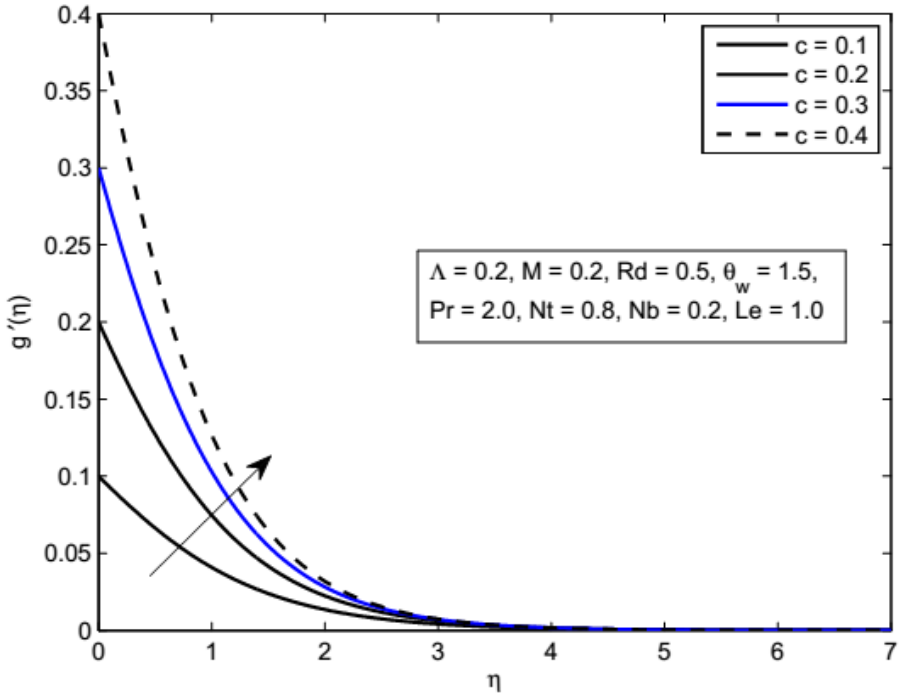

FIGURE 5.16: Influence of c on $g'(\eta)$.

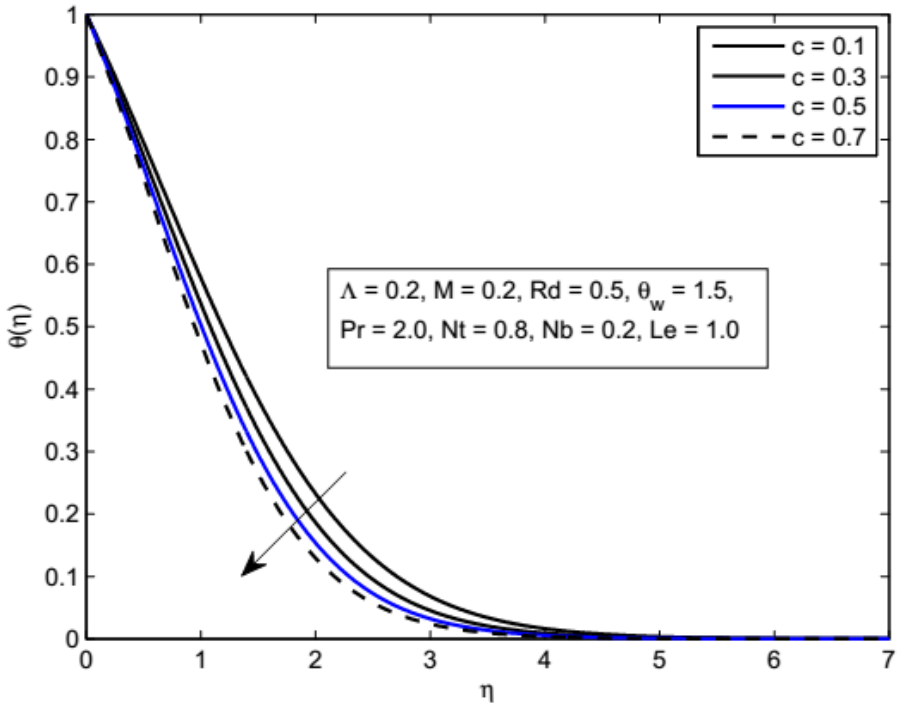

FIGURE 5.17: Influence of c on $\theta(\eta)$.

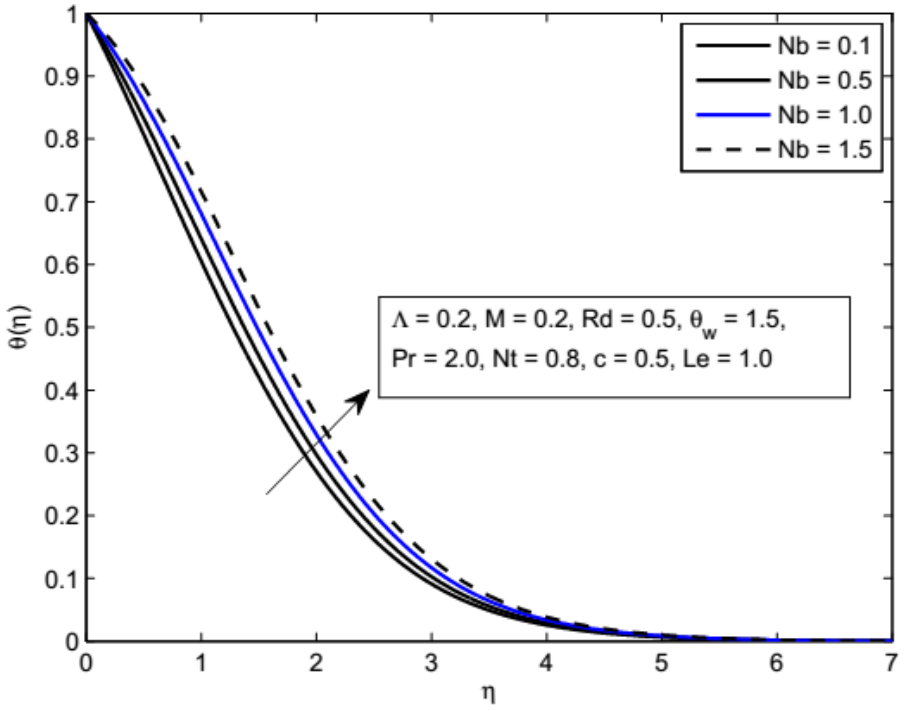

FIGURE 5.18: Influence of Nb on $\theta(\eta)$.

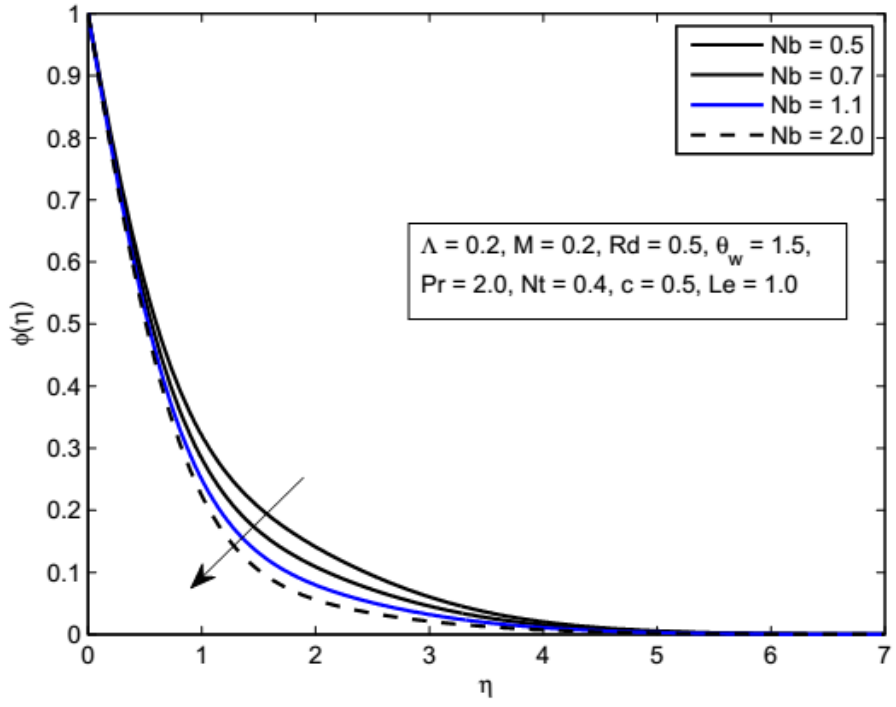

FIGURE 5.19: Influence of Nb on $\phi(\eta)$.

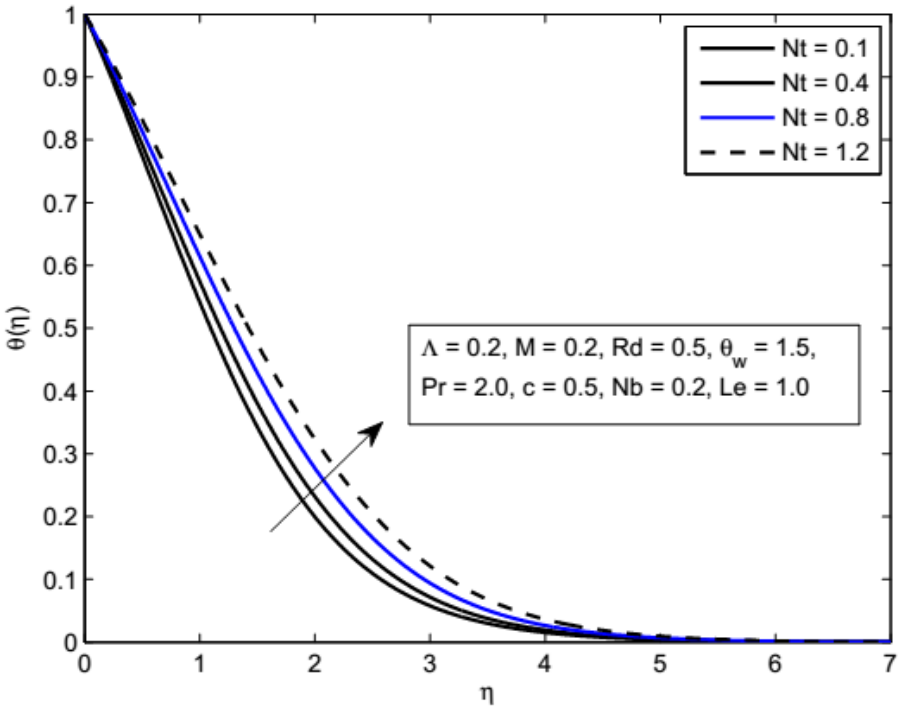

FIGURE 5.20: Influence of Nt on $\theta(\eta)$.

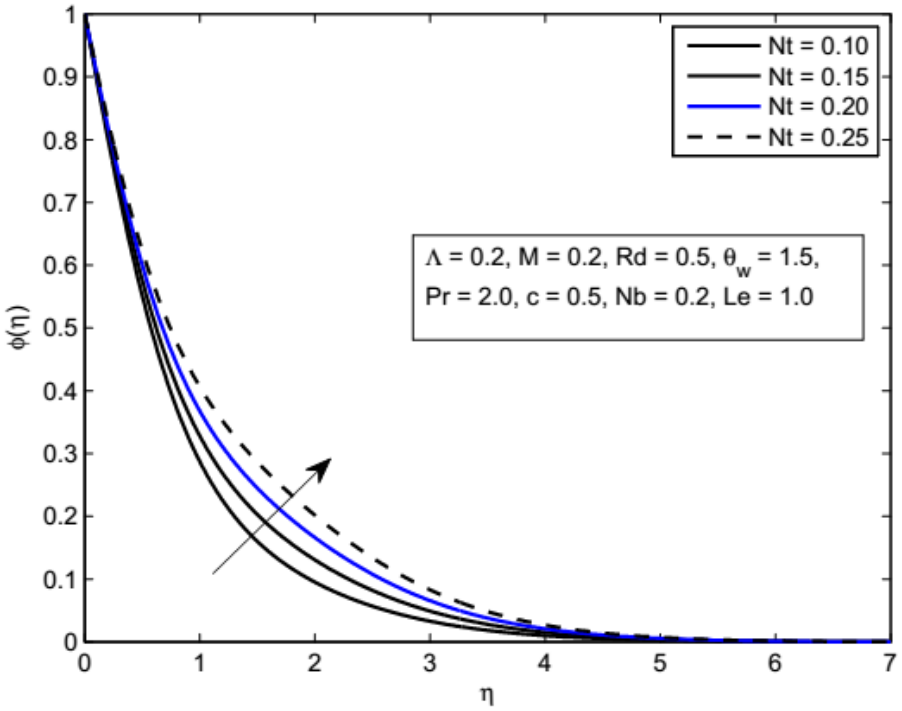

FIGURE 5.21: Influence of Nt on $\phi(\eta)$.

5.5 Concluding Remarks

This study in the present Chapter reveals the influence of non-linear thermal radiation of electrically conducting upper convected Maxwell fluid over a bi-directional stretching surface. Non-linear differential equations are solved numerically by shooting method with fourth order Runge-Kutta integration technique. The main features of the study are as follows:

- UCM fluids have lower boundary layer thickness as compared to Newtonian fluid.
- Nusselt and Sherwood number both are gradually increased when temperature ratio is enhanced.
- Nanoparticle concentration decreases for Nb and increases for Nt.
- Flow velocity decreases for increasing value of thermal radiation parameter, however there is no variation for the linear and non-linear radiation.
- An increase in thermal boundary layer thickness is observed in temperature and concentration profiles for non-linear radiation ($\theta_w = 1.3$), as compared to linear radiation ($\theta_w = 1.0$).

Chapter 6

MHD 3D Upper Convected Maxwell Fluid Flow with Thermophoretic Effect

6.1 Introduction

In this chapter, a three dimensional upper-convected Maxwell (UCM) fluid flow in the presence of the viscous dissipation and Joule heating through a linearly stretching sheet, is considered to examine the effects of thermophoresis and magnetohydrodynamics (MHD) on the heat and mass transfer. The energy equation is formulated under the assumption of the non-linear radiative heat flux. The ODEs are deduced from the governing PDEs with the aid of the similarity transformation. These non-linear ODEs are then numerically tackled by the shooting technique, through the fourth order Runge-Kutta integration process. To strengthen the reliability of our results, the MATLAB built-in function bvp4c is also used. Effects of some prominent physical parameters such as Eckert number, Prandtl number, thermophoretic parameter, magnetic parameter on the velocity, temperature and concentration profiles, are discussed graphically and numerically. It is found that

the concentration profile decreases for the higher values of thermophoretic parameter and Schmidt number. The heat flux rate, is observed to enhance for the increasing values of the thermal radiation and Prandtl number.

6.2 Problem Formulation

Three dimensional steady, incompressible upper-convected Maxwell fluid flow due to stretching surface in xy-plane has been considered in the present Chapter. The flat surface has been stretched in the positive $x-$ direction with velocity $U_w(x) = ax$ and in the positive $y-$ direction with $V_w(y) = by$. A magnetic field with small Reynolds number is applied along the $z-$axis. The effects of viscous dissipation and Joule heating have also been taken into account. Thermophoresis and non-linear thermal radiation effects are incorporated during the formulation of energy equation. T_w and C_w are the constant temperature and concentration respectively on the surface wall, whereas T_∞ and C_∞ denote the ambient temperature and concentration of the fluid as shown in Figure 6.1. The fundamental equations

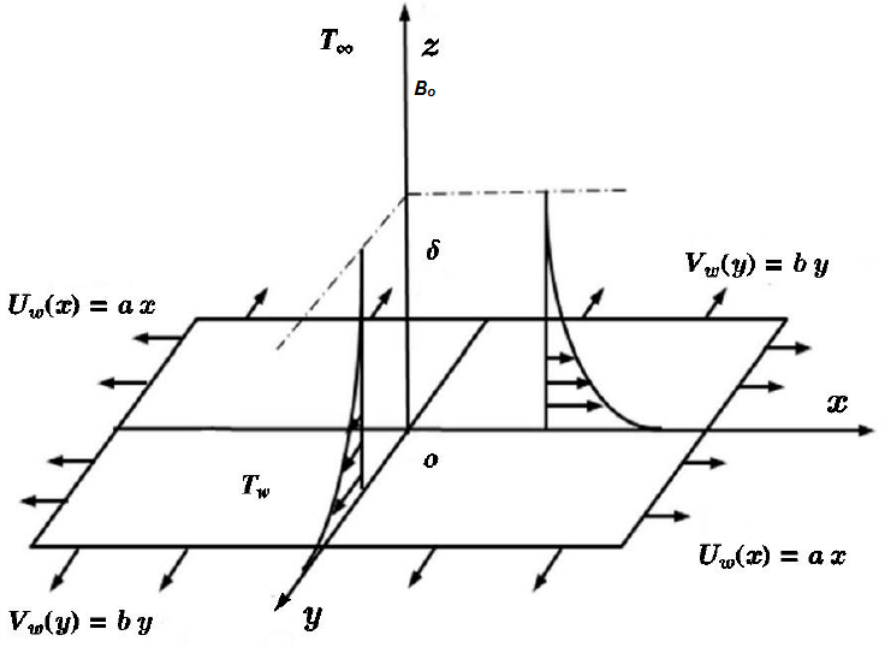

FIGURE 6.1: Geometry of the Problem.

describing the proposed problem for the velocity, temperature and concentration

[116–119] can be expressed in the operator form as follows,

$$\nabla.\mathbf{V} = 0, \tag{6.1}$$

$$\frac{\partial}{\partial t}(\rho\mathbf{V}) + \nabla.[(\rho\mathbf{V})\mathbf{V}] = \nabla.\tau_1 + \mathbf{j}\times\mathbf{B}, \tag{6.2}$$

$$(\mathbf{V}.\nabla)T = \alpha\nabla^2 T - \frac{1}{\rho c_p}\nabla q_r + \frac{\mu}{\rho c_p}(\nabla\mathbf{V}).(\nabla\mathbf{V}) + \frac{\sigma B_0^2}{\rho c_p}(\mathbf{V}.\mathbf{V}), \tag{6.3}$$

$$(\mathbf{V}.\nabla)C = D\ \nabla^2 C - \nabla(V_T C), \tag{6.4}$$

where

$$\tau_1 = -p\mathbf{I} + \mathbf{S}, \tag{6.5}$$

$$\left(1 + \lambda\frac{D}{Dt}\right)\mathbf{S} = \mathbf{S} + \lambda\frac{D\mathbf{S}}{Dt} = \mu A_1, \tag{6.6}$$

$$A_1 = grad\ \mathbf{V} + (grad\ \mathbf{V})^T. \tag{6.7}$$

Here, ρ is the density of the fluid, $\mathbf{V}$ the velocity of the fluid, τ_1 the Cauchy stress tensor, p the pressure, $\mathbf{S}$ the extra stress tensor, $\mathbf{B} = (0, 0, B_0)$ the magnetic field, D/Dt the material time derivative, λ the relaxation time, μ the kinematic viscosity and A_1 the first Rivin-Erickson tensor. After simplifying the above equations, ignoring the pressure gradient and applying the boundary layer approximation, we get

$$\frac{\partial u}{\partial x} + \frac{\partial v}{\partial y} + \frac{\partial w}{\partial z} = 0, \tag{6.8}$$

$$u\frac{\partial u}{\partial x} + v\frac{\partial u}{\partial y} + w\frac{\partial u}{\partial z} + \lambda\left(\begin{array}{c} u^2\frac{\partial^2 u}{\partial x^2} + v^2\frac{\partial^2 u}{\partial y^2} + w^2\frac{\partial^2 u}{\partial z^2} + \\ 2uv\frac{\partial^2 u}{\partial x\partial y} + 2uw\frac{\partial^2 u}{\partial x\partial z} + 2vw\frac{\partial^2 u}{\partial y\partial z}\end{array}\right)$$
$$= \upsilon\frac{\partial^2 u}{\partial z^2} - \frac{\sigma B_0^2}{\rho}\left(u + \lambda w\frac{\partial u}{\partial z}\right), \tag{6.9}$$

$$u\frac{\partial v}{\partial x} + v\frac{\partial v}{\partial y} + w\frac{\partial v}{\partial z} + \lambda\left(\begin{array}{c} u^2\frac{\partial^2 v}{\partial x^2} + v^2\frac{\partial^2 v}{\partial y^2} + w^2\frac{\partial^2 v}{\partial z^2} + \\ 2uv\frac{\partial^2 v}{\partial x\partial y} + 2uw\frac{\partial^2 v}{\partial x\partial z} + 2vw\frac{\partial^2 v}{\partial y\partial z}\end{array}\right)$$
$$= \upsilon\frac{\partial^2 v}{\partial z^2} - \frac{\sigma B_0^2}{\rho}\left(v + \lambda w\frac{\partial v}{\partial z}\right), \tag{6.10}$$

$$u\frac{\partial T}{\partial x} + v\frac{\partial T}{\partial y} + w\frac{\partial T}{\partial z} = \alpha\frac{\partial^2 T}{\partial z^2} - \frac{1}{\rho c_p}\frac{\partial q_r}{\partial z} + \frac{\mu}{\rho c_p}\left(\left(\frac{\partial u}{\partial z}\right)^2 + \left(\frac{\partial v}{\partial z}\right)^2\right) + \frac{\sigma B_0^2}{\rho c_p}\left(u^2 + v^2\right), \tag{6.11}$$

$$u\frac{\partial C}{\partial x} + v\frac{\partial C}{\partial y} + w\frac{\partial C}{\partial z} = D\frac{\partial^2 C}{\partial z^2} - \frac{\partial}{\partial z}\left(V_T C\right). \tag{6.12}$$

The corresponding boundary conditions for the governing PDEs are

$$\left.\begin{aligned} &u = U_w = ax,\ v = V_w = by,\ w = 0, \\ &T = T_w,\ C = C_w \text{ at } z = 0, \\ &u \to 0,\ v \to 0,\ T \to T_\infty,\ C \to C_\infty \text{ as } z \to \infty. \end{aligned}\right\} \tag{6.13}$$

The term q_r in Eq. (6.11) is Rosseland radiative heat flux and V_T is the thermophoretic velocity in Eq. (6.12). These are defined as

$$q_r = \frac{4\sigma^*}{3\aleph}\frac{\partial T^4}{\partial z}, \quad V_T = K_1\frac{\nu}{T_r}\frac{\partial T}{\partial z}. \tag{6.14}$$

Here, $\aleph$ is the Rosseland mean absorption coefficient and σ^* the Steffan-Boltzmann constant. For the conversion of the system of governing non-linear PDEs to the system of ODEs, we use the following dimensionless variables:

$$\left.\begin{aligned} &u = axf'(\eta),\ v = ayg'(\eta),\ w = -\sqrt{a\nu}\left(f(\eta) + g(\eta)\right), \\ &\theta(\eta) = \frac{T - T_\infty}{T_w - T_\infty},\ \phi(\eta) = \frac{C - C_\infty}{C_w - C_\infty},\ \eta = \sqrt{\frac{a}{\nu}}z. \end{aligned}\right\} \tag{6.15}$$

As we are considering the non-linear thermal radiation, so T in (6.15) can be expressed as

$$T = T_\infty\left(\left(\theta_w - 1\right)\theta + 1\right). \tag{6.16}$$

Using Eq. (6.16) into Eq. (6.14), we obtain

$$q_r = -\frac{16\sigma^*}{3\aleph}T_\infty^3\left(\left(\theta_w - 1\right)\theta + 1\right)^3\frac{\partial T}{\partial z}, \tag{6.17}$$

where $\theta_w = \dfrac{T_w}{T_\infty}$ is the temperature ratio parameter. Using the similarity transformation defined in (6.15), Eq. (6.8) is identically satisfied while Eqs. (6.9) to (6.13) are converted to the following ordinary differential equations.

$$f''' - f'^2 + \left(M^2\Lambda + 1\right)(f + g)f'' + 2\Lambda f'(f + g)f'' - (f + g)^2 f''' - M^2 f' = 0, \tag{6.18}$$

$$g''' - g'^2 + \left(M^2\Lambda + 1\right)(f + g)g'' + 2\Lambda g'(f + g)g'' - (f + g)^2 g''' - M^2 g' = 0, \tag{6.19}$$

$$\left(1 + \frac{4}{3}Rd\,(1 + (\theta_w - 1)\,\theta)^3\right)\theta'' + Pr\,(f + g)\,\theta' + 4Rd\,(\theta_w - 1)\,(1 + (\theta_w - 1)\,\theta)^2\,\theta'^2 + + PrEc\left(f''^2 + L^2 g''^2\right) + PrEcM^2\left(f'^2 + L^2 g'^2\right) = 0, \tag{6.20}$$

$$\phi'' - \tau^* Sc\,(\phi\theta'' + \theta'\phi') + Sc\,(f + g)\,\phi' = 0. \tag{6.21}$$

The transformed boundary conditions are:

$$\left.\begin{aligned} &f(0) = 0,\ f'(0) = 1,\ g(0) = 0,\ g'(0) = c,\ \theta(0) = 1,\ \phi(0) = 1, \\ &f'(\eta) \to 0,\ g'(\eta) \to 0,\ \theta(\eta) \to 0,\ \phi(\eta) \to 0 \text{ as } \eta \to \infty. \end{aligned}\right\} \tag{6.22}$$

Different dimensionless parameters appearing in Eqs. (6.18)-(6.22) are defined as

$$\left.\begin{aligned} &M = \frac{\sigma B_0^2}{\rho a},\quad Pr = \frac{\nu}{\alpha} = \frac{\rho c_p \nu}{k},\quad Rd = \frac{4\sigma^* T_\infty^3}{k\aleph},\quad \tau^* = -\frac{K_1(T_w - T_\infty)}{T_r} \\ &\Lambda = \lambda a,\quad Sc = \frac{\nu}{D},\quad Ec = \frac{a^2 x^2}{c_p\,(T_w - T_\infty)},\quad \theta_w = \frac{T_w}{T_\infty},\quad c = \frac{b}{a},\quad L = \frac{y}{x}. \end{aligned}\right\} \tag{6.23}$$

The important quantities of interest, local Nusselt and Sherwood numbers are formulated as

$$Nu_z = \frac{x q_w}{k\,(T_w - T_\infty)},\quad Sh_z = \frac{x j_w}{D\,(C_w - C_\infty)}. \tag{6.24}$$

Here, the heat and mass fluxes are defined as

$$q_w = -k\left(\frac{\partial T}{\partial z}\right)_{z=0},\quad j_w = -D\left(\frac{\partial C}{\partial z}\right)_{z=0}. \tag{6.25}$$

The local Nusselt and Sherwood numbers in the dimensionless form, are

$$Re_z^{-1/2} Nu_z = -[1 + (4/3)\theta_w^3 Rd]\theta'(0), \quad Re_z^{-1/2} Sh_z = -\phi'(0). \tag{6.26}$$

6.3 Solution Methodology

The system of non-linear ordinary differential Eqs. (6.18)-(6.21) along with the boundary conditions (6.22) has been solved iteratively by the shooting method [93] for various values of different physical parameters. To verify the numerical results achieved by the shooting method, we have also implemented the MATLAB built-in function bvp4c. For the solution of the initial value problem arising in the shooting method, Runge-Kutta method of order four has been used. The unbounded domain $[0, \infty)$ has been replaced by the bounded domain $[0, \eta_{max}]$ for some suitable choice of the positive real number η_{max} because no significant variations in the solution are observed for $\eta > \eta_{max}$. For the numerical values presented in Tables 6.1, 6.2 and 6.3, η_{max} is taken as 8 whereas for different figures, we have taken different values of η_{max}. To convert the higher order ODEs (6.18)-(6.21) into a system of first order ODEs, denote f by y_1, g by y_4, θ by y_7 and ϕ by y_9. As a result, the following initial value problem consisting of ten first order ordinary differential equations is obtained.

$$\left.\begin{aligned}
y_1' &= y_2 \\
y_2' &= y_3 \\
y_3' &= \frac{1}{1 - \Lambda (y_1 + y_4)^2} \left[\begin{array}{c} y_2^2 - (M^2\Lambda + 1)(y_1 + y_4) y_3 - \\ 2\Lambda y_2 y_3 (y_1 + y_4) + M^2 y_2 \end{array} \right] \\
y_4' &= y_5 \\
y_5' &= y_6 \\
y_6' &= \frac{1}{1 - \Lambda (y_1 + y_4)^2} \left[\begin{array}{c} y_5^2 - (M^2\Lambda + 1)(y_1 + y_4) y_6 - \\ 2\Lambda y_5 y_6 (y_1 + y_4) + M^2 y_5 \end{array} \right]
\end{aligned}\right\}$$

$$\left.\begin{aligned} y_7' &= y_8 \\ y_8' &= \frac{-3}{3+4Rd\left(1+(\theta_w-1)\,y_7\right)^3}\left[\begin{array}{c} 4Rd\,(\theta_w-1)\left(1+(\theta_w-1)\,y_7\right)^2 y_8^2+ \\ Pr\,(y_1+y_4)\,y_8+PrEc\,(y_3^2+L^2y_6^2) \\ +PrEcM^2\,(y_2^2+L^2y_5^2) \end{array}\right] \\ y_9' &= y_{10} \\ y_{10}' &= -Sc\,(y_1+y_4)\,y_{10}+\tau^*Sc\,(y_9y_8'+y_8y_{10})\,, \end{aligned}\right\} \tag{6.27}$$

with the initial conditions

$$\left.\begin{aligned} &y_1(0)=0, \quad y_2(0)=1, \quad y_3(0)=\varrho_1, \\ &y_4(0)=0, \quad y_5(0)=c, \quad y_6(0)=\varrho_2, \\ &y_7(0)=1, \quad y_8(0)=\varrho_3, \quad y_9(0)=1, \\ &y_{10}(0)=\varrho_4. \end{aligned}\right\}$$

The above initial value problem is solved by Runge-Kutta method of order 4. For the refinement of the choices of $\varrho_1, \varrho_2, \varrho_3$ and ϱ_4 in each iteration of the shooting method, the classical Newton method is used to solve a system of four non-linear algebraic equations in $\varrho_1, \varrho_2, \varrho_3$ and ϱ_4. The stopping criteria for the iterative process is set as

$$\max\left\{\left|y_2(\eta_{max})-0\right|, \left|y_5(\eta_{max})-0\right|, \left|y_7(\eta_{max})-0\right|, \left|y_9(\eta_{max})-0\right|\right\} < \varepsilon.$$

To achieve more sharp numerical results, ε has been given the value 10^{-6} throughout the present numerical investigation.

6.4 Results and Discussion

Although, almost the same numerical results for different quantities of interest are achieved by two different techniques, nevertheless for more satisfaction, the MATLAB code for the current problem has been validated by reproducing some published work of the similar nature. For this purpose, numerical values of $f''(0)$

and $g''(0)$ for different values of c are computed and presented in Table 6.1. The values of $f''(0)$ and $g''(0)$ are compared with those published by Ariel [122] and Hayat et al. [123] and found in an excellent agreement. Numerical values of Nusselt number are also computed for different choices of the values of Deborah number, stretching ratio parameter, Prandtl number and thermal radiation parameter. A convincing comparison of these values with those reported by Mushtaq et al. [14] can be seen in Table 6.2. They have also used the shooting method with RK-4 integration scheme.

Numerical results of local Nusselt number and local Sherwood number for various values of different parameters are tabulated in Table 6.3. From the table, it is observed that the rate of heat flux decreases for the increasing values of Deborah number Λ, magnetic parameter M and Eckert number Ec. The rate of heat flux is found to increase for thermal radiation parameter Rd, stretching ratio c, temperature ratio parameter θ_w and Prandtl number Pr. The rate of mass transfer is observed to reflect the decreasing behavior for Deborah number Λ, magnetic parameter M, thermal radiation parameter θ_w, Eckert number Ec and temperature ratio parameter θ_w whereas it increases for the stretching ratio parameter c and Prandtl number Pr. On the other hand, Sherwood number is enhanced for the higher values of Schmidt number Sc and thermophoretic parameter τ^*.

To visualize the effect of different physical parameters on the velocities $f'(\eta)$, $g'(\eta)$, temperature $\theta(\eta)$ and concentration profile $\phi(\eta)$, Figures 6.2–6.19 are plotted. Figures 6.2 and 6.3 reflect the impact of Deborah number Λ, which is the ratio of the fluid relaxation time to its characteristic time scale, on the velocity and concentration profiles. When the shear stress is applied on the fluid, the time in which it gains its equilibrium position is called the relaxation time. This time is higher for the fluids having high viscosity. So, an increase in Deborah number may increase the viscosity of the fluid resulting in the decreasing behavior of the velocity as shown in Figure 6.2. The fluid becomes Newtonian if we consider $\Lambda = 0$ and its viscosity gradually increases with an increase in Deborah number Λ. From Figure 6.2, it is also concluded that the boundary layer thickness reduces for the upper convected Maxwell fluid. The hydrodynamic boundary layer thickness, is

known to decreases for the increasing values of the Deborah number. In Figure 6.3, the concentration $\phi(\eta)$ is displayed for different values of the Deborah number Λ. It is observed that the concentration increases with an increase in the relaxation time. From this observation, we can conclude that elastic force promotes the heat transfer in the upper-convected Maxwell fluid which resultantly increases the mass transfer.

In Figures 6.4, 6.5 and 6.6, the effect of stretching ratio c on the velocities and concentration profiles is shown. An opposite effect of c on velocity profiles in $x-$ and $y-$ directions is noticed in Figures 6.4 and 6.5. As $c = b/a$, where a and b are the velocity coefficients along the x and y-axes respectively, so an increment in c means a decrement in a, which implies a decrease in the velocity along $x-$ axis. Similarly, an increasing value of c causes an increment in b, which resultantly increases the velocity of the fluid in $y-$ direction. From Figure 6.6, it is seen that the mass transfer decreases for the increasing value of c. To see the variation in the temperature against the increasing values of Prandtl number Pr, Figure 6.7 is plotted. It is observed that if the Prandtl number is augmented, there are thinning effects in the thermal boundary layer thickness. Fluids having larger Prandtl number, have lower thermal diffusivity which results in the fall of temperature.

Figures 6.8–6.10 depict the typical profiles of velocity, temperature and concentration for magnetic parameter M. By increasing the magnetic parameter M, a drag force known as Lorentz force increases which resultantly reduces the velocity of the fluid and hence the rate of heat and mass transfer is reduced and this leads to an increment in the temperature and concentration. In Figure 6.11, the effect of thermal radiation parameter Rd on temperature for both linear and non-linear radiation, is shown. It is seen that $\theta(\eta)$ has increasing trend for increasing values of Rd. It is also noticed that temperature rises more quickly in non-linear radiation case ($\theta_w = 1.3$) as compared with the linear radiation case ($\theta_w = 1.0$). The thermal radiation is increased due to the fact that more energy is released in the fluid.

To see the effect of Eckert number Ec on temperature, Figure 6.12 is presented. From this figure, it is clear that temperature increases with an increase in Ec. Due to friction, the heat energy is stored in the fluid for increasing values of Ec, which results in the enhancement of the temperature profile. The effect of the variation in the Schmidt number Sc on the mass transfer, is shown in Figure 6.13. From this figure, it is noticed that the concentration boundary layer and hence the concentration field $\phi(\eta)$ is reduced with the increment in the Schmidt number Sc. This is due to the fact that Sc is inversely proportional to the diffusion coefficient. Because an increase in the diffusion coefficient decreases the mass transfer rate, therefore an increase in Sc results in a decrease in the concentration profile. The effect of the thermophoretic parameter τ^* on the concentration profile, is shown in Figure 6.14. We observe that the increasing values of the thermophoretic parameter τ^* induce a decrement in the concentration of the particles throughout the flow domain. In Figure 6.15, the variation in the temperature ratio parameter θ_w is analyzed for the temperature profile. From this figure, it is observed that temperature is enhanced for the increasing values of θ_w. An increase in θ_w implies an increase in the wall temperature T_w, which leads to an increase in the temperature of the fluid within the boundary layer. In Figure 6.16, the temperature profile is found to increase, when L increases. Remember that L is the ratio of the thickness of the plate along $y-$axis to that along the $x-$axis.

Through Figure 6.17, the effects of the non-linear thermal radiation and the temperature ratio parameter on the Nusselt number, have been analyzed. It is observed that both of these parameters cause the increasing behavior in the Nusselt number. Figure 6.18 is plotted to see the trend of the Sherwood number due to the rise in the Schmidt number Sc and the thermophoretic parameter τ^*. Here, the rate of mass transfer is found to enhance for the higher values of τ^* and Sc. When the Prandtl number increases form 0.2 to 0.5, the value of Nusselt number is also enhanced, as shown in Figure 6.19. However, the Eckert number has the opposite effect on the Nusselt number.

c	$f''(0)$				$g''(0)$			
	[122]		[123]	Present	[122]		[123]	Present
	HPM	Exact	HAM		HPM	Exact	HAM	
0.0	1.0	1.0	1.0	1.0	0.0	0.0	0.0	0.0
0.1	1.017027	1.020260	1.020259	1.020246	0.073099	0.066847	0.066847	0.066835
0.2	1.034587	1.039495	1.039495	1.039462	0.158231	0.148737	0.148736	0.148721
0.3	1.052470	1.057955	1.057954	1.057922	0.254347	0.243360	0.243359	0.243338
0.4	1.070529	1.075788	1.075788	1.075750	0.360599	0.349209	0.349208	0.349182
0.5	1.088662	1.093095	1.093095	1.093062	0.476290	0.465205	0.465204	0.465193
0.6	1.106797	1.109947	1.109946	1.109928	0.600833	0.590529	0.590528	0.590518
0.7	1.124882	1.126398	1.126397	1.126373	0.733730	0.724532	0.724531	0.724526
0.8	1.142879	1.142489	1.142488	1.142461	0.874551	0.866683	0.866682	0.866670
0.9	1.160762	1.158254	1.158253	1.158230	1.022922	1.016539	1.016538	1.016523
1.0	1.178511	1.173721	1.173720	1.173710	1.178511	1.173721	1.173720	1.173714

TABLE 6.1: Comparison of the present results of $f''(0)$ and $g''(0)$ with those computed by Ariel [122] and Hayat et al. [123] for different values of c

			$Rd = 0$		$Rd = 1.0$			
			$\theta_w = 0$		$\theta_w = 0$		$\theta_w = 1.1$	
Λ	c	Pr	[14]	Present	[14]	Present	[14]	Present
1	0.5	2	1.01695	1.0169493	0.61177	0.6127148	0.53932	0.5395022
		4	1.60165	1.6016506	1.01695	1.0169493	0.90348	0.9034844
		7	2.24393	2.2439298	1.47271	1.4727082	1.31435	1.3143535
		10	2.75508	2.7550740	1.83692	1.8369216	1.64284	1.6428361
1	0	7	1.82603	1.8260260	1.20254	1.2025347	1.07372	1.0737145
	0.3		2.09403	2.0940290	1.37824	1.3782398	1.23051	1.2305095
	0.6		2.31293	2.3129240	1.51544	1.5154397	1.35219	1.3609931
	1		2.55918	2.5591800	1.66440	1.6644187	1.48361	1.4836290
0	0.5	7	2.35436	2.3543502	1.59321	1.5922506	1.42760	1.4275931
0.5			2.29665	2.2966491	1.53021	1.5302076	1.36840	1.3684014
1.0			2.24393	2.2439299	1.47271	1.4727082	1.31435	1.3143533
1.5			2.19501	2.1950047	1.41998	1.4200796	1.26482	1.2649215

TABLE 6.2: Comparison of the presently computed values of the wall temperature gradient $-\theta'(0)$ with those of Mushtaq et al. [14] for different values of Λ, c, Pr, Rd and θ_w.

										$Nu_z Re_z^{-1/2}$		$Sh_z Re_z^{-1/2}$	
Λ	M	c	Rd	θ_w	Pr	Ec	L	Sc	τ^*	Shooting	bvp4c	Shooting	bvp4c
0.1	0.2	0.5	1.0	1.3	0.2	0.1	1.0	0.3	0.2	0.3202000	0.3202000	0.2956925	0.2956921
0.2										0.3127308	0.3127305	0.2855532	0.2855529
0.3										0.3061861	0.3061856	0.2763398	0.2763395
0.4										0.3003928	0.3003922	0.2679526	0.2679521
	0.3									0.3175056	0.3175050	0.2926446	0.2926442
	0.4									0.3139047	0.3139041	0.2885396	0.2885391
	0.5									0.3095445	0.3095438	0.2835238	0.2835234
		0.2								0.3071753	0.3071747	0.2636041	0.2636038
		0.3								0.3122098	0.3122091	0.2751217	0.2751215
		0.4								0.3165321	0.3165316	0.2857615	0.2857612
			0.9							0.3068894	0.3068890	0.2959023	0.2959020
			1.0							0.3202000	0.3202000	0.2956924	0.2956921
			1.1							0.3336676	0.3336672	0.2955106	0.2955102
				1.0						0.2777206	0.2777203	0.2981455	0.2981451
				1.1						0.2901385	0.2901382	0.2972483	0.2972480
				1.2						0.3042220	0.3042217	0.2964293	0.2964290
					0.3					0.3830036	0.3830032	0.2967939	0.2967934
					0.4					0.4522845	0.4522842	0.2978659	0.2978655
					0.5					0.5261987	0.5261983	0.2988827	0.2988824
						0.2				0.3050372	0.3050368	0.2954590	0.2954589
						0.3				0.2898744	0.2898740	0.2952253	0.2952251
						0.4				0.2747115	0.2747112	0.2949912	0.2949911
							0.5			0.3223145	0.3223141	0.2957250	0.2957250
							1.0			0.3202000	0.3202000	0.2956925	0.2956922
							1.5			0.3166757	0.3166753	0.2956381	0.2956376
								0.1		0.3202000	0.3202000	0.1369700	0.1369700
								0.2		0.3202000	0.3202000	0.2156863	0.2156862
								0.3		0.3202000	0.3202000	0.2956924	0.2956921
									0.1	0.3202000	0.3202000	0.2935038	0.2935037
									0.2	0.3202000	0.3202000	0.2956924	0.2956922
									0.3	0.3202000	0.3202000	0.2978858	0.2978854

TABLE 6.3: Numerical values of local Nusselt number and Sherwood number

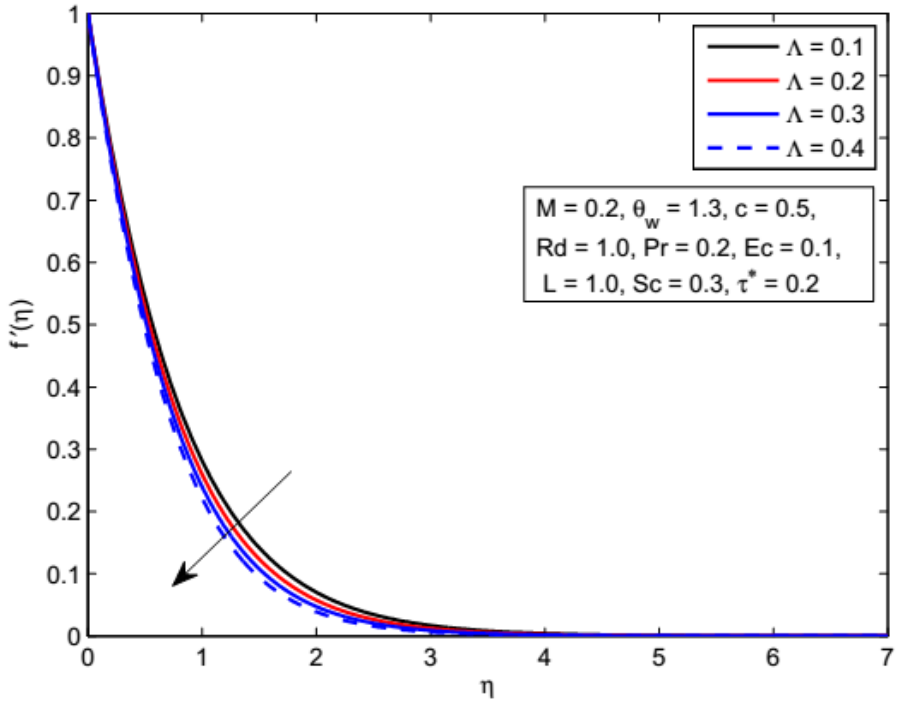

FIGURE 6.2: Influence of Λ on $f'(\eta)$.

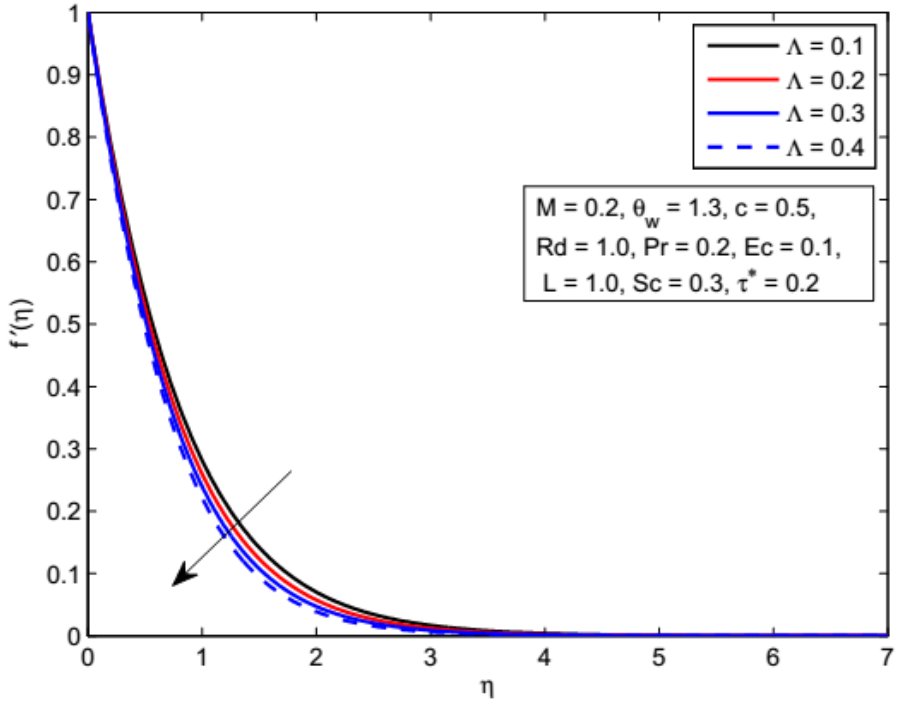

FIGURE 6.3: Influence of Λ on $\phi(\eta)$.

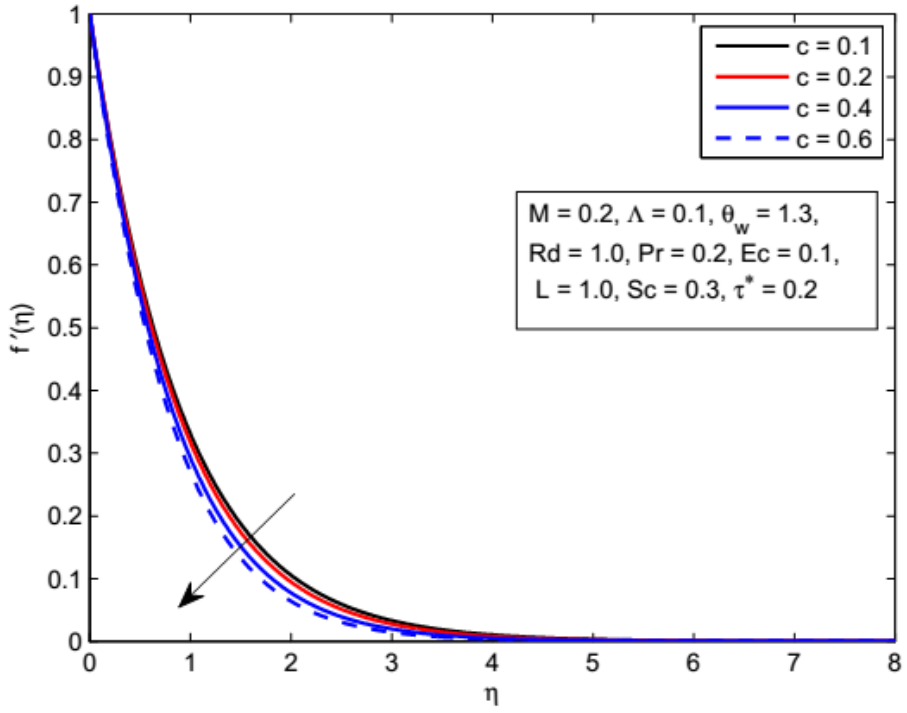

FIGURE 6.4: Influence of c on $f'(\eta)$.

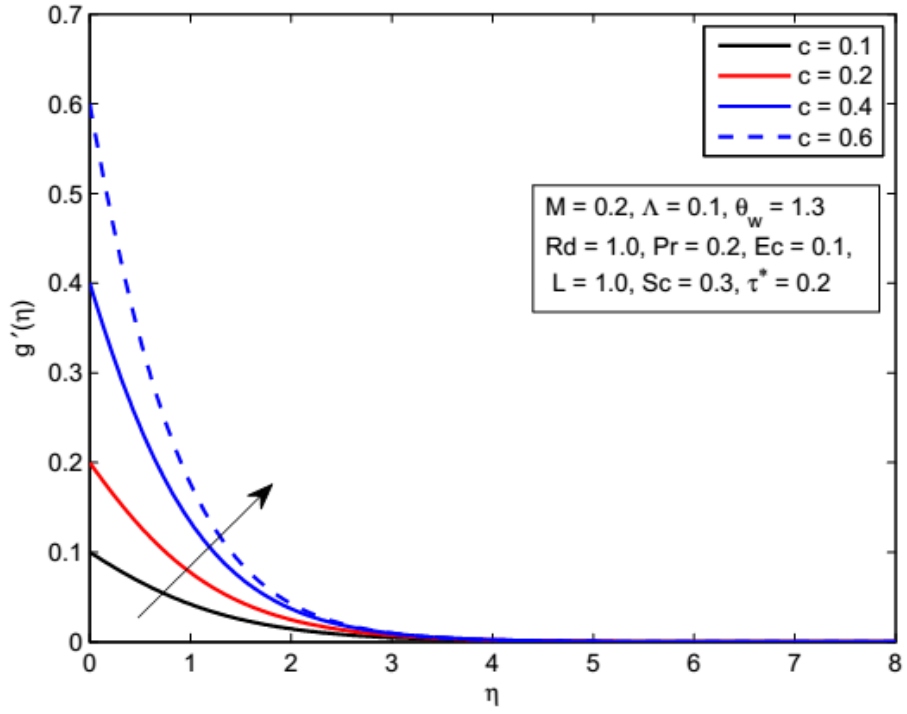

FIGURE 6.5: Influence of c on $g'(\eta)$.

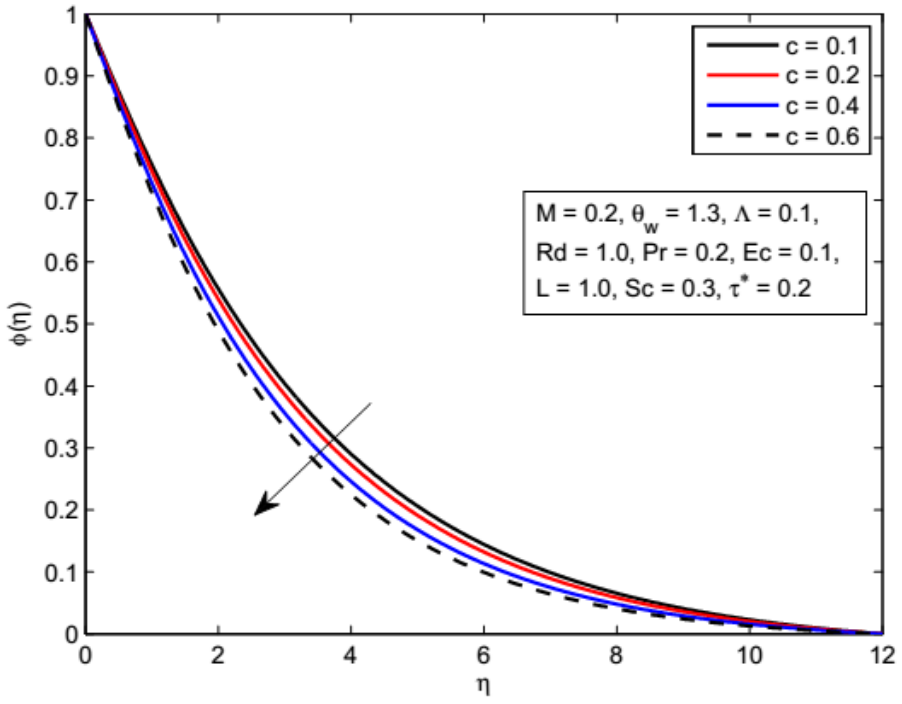

FIGURE 6.6: Influence of c on $\phi(\eta)$.

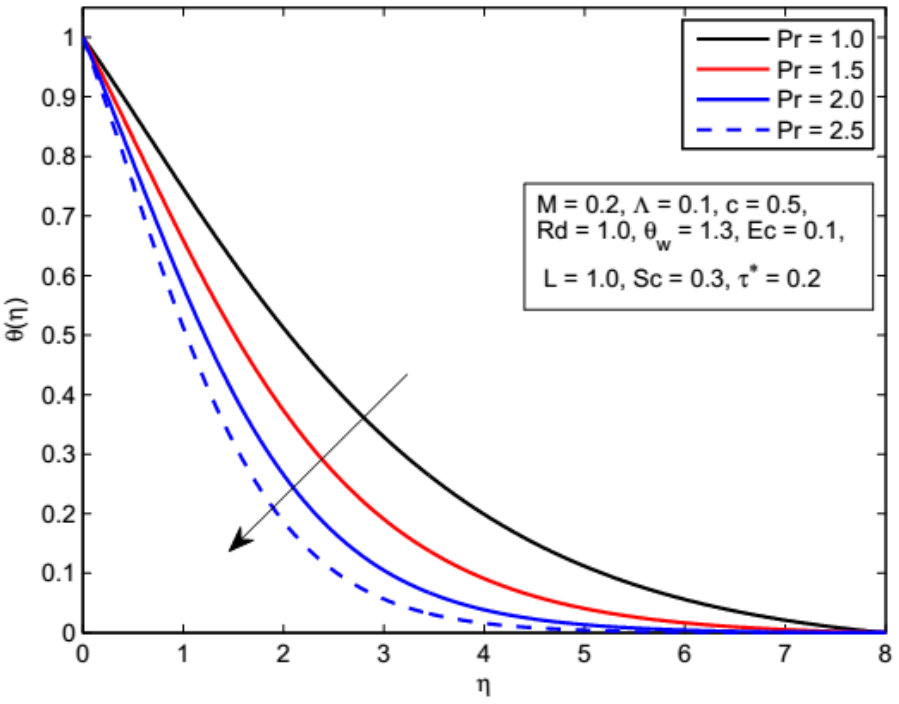

FIGURE 6.7: Influence of Pr on $\theta(\eta)$.

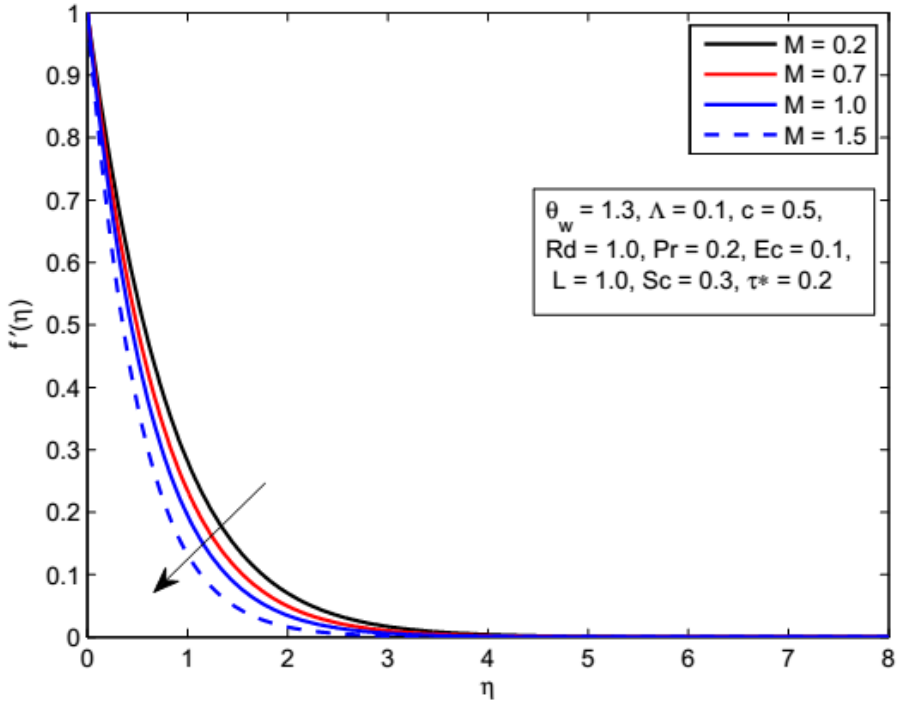

FIGURE 6.8: Influence of M on $f'(\eta)$.

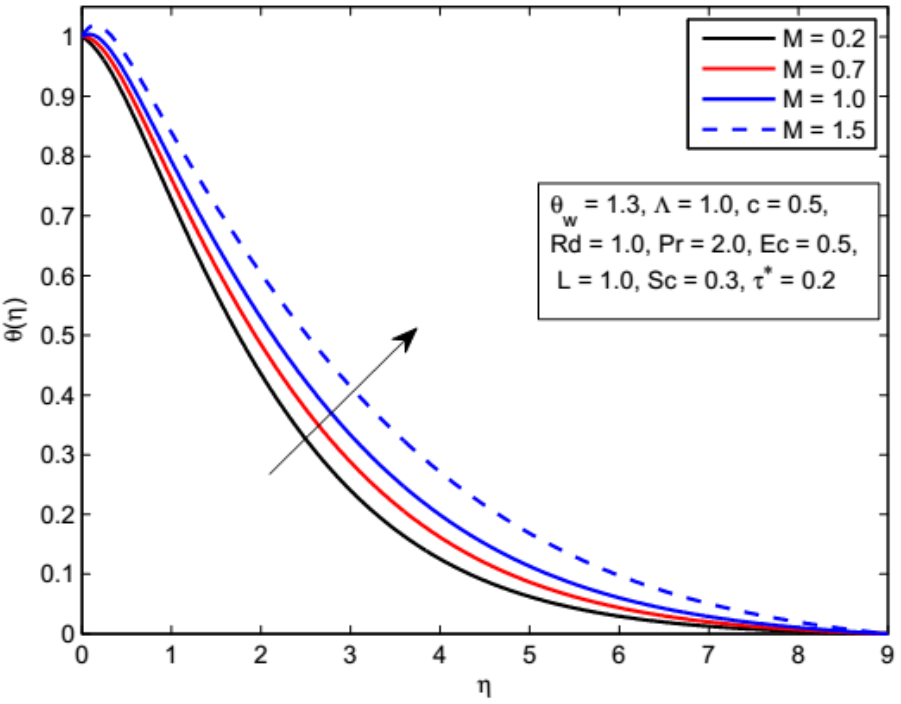

FIGURE 6.9: Influence of M on $\theta(\eta)$.

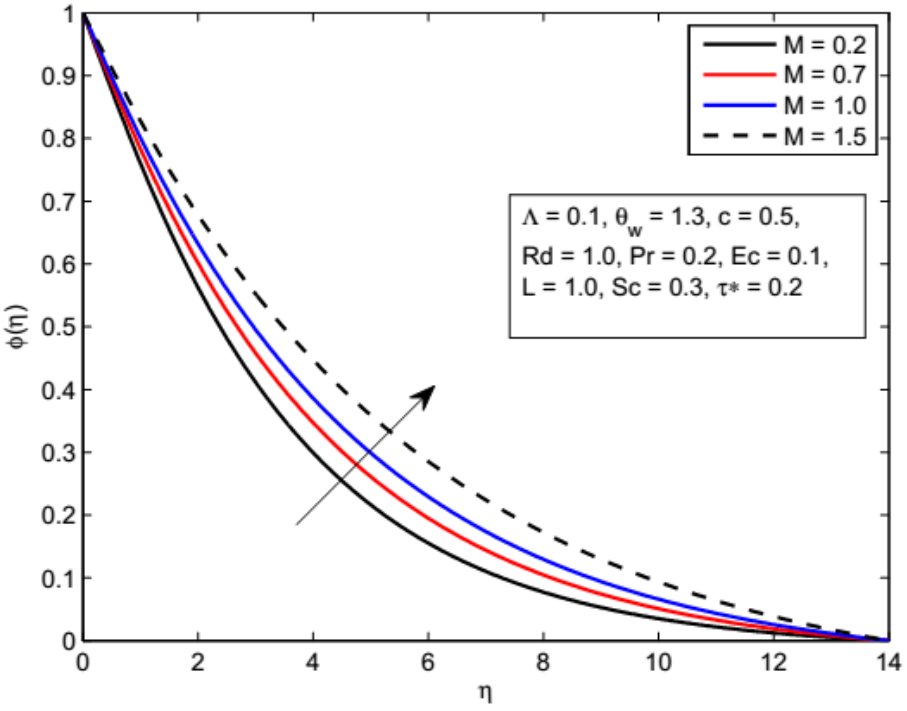

FIGURE 6.10: Influence of M on $\phi(\eta)$.

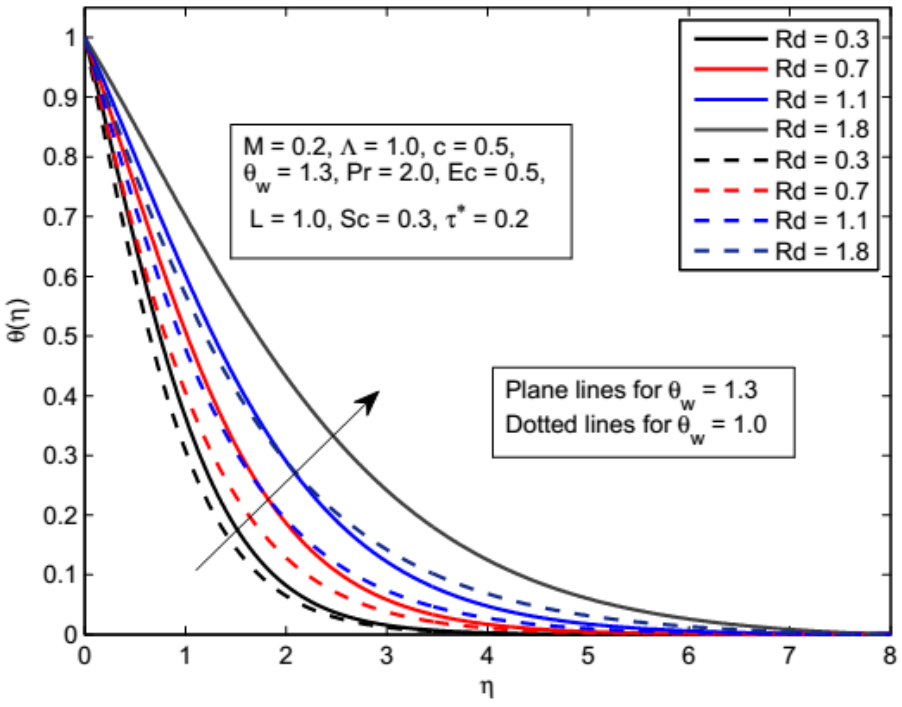

FIGURE 6.11: Influence of Rd on $\theta(\eta)$.

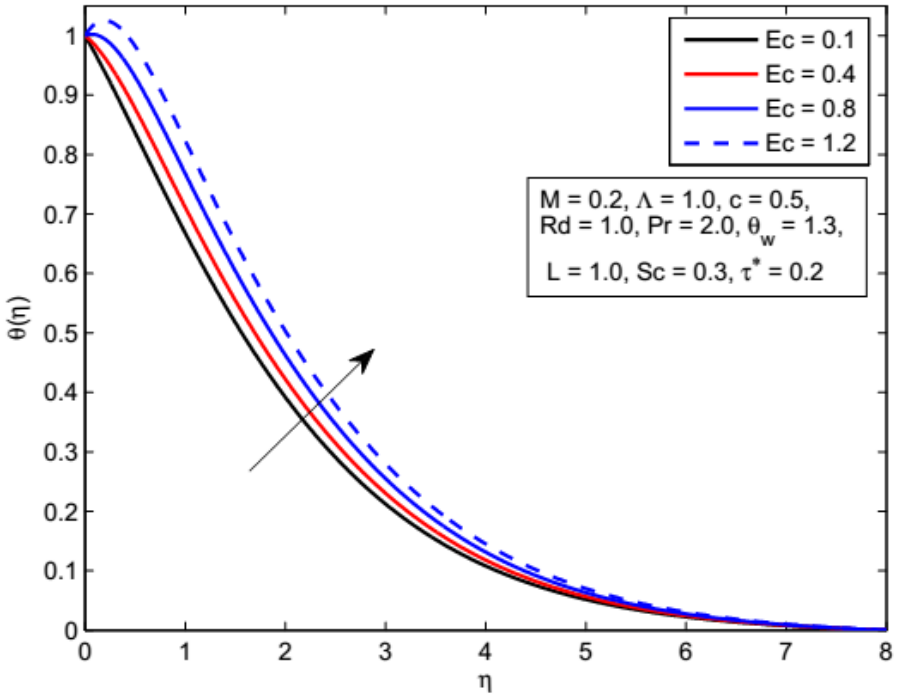

FIGURE 6.12: Influence of Ec on $\theta(\eta)$.

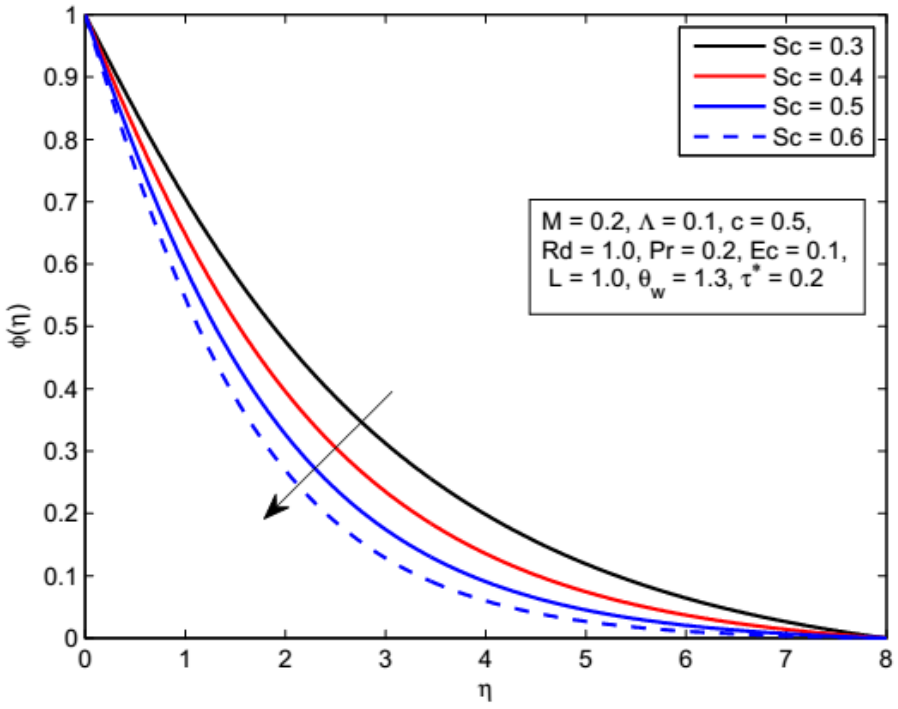

FIGURE 6.13: Influence of Sc on $\phi(\eta)$.

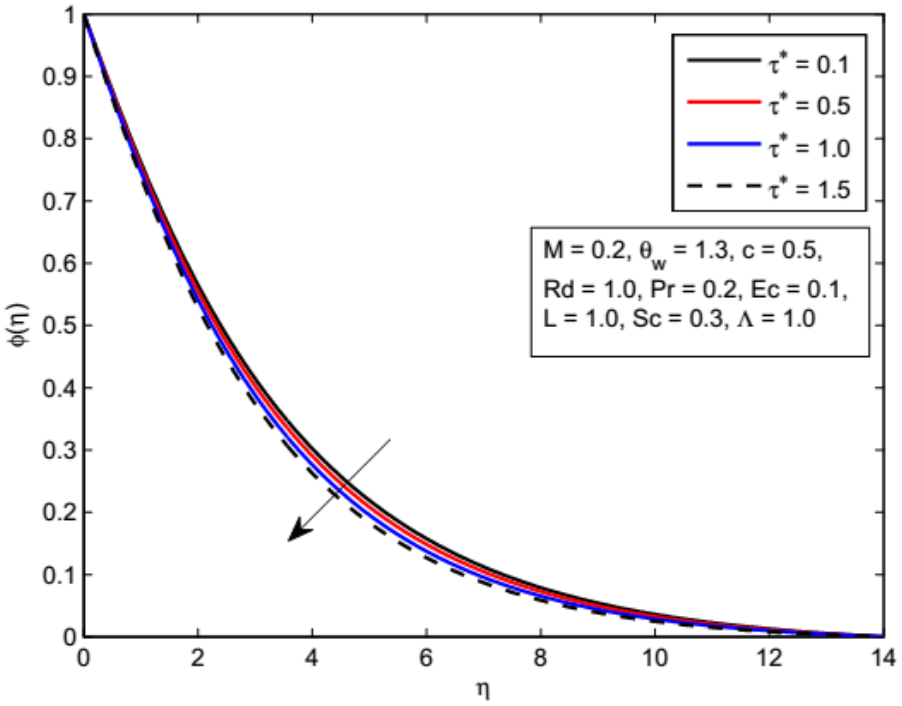

FIGURE 6.14: Influence of τ^* on $\phi(\eta)$.

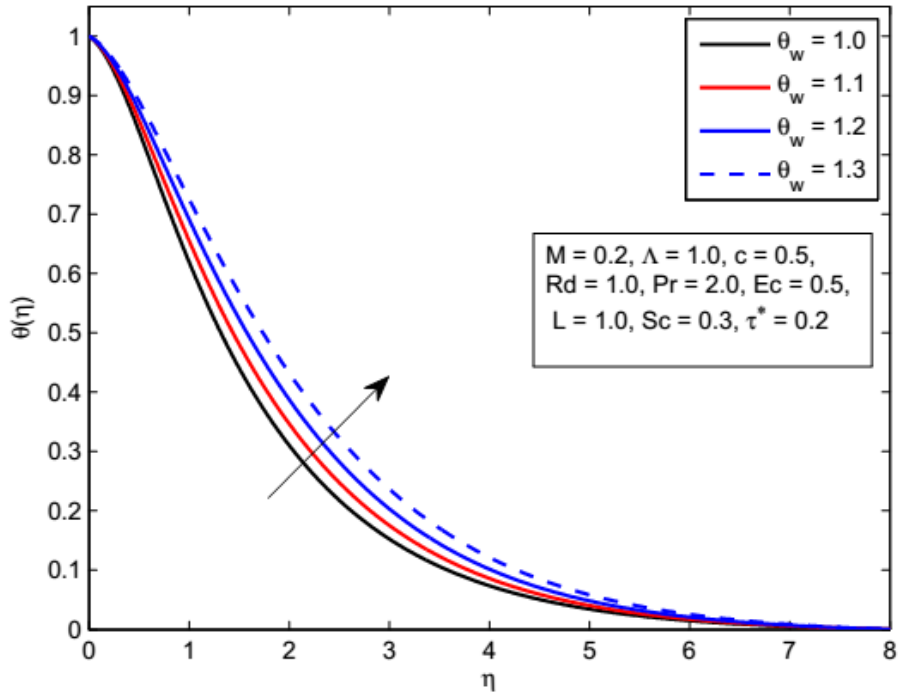

FIGURE 6.15: Influence of θ_w on $\theta(\eta)$.

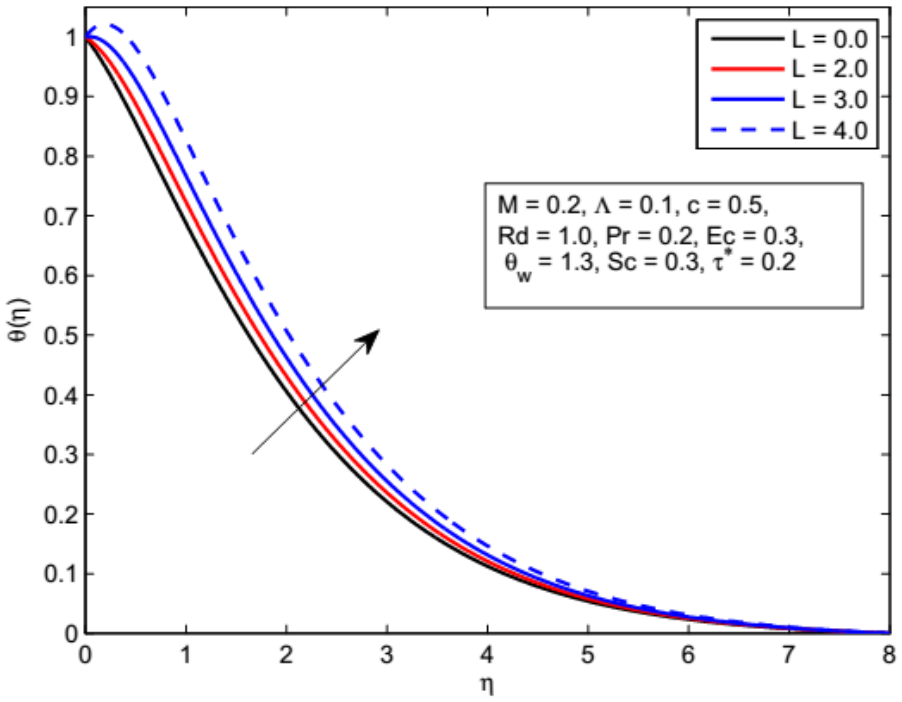

FIGURE 6.16: Influence of L on $\theta(\eta)$.

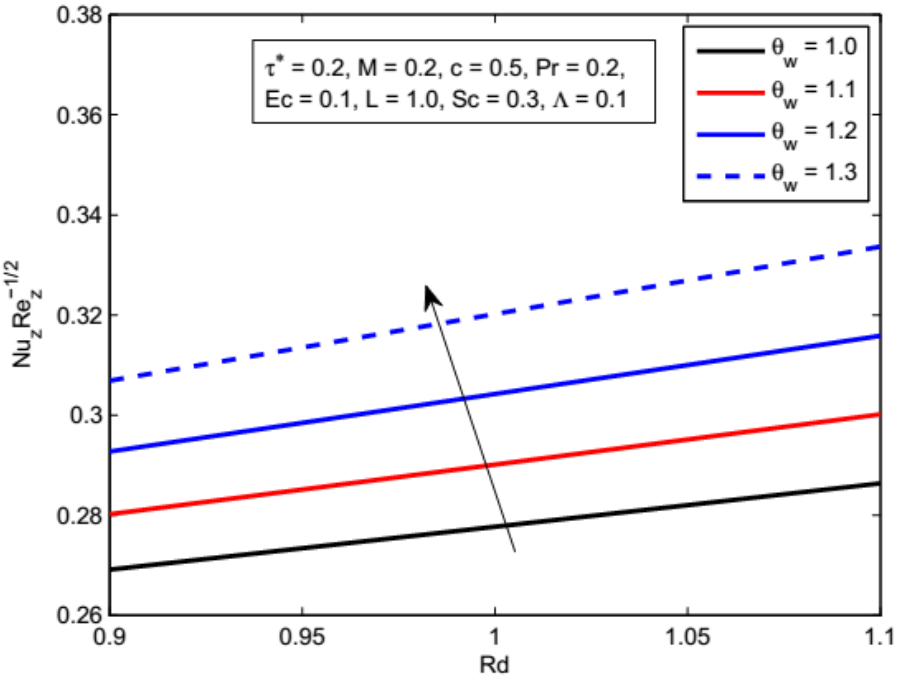

FIGURE 6.17: Influence of θ_w, Rd on $Nu_z Re_z^{-1/2}$.

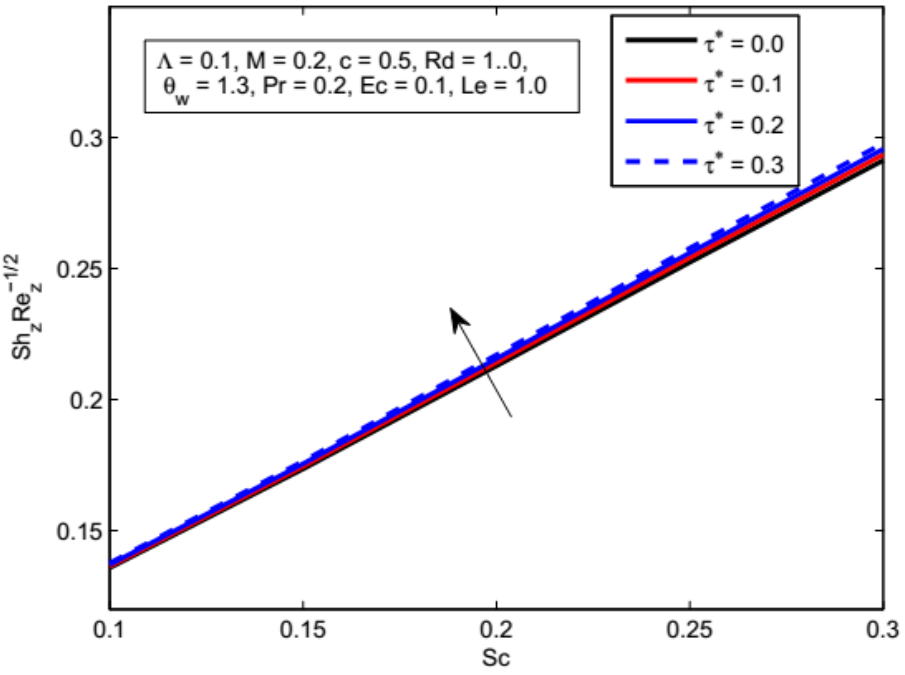

FIGURE 6.18: Influence of τ^*, Sc on $Sh_z Re_z^{-1/2}$.

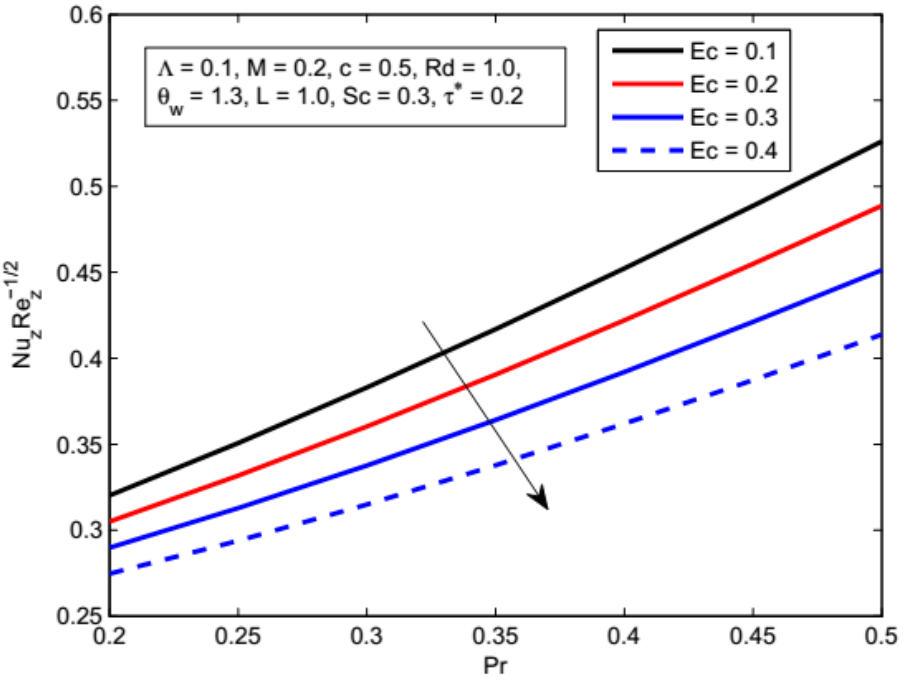

FIGURE 6.19: Influence of Pr, Ec on $Nu_z Re_z^{-1/2}$.

6.5 Concluding Remarks

This study reveals the influence of non-linear thermal radiation of electrically conducting upper convected Maxwell nanofluid over a bi-directional stretching surface. Non-linear boundary value problem is solved numerically by the shooting method involving the fourth order Runge-Kutta integration technique. The main findings of the study are as follows:

- UCM fluids have lower boundary layer thickness as compared to the Newtonian fluids.
- The present results are valid for both the linear radiation ($\theta_w = 1.0$) as well as for the non-linear radiation ($\theta_w > 1$).
- There is a decrease in the concentration profile when thermophoretic parameter and Schmidt number are increased.
- An increase in the temperature is observed, when the thermal radiation parameter Rd is increased for linear and non-linear radiation θ_w. However, the boundary layer thickness increases more quickly for the non-linear radiation ($\theta_w = 1.3$) as compared with the linear radiation ($\theta_w = 1.0$).
- Eckert number and magnetic parameter, have the increasing impact on the temperature profile.

Chapter 7

Conclusion

7.1 Conclusion

In this treatise, the numerical results of non-linear equations, governing the flow of Newtonian and non-Newtonian fluids (upper convected Maxwell fluid) for the heat, flow and mass transfer over a stretching sheet are obtained for different geometries and for the distinct values of the emerging parameters. Boundary layer approximations are used to acquire the mathematically modeled equations based on the laws of conservations. Continuity equation is derived from the law of conservation of mass, momentum equations based on the Newton's second law of motion, energy equations is obtained from the first law of thermodynamics, and Fick's law is used to derive the concentration equations. These governing partial differential equations are transformed to the non-linear coupled ordinary differential equations by the implementation of similarity transformations. In all the cases, these differential equations are solved numerically by the shooting method through the integration scheme RK-4. Results are further supported by a MATLAB built-in function bvp4c. In all the Chapters, results are analogized with the previously published articles in limiting cases. The main findings of the thesis are as follows:

- Due to the enhancement of Lorentz forces, the increasing magnetic parameter reduces the speed of the fluid. Because of the reduction in the speed of the fluid, the concentration and temperature profiles are increased.
- When the thermophoresis parameter is increased, the concentration and the thermal boundary layer thickness are also increased, and consequently the temperature and nanoparticles concentration are raised.
- The temperature distribution is a growing function of the Brownian motion parameter but a reverse relation is noticed in the case of the concentration distribution.
- The mass and temperature profiles both are decreasing functions of Prandtl number.
- The velocity profile always shows a decreasing role for the thermal radiation parameter regardless of the linear and the non-linear thermal radiation.
- The thermal boundary layer thickness increases more quickly for the non-linear thermal radiation as compared to the linear one.
- The concentration profile is a decreasing function of the thermophoretic parameter and Schmidt number.
- The transverse and the tangential velocity both increase for the higher values of the Hall current and ion-slip parameter.
- The wall shear stress decreases when the Hall current parameter is increased.
- The value of the mass transfer rate is getting high for the higher values of Prandtl number but it reduces for the Eckert number.

7.2 Future Outlooks

The work described in this thesis contributes to the importance of nanofluid for heat and mass transfer over the stretching sheet. In the 3rd and 4th chapters,

the effects of Hall current and ion-slip along with thermal diffusivity and heat generation absorption are also studied, whereas in 5th and 6th chapters, upper convected Maxwell fluid on bidirectional stretching sheet is investigated with MHD and non-linear thermal radiation effects. The described work can be extended in the following directions.

- The effects of Hall and ion-slip with nanofluid over the stretching cylinder and between the rotating disks is still missing in the literature. So the articles mentioned in 3rd and 4th chapters can be extended for the stretching cylinder and rotating disks with some other prominent effects such as non-linear thermal radiation, Joule heating and viscous dissipation.

- As in 3rd and 4th chapters, we have considered the Newtonian fluid. Attempts can be made to model the same problem for the non-Newtonian fluid such as Williamson fluid, Maxwell fluid, Oldroyd-B fluid etc.

- Different boundary conditions can be imposed such as convective boundary condition, velocity, thermal and concentration slip conditions, Melting heat, zero mass flux conditions etc.

- The problem described in 5th and 6th chapters can be further extended for the cylinder and rotating disk geometries. Some other parameters can also be incorporated e.g. variable thermal conductivities, porous media, Soret and Dufour effects, permeable sheets, heat generation absorption effects, chemical reaction, homogeneous/heterogeneous effects, Joule heating etc. The nature of the non-Newtonian fluid can also be varied.

- All the problems solved here are based on the linearly stretching sheets. The same problems can be modified for the non-linear stretching sheet and exponential stretching sheets.

Bibliography

[1] R. B. Bird, R. C. Armstrong, and O. Hassager, "Dynamics of polymeric liquids," *John Wiley and Sons Inc.,New York*, vol. 1, 1987.

[2] R. L. Fosdick and K. R. Rajagopal, "Anamolous features in the model of second-order fluids," *Arch. Ration. Mech. Anal.*, vol. 70, p. 145, 1979.

[3] T. Hayat, Z. Abbas, and M. Sajid, "Series solution for the upper-convected Maxwell fluid over a porous stretching plate," *Phys. Lett. A.*, vol. 358, pp. 396–403, 2006.

[4] K. Sadeghy, A. H. Najafi, and M. Saffaripour, "Sakiadis flow of an upper-convected Maxwell fluid," *Int. J. Non-Linear Mech*, vol. 40, pp. 1220–1228, 2005.

[5] K. R. Rajagopal, A. S. Gupta, and A. S. Wineman, "On a boundary layer of non-Newtonian fluids," *Int. J. of Engr. Sci.*, vol. 18, pp. 875–883, 1980.

[6] M. Ali and N. Ashrafi, "Similarity solution for high Weissenberg number flow of upper-convected Maxwell fluid on a linearly stretching sheet," *J. Engr.*, vol. 2016, pp. 1–10, 2016.

[7] A. Mushtaq, S. Abbasbandy, M. Mustafa, T. Hayat, , and A. Alsaedi, "Numerical solution for Sakiadis flow of upper-convected Maxwell fluid using Cattaneo-Christov heat flux model," *AIP Adv.*, vol. 6, p. 015208, 2016.

[8] A. J. Omowaye and I. L. Animasaun, "Upper-convected Maxwell fluid flow with variable thermo-physical properties over a melting surface situated in

hot environment subject to thermal stratification," *J. App. Fluid Mech.*, vol. 9(4), pp. 1777–1790, 2016.

[9] K. L. Krupalakshmi, B. J. Gireesha, B. Mahanthesh, and R. S. R. Gorla, "Influence of nonlinear thermal radiation and magnetic field on upper-convected Maxwell fluid flow due to a convectively heated stretching sheet in the presence of dust particles," *Commun. Numer. Analy.*, vol. 2016(1), pp. 57–73, 2016.

[10] I. Waini, N. A. Zainal, and N. S. Khashi'ie, "Aligned magnetic field effects on flow and heat transfer of the upper-convected Maxwell fluid over a stretching/shrinking sheet," *MATEC Web Conferences*, vol. 97, p. 01078, 2017.

[11] S. Saleem, M. Awais, S. Nadeem, N. Sandeep, and T. Mustafa, "Theoretical analysis of upper-convected Maxwell fluid flow with Cattaneo-Christov heat flux model," *Chinese J. Phy.*, p. doi: 10.1016/j.cjph.2017.04.005, 2017.

[12] M. S. Abel, V. Jagadish, M. Tawade, and M. Mahantesh, "MHD flow and heat transfer for the upper-convected Maxwell fluid over a stretching sheet," *Meccanica*, vol. 47, pp. 385–393, 2012.

[13] M. Mustafa, J. A. Khan, T. Hayat, and A. Alsaedi, "Sakiadis flow of Maxwell fluid considering magnetic field and convective boundary conditions," *AIP Adv.*, vol. 5, p. 027106, 2015.

[14] A. Mushtaq, M. Mustafa, T. Hayat, and A. Alsaedi, "A numerical study for three-dimensional viscoelastic flow inspired by non-linear radiative heat flux," *Non-linear Mech.*, vol. 79, pp. 83–87, 2016.

[15] S. Rana, R. Mehmood, and N. S. Akbar, "Mixed convective oblique flow of a Casson fluid with partial slip, internal heating and homogeneous-heterogeneous reactions," *J. Mol. Liq.*, vol. 222, pp. 1010–1019, 2016.

[16] W. Ibrahim, "Magnetohydrodynamic (MHD) stagnation point flow and heat transfer of upper-convected Maxwell fluid past a stretching sheet in the presence of nanoparticles with convective heating," *Front. Heat Mass Trans.*, vol. 7, 2016.

[17] R. Mehmood, S. Rana, N. S. Akbar, and S. Nadeem, "Non-aligned stagnation point flow of radiating Casson fluid over a stretching surface," *Alex. Engr. J.*, p. doi.org/10.1016/j.aej.2017.01.010, 2017.

[18] B. C. Sakiadis, "Boundary-layer equations for two-dimensional and axisymmetric flow," *American Inst. Chem. Engr. J.*, vol. 1, p. 26, 1961.

[19] ——, "The boundary layer on a continuous flat surface," *American Inst. Chem. Engr. J.*, vol. 7, p. 121, 1961.

[20] L. E. Erickson, L. T. Fan, and V. G. Fox, "Heat and mass transfer on a moving continuous flat plate with suction or injection," *Ind. Engr. Chem. Fundamentals*, vol. 5, p. 19, 1966.

[21] R. U. Haq, S. Nadeem, Z. H. Khan, and N. F. M. Noor, "Convective heat transfer in MHD slip flow over a stretching surface in the presence of carbon nanotubes," *Phy. B*, vol. 5, p. 19, 2014.

[22] G. K. Ramesh, "Numerical study of the influence of heat source on stagnation point flow towards a stretching surface of a Jeffrey nanoliquid," *J. Engr*, vol. 2015, p. 10, 2015.

[23] B. J. Gireesha, B. Mahanthesh, and M. M. Rashidi, "MHD boundary layer heat and mass transfer of a chemically reacting Casson fluid over a permeable stretching surface with non-uniform heat source/sink," *Int. J. Ind. Math.*, vol. 7, pp. 247–260, 2015.

[24] S. U. S. Choi, "Enhancing thermal conductivity of fluids with nanoparticles, development and applications of non-Newtonian flows," *ASME J. Heat Trans.*, pp. 0–8, 1995.

[25] S. M. S. Murshed, K. C. Leong, and C. Yang, "Thermophysical and electrokinetic properties of nanofluids - a critical review," *Appl. Therm. Engr.*, vol. 28, pp. 2109–2125, 2008.

[26] S. Ozerinc, S. Kakac, and A. Yazicioglu, "Enhanced thermal conductivity of nanofluids: a state-of-the-art review," *Microfluids Nanofluids*, vol. 8, pp. 145–170, 2010.

[27] S. U. S. Choi, "Nanofluids: from vision to reality through research," *J. Heat Trans.*, vol. 131, pp. 1–9, 2009.

[28] K. V. Wong and O. Leon, "Applications of nanofluids: current and future," *Adv. Mech. Engr.*, vol. 2010, pp. 1–10, 2010.

[29] J. Buongiorno, "Convective transport in nanofluids applications of nanofluids: current and future," *ASME J. Heat Trans.*, vol. 2010, pp. 240–250, 2006.

[30] R. Tiwari and S. Das, "Heat transfer augmentation in a two-sided lid-driven differentially heated square cavity utilizing nanofluids," *Int. J. Heat Mass Transf.*, vol. 50, pp. 2002–2018, 2007.

[31] N. Ashikin, K. Zaimi, and R. A. Hamid, "MHD boundary layer flow of a Maxwell nanofluid over a permeable vertical surface," *AIP Conference Proceedings*, 2014.

[32] S. Mansur, A. Ishak, and I. Pop, "Magnetohydrodynamic stagnation point flow of a nanofluid over a stretching/shrinking sheet with suction," *PLOS ONE*, vol. 10(3), p. e0117733, 2015.

[33] S. Noreen and M. Qasim, "Influence of Hall current and viscous dissipation on pressure driven flow of pseudoplastic fluid with heat generation: A mathematical study," *PLOS ONE*, vol. 10, p. e0129588, 2015.

[34] T. Hayat, B. Ashraf, S. A. Shehzad, A. Alsaedi, and N. Bayomi, "Three-dimensional mixed convection flow of viscoelastic nanofluid over an exponentially stretching surface," *Int. J. Numer. Meth. Heat Fluid Flow*, vol. 25, pp. 333–357, 2015.

[35] T. Hayat, M. Imtiaz, and A. Alsaedi, "Unsteady flow of nanofluid with double stratification and magnetohydrodynamics," *Int. J. Heat Mass Trans.*, vol. 92, pp. 100–109, 2016.

[36] S. A. Shehzad, F. M. Abbasi, T. Hayat, and B. Ahmad, "Doubly stratified mixed convection flow of Maxwell nanofluid with heat generation/absorption," *J. Magn. Magn. Mater.*, vol. 404, pp. 159–165, 2016.

[37] T. Hayat, S. Qayyum, S. A. Shehzad, and A. Alsaedi, "Simultaneous effects of heat generation/absorption and thermal radiation in magnetohydrodynamics MHD flow of Maxwell nanofluid towards a stretched surface," *Results Phy.*, vol. 7, pp. 562–573, 2017.

[38] A. Alsaedi, M. I. Khan, M. Farooq, N. Gull, and T. Hayat, "Magnetohydrodynamic MHD stratified bioconvective flow of nanofluid due to gyrotactic microorganisms," *Adv. Powder Tech.*, vol. 28, pp. 288–298, 2017.

[39] T. Hayat, Z. Hussain, A. Alsaedi, and M. Mustafa, "Nanofluid flow through a porous space with convective conditions and heterogeneous-homogeneous reactions," *J. Taiwan Inst. Chem. Engr.*, vol. 70, pp. 119–126, 2017.

[40] M. Mustafa, M. Wasim, T. Hayat, and A. Alsaedi, "A revised model to study the rotating flow of nanofluid over an exponentially deforming sheet: Numerical solutions," *J. Mol. Liq.*, vol. 225, pp. 320–327, 2017.

[41] A. Hussanan, M. Z. Salleh, I. Khan, and S. Shafie, "Convection heat trasnfer in micropolar nanofluids with oxide nanoparticles in water, kerosene and engine oil," *J. Mol. Liq.*, vol. 229, pp. 482–488, 2017.

[42] A. C. Eringen, "Theory of micropolar fluids," *J. Math. Mech*, vol. 16, pp. 1–18, 1966.

[43] ——, "Theory of thermomicropolar fluids," *J. Math. Anal. Appl*, vol. 38, pp. 480–496, 1972.

[44] F. Mabood, S. M. Ibrahim, M. M. Rashidi, M. S. Shadloo, and G. Lorenzini, "Non-uniform heat source/sink and Soret effects on MHD non-Darcian convective flow past a stretching sheet in a micropolar fluid with radiation," *Int. J. Heat . Mass Trans.*, vol. 93, pp. 674–682, 2016.

[45] A. Mirzaaghaian and D. D. Ganji, "Application of differential transformation method in micropolar fluid flow and heat transfer through permeable walls," *Alex. Engr J.*, vol. 55, pp. 2183–2191, 2016.

[46] M. A. Ali, N. Faraz, Y. Q. Bai, and Y. Khan, "Analytical study of the non orthogonal stagnation point flow of a micro polar fluid," *J. King Saud Uni. Sci.*, vol. 29, pp. 126–132, 2017.

[47] M. Turkyilmazoglu, "Mixed convection flow of magnetohydrodynamic micropolar fluid due to a porous heated/cooled deformable plate: Exact solutions," *Int. J. Heat Mass Trans.*, vol. 106, pp. 127–134, 2017.

[48] S. A. Shehzad, M. Waqas, A. Alsaedi, and T. Hayat, "Flow and heat transfer over an unsteady stretching sheet in a micropolar fluid with convective boundary condition," *J. App. Fluid Mech.*, vol. 9(3), pp. 1437–1445, 2016.

[49] G. Lukaszewicz, "Micropolar Fluids: Theory and Applications," *Basel Birkhauser*, 1999.

[50] A. C. Eringen, "Microcontinuum Field Theories," *Fluent Media, Springer, New York*, 2001.

[51] N. A. A. Latiff, M. J. Uddin, O. A. Beg, and A. I. Ismail, "Unsteady forced bioconvection slip flow of a micropolar nanofluid from a stretching/shrinking sheet," *J. Nano. engr. Nano. sys.*, p. 11, 2015.

[52] S. E. Ahmed, M. A. Mansour, A. K. Hussein, and S. Sivasankaran, "Mixed convection from a discrete heat source in enclosures with two adjacent moving walls and filled with micropolar nanofluids," *Engr. Sci. Tech., Int. J.*, p. 13, 2015.

[53] P. V. S. Narayana, B. Venkateswarlu, and S. Venkataramana, "Effects of Hall current and radiation absorption on MHD micropolar fluid in a rotating system," *Ain Shams Engr. J.*, vol. 4, pp. 843–854, 2013.

[54] R. U. Haq, S. Nadeem, N. S. Akbar, and Z. H. Khan, "Buoyancy and radiation effect on stagnation point flow of micropolar nanofluid along a vertically convective stretching surface," *IEEE Trans. Nanotech.*, vol. 14, pp. 42–50, 2015.

[55] M. F. El-Amin, "Combined effect of viscous dissipation and Joule heating on MHD forced convection over a non-isothermal horizontal cylinder embedded in a fluid saturated porous medium," *J. Magn. Mag. Mater.*, vol. 263, p. 337343, 2003.

[56] M. S. Alam, M. M. Rahman, and M. A. Sattar, "On the effectiveness of viscous dissipation and Joule heating on steady magnetohydrodynamic heat and mass transfer flow over an inclined radiate isothermal permeable surface in the presence of thermophoresis," *Comm. Non-linear Sci. Num. Sim.*, vol. 14, pp. 2132–2143, 2009.

[57] S. M. Ibrahim and N. B. Reddy, "Similarity solution of heat and mass transfer for natural convection over a moving vertical plate with internal heat generation and a convective boundary condition in the presence of thermal radiation, viscous dissipation, and chemical reaction," *ISRN Thermodynamics*, vol. 2013, p. 10, 2013.

[58] T. Hayat, A. Naseem, M. Farooq, and A. Alsaedi, "Unsteady MHD three-dimensional flow with viscous dissipation and Joule heating," *Eur. Phys. J. Plus*, vol. e0124699, pp. 128–158, 2013.

[59] A. Mushtaq, S. Abbasbandy, M. Mustafa, T. Hayat, and A. Alsaedi, "Numerical solution for Sakiadis flow of upper-convected Maxwell fluid using Cattaneo-Christov heat flux model," *AIP Adv.*, vol. 6, p. 015208, 2016.

[60] S. Das, S. Chakraborty, R. N. Jana, and O. D. Makinde, "Entropy analysis of unsteady magneto-nanofluid flow past accelerating stretching sheet with convective boundary condition," *Appl. Math. Mech*, vol. 36, pp. 1593–1610, 2015.

[61] M. Sheikholeslami, M. M. Rashidi, and D. D. Ganji, "Numerical investigation of magnetic nanofluid forced convective heat transfer in existence of variable magnetic field using two phase model," *J. Mol. Liq.*, vol. 212, pp. 117–126, 2015.

[62] F. M. Abbasi, S. A. Shehzad, T. Hayat, A. Alsaedi, and M. A. Obid, "Influence of heat and mass flux conditions in hydromagnetic flow of Jeffrey nanofluid," *AIP Adv.*, vol. 5, p. 037111, 2015.

[63] H. A. Attia, "Effect of the ion slip on the MHD flow of a dusty fluid with heat transfer under exponential decaying pressure gradient." *Cent. Eur. J. Phys.*, vol. 3, pp. 484–507, 2005.

[64] K. Cramer and S. Pai, "Magnetofluid dynamics for engineers and applied physicists," *McGraw-Hill, New York*, vol. 93, 1973.

[65] M. S. Alam, M. Ali, M. A. Alim, and A. Saha, "Steady MHD boundary free convective heat and mass transfer flow over an inclined porous plate with variable suction and Soret effect in presence of Hall current," *J. Heat Mass Trans.*, vol. 49, pp. 155–164, 2014.

[66] E. M. Abo-Eldahab, "Hall effects on magnetohydrodynamic free convective flow at a stretching surface with a uniform free stream," *Phys. Scr.*, vol. 63, pp. 29–35, 1999.

[67] M. Thamizsudar and J. Pandurangan, "Hall effects and rotation effects on MHD flow past an exponentially accelerated vertical plate with combined

heat and mass transfer effects," *Int. J. Appl. Mech. Engr.*, vol. 20, pp. 605–616, 2015.

[68] T. M. E. Nabil, A. Y. Ghaly, S. N. Sallam, K. Elagamy, and Y. M. Younis, "Hall effect on peristaltic flow of third order fluid in a porous medium with heat and mass transfer." *J. Appl. Math. Phy.*, vol. 3, pp. 1138–1150, 2015.

[69] M. R. Islam, M. Asaduzzaman, and M. M. Alam, "Hall current effects on one dimensional unsteady MHD micropolar fluid flow past an impulsive started plate," *Int. J. Engr. Tech. Sci. Res.*, vol. 2, pp. 79–88, 2015.

[70] H. A. Attia, W. Abbas, Mostafa, and A. M. Abdeen, "Ion slip effect on unsteady Couette flow of a dusty fluid in the presence of uniform suction and injection with heat transfer," *J. Braz. Soc. Mech. Sci. Eng.*, pp. 1–11, 2015.

[71] N. N. Anika, M. M. Hoque, S. I. Hossain, and M. M. Alam, "Thermal diffusion effect on unsteady viscous MHD micropolar fluid flow through an infinite vertical plate with Hall and ion-slip current," *Proc. Engr.*, vol. 105, pp. 160–166, 2015.

[72] Z. Uddin and M. Kumar, "Hall and ion-slip effect on MHD boundary layer flow of a micro polar fluid past a wedge," *Scientia Iranica B*, vol. 20(3), pp. 467–476, 2013.

[73] S. S. Motsa and S. Shatery, "The effects of chemical reaction, Hall and ion-slip currents on MHD micropolar fluid flow with thermal diffusivity using a noval numerical technique," *J. Appl. Math.*, vol. 2012, 2012.

[74] K. Vafai, "A handbook of porous media, 2nd edition," *CRC Press, Taylor & Francis Group, 6000 Broken Sound Parkway NW, Suite 300*, vol. 2, 2005.

[75] T. Hayat, M. Imtiaz, A. Alsaedi, and R. Mansoor, "MHD flow of nanofluids over an exponentially stretching sheet in a porous medium with convective boundary conditions," *Chin. Phys. B*, vol. 23, no. 5, p. 054701, 2014.

[76] A. Rauf, S. A. Shahzad, M. K. Siddiq, J. Raza, and M. A. Meraj, "Mixed convective thermally radiative micro nanofluid flow in a stretchable channel with porous medium and magnetic field," *AIP Adv.*, vol. 6, p. 035126, 2016.

[77] S. Nadeem and N. Muhammad, "Impact of stratification and Cattaneo-Christov heat flux in the flow saturated with porous medium," *J. Mol. Liq.*, vol. 224, no. Part A, pp. 423 – 430, 2016.

[78] M. Sheikholeslami, "Numerical simulation of magnetic nanofluid natural convection in porous media," *Phy. Lett. A*, vol. 381, no. 5, pp. 494 – 503, 2017.

[79] W. C. Hinds, "Aerosol technology: properties, behavior, and measurement of airborne particles," *John Wiley and Sons, New York*, 1982.

[80] A. Y. Bakiera and M. A. Mansour, "Combined magnetic field and thermophoresis particle deposition in free convection boundary layer from a vertical flat plate embedded in a porous medium," *Int. J. Thermal. Sci.*, vol. 11, pp. 65–74, 2007.

[81] C. J. Tsai, J. S. Lin, I. Shankar, G. Aggarwal, and D. R. Chen, "Thermophoretic deposition of particles in laminar and turbulent tube flows," *Aerosol Sci. Technol.*, vol. 38, pp. 131–139, 2004.

[82] P. Goldsmith and F. G. May, "Diffusiophoresis and thermophoresis in water vapour systems, in: Aerosol science," *C. N. Davies (Ed.), Academic Press, London,*, pp. 163–194, 1966.

[83] S. L. Goren, "Thermophoresis of aerosol particles in laminar boundarylayer on flat plate," *J. Colloid Interface Sci.*, vol. 61, pp. 77–85, 1977.

[84] T. Hayat, M. Rafiq, and B. Ahmad, "Influences of rotation and thermophoresis on MHD peristaltic transport of Jeffrey fluid with convective conditions and wall properties," *J. Magn. Magn. Mater.*, vol. 410, pp. 89 – 99, 2016.

[85] M. Sheikh and Z. Abbas, "Effects of thermophoresis and heat generation/absorption on MHD flow due to an oscillatory stretching sheet with chemically reactive species," *J. Magn. Magn. Mater.*, vol. 396, pp. 204–213, 2015.

[86] D. Pal and H. Mondal, "Influence of thermophoresis and Soret–Dufour on magnetohydrodynamic heat and mass transfer over a non-isothermal wedge with thermal radiation and Ohmic dissipation," *J. Magn. Magn. Mater.*, vol. 331, pp. 250–255, 2013.

[87] B. R. Rout and C. Sahoo, "Effect of thermal radiation on steady MHD thermal slip boundary layer flow over a flat plate with variable fluid properties," *Int. J. Innov. Res. Dev.*, vol. 5, pp. 393–398, 2016.

[88] N. Khan and T. Mahmood, "Thermophoresis particle deposition and internal heat generation on MHD flow of an Oldroyd-B nanofluid between radiative stretching disks," *J. Mol. Liq.*, vol. 216, pp. 571–582, 2016.

[89] http://www.freestudy.co.uk/fluid%20mechanics/t3203.pdf.

[90] T. C. Papanastasiou and G. C. Georgiou, "Viscous fluid flow," *CRC Press, LLC, 2000 N.W. Corporate Blvd., Boca Raton, Florida*, 1999.

[91] https://warwick.ac.uk/fac/sci/physics/research/cfsa/people/valery/teaching/px420/addres/mhd_int1.pdf.

[92] M. Sajid, Z. Abbas, N. Ali, and T. Javed, "Note on effect of Joule heating and MHD in the presence of convective boundary condition for upper-convected Maxwell fluid through wall jet," *J. Mol. Liq.*, vol. 230, pp. 235 – 236, 2017.

[93] T. Y. Na, "Computational methods in engrineering boundary value problem," *Academic Press*, pp. 71–76, 1979.

[94] M. Khan, S. Abelman, D. Mason, and F. Mahomed, "Self-similar unsteady flow of a sisko fluid in a cylindrical tube undergoing translation," *Mathematical Problems in Engineering*, vol. 2015, 2015.

[95] L. F. Shampine, M. W. Reichelt, and J. Kierzenka, "Solving boundary value problems for ordinary differential equations in MATLAB with bvp4c," *http://www.mathworks.com/bvp_tutorial*.

[96] L. Cao, X. Si, and L. Zheng, "Convection of Maxwell fluid over stretching porous surface with heat source/sink in presence of nanoparticles: Lie group analysis," *Appl. Math. Mech. -Engl. Ed.*, vol. DOI 10.1007/s10483-016-2052-9, 2016.

[97] L. L. J. Li, L. Zheng, "MHD viscoelastic flow and heat transfer over a vertical stretching sheet with Cattaneo-Christov heat flux effects," *J. Mol. Liq.*, vol. 221, pp. 19–25, 2016.

[98] N. S. Elgazery, "The effects of chemical reaction, Hall and ion-slip currents on MHD flow with temperature dependent viscosity and thermal diffusivity," *Comm. Nonlinear Sci. Num. Sim.*, vol. 14, pp. 1267–1283, 2009.

[99] Z. Abbas and M. Sheikh, "Numerical study of homogeneous-heterogeneous reactions on stagnation point flow of ferrofluid with non-linear slip condition," *Chinese J. Chem. Engr.*, vol. doi.org/10.1016/j.cjche.2016.05.019, 2016.

[100] F. M. Abbasi and S. A. Shehzad, "Heat transfer analysis for three-dimensional flow of Maxwell fluid with temperature dependent thermal conductivity: Application of Cattaneo-Christov heat flux model," *J. Mol. Liq.*, vol. 220, p. 848854, 2016.

[101] M. Awais, T. Hayat, S. Irum, and A. Alsaedi, "Heat generation/absorption effects in a boundary layer stretched flow of Maxwell nanofluid: Analytic and numeric solutions," *PLOS One*, vol. 10(6), p. e0129814, 2015.

[102] J. A. Khan, M. Mustafa, T. Hayat, and A. Alsaedi, "Numerical study of Cattaneo-Christov heat flux model for viscoelastic flow due to an exponentially stretching surface," *PLOS One*, vol. 10(9), p. e0137363, 2015.

[103] M. Mustafa, A. Mushtaq, T. Hayat, and B. Ahmad, "Nonlinear radiation heat transfer effects in the natural convective boundary layer flow of nanofluid past a vertical plate: A numerical study," *PLOS One*, vol. 9(9), p. e103946, 2014.

[104] A. Mushtaq, M. Mustafa, T. Hayat, and A. Alsaedi, "Numerical study of the non-linear radiation heat transfer problem for the flow of a second-grade fluid," *Bulg. Chem. Comm.*, vol. 47(2), pp. 725–732, 2015.

[105] B. I. Olajuwon, "Convection heat and mass transfer in a hydromagnetic flow of a second grade fluid in the presence of thermal radiation and thermal diffusion," *Int. Comm. Heat and Mass Trans.*, vol. 38, p. 377382, 2011.

[106] G. W. Sutton and A. Sherman, "Engineering magnetohydrodynamics," *McGraw-Hill, New York. USA*, 1965.

[107] E. M. Abo-Eldahab and M. A. El-Aziz, "Hall and ion-slip effects on MHD free convective heat generating flow past a semi-infinite vertical flat plate," *Phys. Scripta*, vol. 61, p. 344, 2000.

[108] A. J. Chamkha and A. A. Khaled, "Similarity solutions for hydromagnetic simultaneous heat and mass transfer by natural convection from an inclined plate with internal heat generation or absorption," *Heat Mass Trans.*, vol. 37, p. 117, 2001.

[109] E. M. Abo-Eldahaba and M. A. El-Aziz, "Blowing/suction effect on hydromagnetic heat transfer by mixed convection from an inclined continuously stretching surface with internal heat generation/absorption," *Int. J. Therm. Sci.*, vol. 43, pp. 709–719, 2004.

[110] N. Acharya, K. Das, and P. K. Kundu, "Fabrication of active and passive controls of nanoparticles of unsteady nanofluid flow from a spinning body using HPM," *Eur. Phys. J. Plus*, vol. 132, p. 323, 2017.

[111] M. Ramzan and M. Bilal, "Time dependent MHD nano-second grade fluid flow induced by permeable vertical sheet with mixed convection and thermal radiation," *PLoS ONE*, vol. 10(5), p. e0124929, 2015.

[112] M. Ramzan, M. Bilal, J. D. Chung, and U. Farooq, "Mixed convective flow of Maxwell nanofluid past a porous vertical stretched surface - An optimal solution," *Results Phy.*, vol. 6, pp. 1072–1079, 2016.

[113] W. U. Lei, Z. Feng-De, and Z. Jie-Fang, "Adomian decomposition method for nonlinear differential-difference equation," *Commun. Theor. Phys.*, vol. 48, pp. 983–986, 2007.

[114] E. F. Elshehawey, N. T. Eldabe, E. M. E. Elbarbary, and N. S. Elgazery, "Chebyshev finite-difference method for the effects of Hall and ion-slip currents on magnetohydrodynamic flow with variable thermal conductivity," *Can. J. Phys.*, vol. 82, pp. 701–715, 2004.

[115] A. M. Salem and M. A. El-Aziz, "Effect of Hall currents and chemical reaction on hydromagnetic flow of a stretching vertical surface with internal heat generation/absorption," *Appl. Math. Model.*, vol. 32, pp. 1236–1254, 2008.

[116] I. C. Liu and H. I. Andersson, "Heat transfer over a bidirectional stretching sheet with variable thermal conditions," *Int. J. Heat Mass Transf.*, vol. 51, pp. 4018–4024, 2008.

[117] M. Awais, T. Hayat, A. Alsaedi, and S. Asghar, "Time-dependent three-dimensional boundary layer flow of a Maxwell fluid," *Comp. Fluids*, vol. 91, pp. 21–27, 2014.

[118] K. Jafar, R. Nazar, A. Ishak, and I. Pop, "MHD stagnation point flow towards a shrinking sheet with suction in an upper-convected Maxwell (UCM) fluid," *Int. J. Math,, Compt., Phy., Elect. Comp. Engr.*, vol. 8(5), pp. 1–9, 2014.

[119] T. Hayat, M. Awais, M. Qasim, and A. A. Hendi, "Effects of mass transfer on the stagnation point flow of an upper-convected Maxwell (UCM) fluid," *Int. J. Heat. Mass Trans.*, vol. 54, pp. 3777–3782, 2011.

[120] W. Ibrahim, "Nonlinear radiative heat transfer in magnetohydrodynamic MHD stagnation point flow of nanofluid past a stretching sheet with convective boundary condition," *J. Propul. Power*, vol. 4(4), pp. 230–239, 2015.

[121] S. A. Shehzad, Z. Abdullah, A. Alsaedi, F. M. Abbasi, and T. Hayat, "Thermally radiative three-dimensional flow of Jeffrey nanofluid with internal heat generation and magnetic field," *J. Magn. Magn. Mater.*, vol. 108–114, p. 397, 2016.

[122] P. D. Ariel, "The three-dimensional flow past a stretching sheet by the homotopy perturbation method," *Comput. Math. Appl.*, vol. 54, pp. 920–925, 2007.

[123] T. Hayat, M. Awais, and S. Obaidat, "Mixed convection three-dimensional flow of an upper-convected Maxwell fluid under magnetic field, thermal-diffusion, and diffusion-thermo effects," *J. heat trans.*, vol. 134, pp. 044 503–1, 2012.